Cellulose-based Hydrogels and Aerogels for Hemostatic Applications

By

Peiyu Yu

A Thesis Submitted to the Faculty of Graduate Studies of

The University of Manitoba

in partial fulfillment of the requirements of the degree of

Master of Science

Department of Biosystems Engineering

University of Manitoba

Winnipeg, Manitoba

Table of Contents

Abstract

Hemostasis is an important issue in-clinic treatments for acute wounds. Existing hemostatic materials may not fully meet the demands in emergency situations in terms of hospitals and battlefields which calls for the development of cost-effective hemostatic materials for clinical applications.

Cellulose as a natural polymer is abundant in nature and has been widely used in different applications, like food, cosmetics, and hemostatic applications. Cellulose-based materials can absorb water from blood upon contact with wounds, which helps to stop bleeding. In this work, cellulose-based aerogels and hydrogels were prepared and their potential applications as hemostatic materials were explored.

Aerogels with ultra-high porosity and large surface area can absorb water from blood and form barriers in the trauma site to stop bleeding. In this thesis, an aerogel with lightweight, injectability, antibacterial ability, water-induced shape memory behavior, and excellent compressibility was developed from carboxymethylated nanocellulose fibers (NCFs), alginate and zinc chloride. The obtained NCFs-alginate aerogels have dual networks which are the physical network of NCFs formed by freeze-drying and physical crosslinking between alginate and zinc ions. Here, zinc chloride endowed the aerogels with the antibacterial ability to prevent infection and reduce the probability of complications due to microorganisms. The NCFs-alginate aerogels with high water absorption can absorb water when contacting blood to stop bleeding. Meanwhile, in the presence of NCFs and alginate, the aerogels can promote wound healing quickly. Besides, injectability and rapid water-induced shape recovery ability (4s) allowed the NCFs-alginate aerogels to be used for penetrating wounds.

Carboxymethylated cellulose (CMC) is an important derivation of cellulose and has been widely used in biomedical applications. A facile and environmentally friendly

method for preparing self-healing hydrogels using CMC, polyvinyl alcohol (PVA), and borax has been developed. The CMC was grafted with double bonds via triethylamine and methacrylic anhydride (MA). Herein, the hydrogel contains double networks: the chemically crosslinked network formed by methacrylate carboxymethylated cellulose (MACMC) and the physical crosslinking between PVA and borax. The MACMC-PVA hydrogel has rapid self-healing efficiency (8s) due to the presence of reversible hydrogen bonds, including hydrogen bonds between CMC and PVA and dynamic complexation of diol-borax between PVA and borax. Additionally, the MACMC-PVA hydrogel with good tissue-adhesive properties and remarkable stretchability can closely adhere to wound sites of different shapes, including penetrating wounds. The hydrophilicity and higher water absorption rate allow the hydrogel to absorb water from the blood to block bleeding and to provide a moisture environment that promotes wound healing.

Based on the above studies, cellulose-based aerogels and hydrogels with high water absorption and outstanding properties can provide an optimum environment to stop bleeding, avoid infection and accelerate wound healing. Therefore, the developed cellulose-based materials have great potential in hemostatic applications.

Keywords: NCFs, alginate, zinc chloride, aerogel, CMC, PVA, borax, self-healing hydrogel, hemostasis

Acknowledgment

I would like to express my gratitude to Dr. Wen Zhong, my supervisor, for her professional guidance and support throughout my studies. She and Dr. Malcolm Xing have motivated me not just academically, but also in terms of thinking freely and being unique.

Thanks to all my lab colleagues especially Dr. Yuqing Liu and Xingying Zhang for teaching me the usage of instruments and giving me suggestions during the project, and Dr. Ying Wang who helped me with the animal test.

I would also want to express my gratitude to Dr. Malcolm Xing and Dr. David Levin as my committee members making comments to help me improve my research.

I am also thankful for the love and support of my mom and friend.

Lastly, thanks for the financial support from the Natural Sciences and Engineering Research Council of Canada (NSERC) Discovery Grant and NESRC Discovery Accelerator Supplements Awards.

List of Figures

List of Tables

Chapter 1 Introduction

1.1 General introduction

Uncontrolled hemorrhage is the main cause of trauma-related death on battlefields and in hospitals (1). Around the world, over 30% of trauma death is caused by uncontrolled hemorrhage (2). Prolonged bleeding may lead to such complications as hemorrhagic shock, hypothermia, and multiple organ failure (3,4). Thus, effective hemostatic methods are critical for increasing the survival rate from acute injuries. The human body has a limited capacity for wound healing. However, the natural hemostasis mechanism of humans cannot timely control massive bleeding in surgery and heavy wounds (5). Herein, hemostatic dressing and/or devices have been used to block bleeding and/or promote wound healing. An ideal hemostatic material is expected to effectively promote wound healing, especially for massive bleeding, and to have outstanding properties, including biocompatibility, biodegradability, non-cytotoxicity, cost-effectiveness, ultralightweight, stability, and easy for applications (2,5–7).

Hydrogels, a soft material with three-dimension network structures and tunable physical and chemical characteristics, has been widely used in different fields, including sensors and biomedical fields (8,9). In recent years, self-healing hydrogels have attracted widespread attention, as they enable a structure or material to restore its mechanical properties and original integrity after being damaged. Thus, the lifetime of hydrogels can be prolonged, and their stability can be maintained (9–11). Additionally, self-healing hydrogels have been vastly used as hemostatic materials and drug delivery carriers because of their self-recovery ability, high mechanical durability, high water content (maximum 99.5%), and long lifespan (12). Meanwhile, self-repairable hydrogels have been considered to be one of the best choices for injectable materials (13). Therefore, self-healing hydrogels are promising for wound dressings.

Aerogel is an ultralight material with a highly porous structure produced by sublimating the liquid component from a hydrogel via freezing-drying or critical point drying (14,15). Aerogels show the merits of low density, large specific surface area, high porosity, and low thermal conductivity (16). Compared with other aerogel building blocks, nanocellulose aerogels offer tunable interfacial chemistry, excellent mechanical property, extremely high specific surface area, and beneficial renewable origins (14). Aerogels have high water absorption, great mechanical properties, and rapid shape recovery ability, making them a promising hemostatic material (17). Because of the large specific surface area and high porosity, aerogels can adsorb liquid upon contact with the blood and swell to provide a haemostat in a bleeding site: Aerogels can entangle proteins, platelets, and red blood cells to form a "barrier" which prevents the flow of blood, and serves as a matrix for fibrin to form the solid fibrin clot (18).

Nanocellulose fibers are a natural polymer that can be obtained from various sources, such as bacteria, algae, and wood, among which the wood-based nanocellulose fibers (NCFs) have been mostly studied due to their great environmental and industrial importance (19). Nanocellulose is a linear natural polymer with a highly ordered, long, and thin nanostructure (15). NCFs have the advantages of natural abundance, biodegradation, low thermal conductivity, lightweight, and high strength, therefore, are becoming a promising material for wound care applications (16,19). Nanocellulose has abundant active hydroxyl groups, which can be chemically modified into functional groups, such as carboxymethyl. Some recent studies showed promising results for NCFs-based wound dressings for wound healing (19). Carboxymethylated cellulose (CMC), one of the important cellulose derivations, is widely used in the food industry, biomedical, and pharmaceutical areas, because of its biocompatibility, biodegradability, non-toxicity, and low cost (20–22).

1.2 Problem statement

A number of materials have been widely used for hemostasis, such as collagen (Col), gelatin (GE), alginate (AE), chitosan (CS), oxidized cellulose, cyanoacrylic acid tissue adhesive, and porous zeolite (7). Although these materials are commonly used and effective hemostatic agents, they still have limitations on hemostatic efficiency. For example, collagen and gelatin are the main components of the extracellular matrix and connective tissues, respectively. They can therefore facilitate the formation of fibrin. However, collagen and gelatin have poor tissue adhesion because they need ample platelets to form clots. Alginate can also accelerate the formation of fibrin (5). Nevertheless, alginate dressings have poor chemical stability, and their structure degradation is unpredictable (5,6,17,23). Porous zeolite can absorb water from the blood, aggregate proteins, and cellular matrix to promote the formation of platelet plugs. However, porous zeolite undergoes an exothermic reaction upon absorbing water from wounds and may cause wound burn and inflammation (17,24). New hemostatic techniques or materials have been developed, such as the XStat device, which is a syringe-like device that injects cellulose-based sponges coated with chitosan into penetrated wounds to absorb blood quickly (25). However, the preparation and synthesis of the new hemostatic materials can be intricate and costly (2,17). Therefore, a hemostatic material that is cost-effective, easy to prepare and use, and high in blood absorption capacity is highly demanded.

1.3 General Objectives

Although the commercial hemostatic materials exhibit good hemostatic performance, the drawbacks are also obvious, like causing additional injury, poor adhesion, expensive, and difficult operation. Therefore, the general objective of this thesis is to develop cellulose-based multifunctional aerogels and hydrogels which can be

potentially used in hemostatic applications. This thesis is composed of two projects with the following specific objectives:

1) To design NCFs-alginate aerogels which have lightweight, high porosity, injectability, antibacterial ability, and excellent hemostatic efficiency.

2) To develop self-healing hydrogels with high water absorption and good mechanical property that are prepared by carboxymethylated cellulose (CMC), polyvinyl alcohol (PVA), and borax.

1.4 Layout of thesis

The layout of this thesis will be as follows:

In chapter 2, an overview of the development and application of hemostatic materials is provided, beginning with a description of the physiological mechanism of hemostasis and existing hemostatic methods, followed by an explanation of the hemostatic materials in clinical use. A discussion will be provided on high-performance hemostatic materials, including antibacterial hemostatic materials, and biomimetic hemostatic materials. The prospects for hemostatic materials will be discussed at the end of this chapter.

Chapter 3 reports the nanocellulose fibers (NCFs)-based aerogels. Firstly, the NCFs-alginate aerogels are briefly introduced in this chapter, followed by the discussion of materials and methods which were used in preparing and testing the aerogels. Finally, the results are demonstrated and discussed, including the characteristics, compressive ability, water absorption, rheology assay, and water-induced shape memory behavior. The hemostatic efficiency of NCFs-alginate aerogels was evaluated by *in vitro* hemostatic tests and *in vivo* rat liver and heart injury models. The results showed that the NCFs-alginate aerogels have excellent antibacterial ability, hemocompatibility,

coagulation ability, and rapid hemostasis capacity as compared to NCFs aerogels and gelatin hemostatic sponges.

In chapter 4, a CMC-based hydrogel is prepared with CMC, PVA, and borax. A brief introduction of this hydrogel is provided at the beginning of this chapter, followed by the materials and methods for preparing the hydrogels. Finally, there are presentations and discussions on the results of characterization tests, including adhesion, rheology, self-healing, water contact angles, water absorption rates, and rewet assay.

In the end, a general conclusion and future outlook of the cellulose-based materials are briefly discussed in chapter 5.

Chapter 2 Literature Review

This chapter starts with an introduction to hemostatic mechanisms and the performance of the most commonly used hemostatic materials, including fibrin, collagen, zeolite, gelatin, alginate, chitosan, cellulose, and cyanoacrylate, and the commercial wound dressings based on these materials. Then, the properties and clinical applications of high-performance hemostatic materials, such as those with antibacterial capacity, superhydrophobicity/superhydrophilicity, superelasticity, high porosity, and/or biomimicry, are introduced. The prospects of high-performance hemostatic materials are briefly discussed at the end of this chapter.

2.1 Introduction

Blood is composed of erythrocytes, leukocytes, platelets, and plasma, making up about 7-8% of total body weight. Blood in the human body is involved in several essential processes, including transporting oxygen and other nutrients to different organs, preventing excessive blood loss, and regulating body temperature (26). However, in battlefields, hospitals, and other emergencies, uncontrolled hemorrhage causes over 30% of traumatic deaths, half of which happen at the prehospital stage. It is also suggested that 50% of military mortality is caused by bleeding (2,27). Excessive bleeding can cause severe damage, including hemorrhagic shock, hypothermia, hypotension, multiple organ failure, acidosis, and infections (3,4). Therefore, hemostasis becomes an important step in trauma treatment.

The intrinsic hemostatic mechanism of the human body has a limited capacity and may need assistance via hemostatic materials or devices for rapid hemostasis, particularly in emergency situations (5). In clinical practice, compression with cotton gauze and wound closure with sutures or staples are the most frequently used methods to stop bleeding. Recently, a variety of hemostatic materials have been generated for the industry, namely, collagen (28), zeolite (24), gelatin (29), alginate (30), chitosan (31),

cellulose (32), and cyanoacrylate (33). However, the hemostatic efficiency of these materials cannot fully meet clinical requirements (5,34,35). Therefore, considerable efforts have been made in recent years to improve high-performance hemostatic materials.

A desirable hemostatic material should generally have rapid and sustainable hemostatic efficacy, biocompatibility, biodegradability, non-cytotoxicity, and firm adhesion in a moist environment. Furthermore, ease of use, shelf life, and cost are also major factors to be considered in the design and engineering of hemostatic materials (5,35).

In this review, a description of the progress of hemostatic materials is given, starting with an introduction to the intrinsic hemostatic mechanism of the human body and existing hemostatic methods, followed by a discussion on hemostatic materials that have been used clinically. High-performance hemostatic materials, including those that are antibacterial hemostatic materials, and biomimetic hemostatic materials will be described. The future outlook of high-performance hemostatic materials will be briefed by the end of this review.

2.2 Hemostatic mechanisms and current hemostatic methods

Hemostasis is a complicated process that converts an unstable platelet plug into stable fibrin and includes two steps, the primary hemostasis and the secondary hemostasis (the coagulation cascade) (3). In the primary hemostasis stage, vessels contract to diminish blood loss from the wound, and procoagulant proteins and factors are secreted. Meanwhile, activated platelets form an initial platelet plug in the injured vascular wall. Other platelets are also activated and aggregated in the blood to form a hemostatic plug to mainly avoid hemorrhage. The secondary hemostasis stage (coagulation cascade) is the process of forming fibrin clotting at the site of the initial hemostatic plug, including the intrinsic pathway, extrinsic pathway, and common pathway. In the intrinsic pathway, coagulation factor X is activated in the presence of Ca^{2+} and platelet-secreted

phospholipid membrane. In the extrinsic pathway, in the presence of Ca^{2+}, tissue factor can combine with activated coagulation factor VII to form a factor VII-tissue factor complex. In the common pathway, activated factor X can synthesize fibrin with the participation of Ca^{2+}, platelet-secreted phospholipid membrane, and activated factor XIII. The fibrin is used to bolster the platelet plug that is formed in the primary hemostasis stage (3,5).

Various hemostatic methods have been used to stop bleeding in different situations. For example, Ferreira1et al. (36) used nylon cable ties to prevent hemorrhage for castration of male cattle and found that the nylon cable ties are an effective and economic hemostatic material. Itoi et al. (37) used an endoscopic hemoclip to treat uncontrolled sphincterotomy bleeding. Cho et al. (38) used sutures for uterine hemostasis in cesarean delivery to prevent uncontrolled postpartum bleeding to avoid hysterectomy. Maeda et al. (39) illustrated that the stapler can completely stop bleeding for mesenteric vessels in the surgery for a prolapsed transverse colostomy compared with a hand-sewn technique. Other common hemostatic methods can be found in other review papers (40,41). However, surgical procedures such as sutures and staples may not be suitable for all types of wounds, especially wounds with significant tissue loss or necrosis, uneven edges, or infections (42). In such situations, hemostatic materials or wound dressings are more effective in controlling hemorrhage and assisting wound healing.

2.3 Conventional hemostatic materials

When hemorrhage is severe and beyond the capacity of the intrinsic hemostasis mechanism of the human body, hemostatic materials are needed to stop bleeding. The mechanism of hemostatic materials usually involves two pathways, namely, the active pathway and the passive pathway. The active pathway works to trigger the hemostasis process by specifically initiating the coagulation cascade, while the passive pathway achieves hemostasis via the specific surface properties of the hemostatic materials, such

as hemocompatibility and anti-infection. In the hemostatic process, metal ions, particularly Ca^{2+}, play an important role because Ca^{2+} participates in several essential steps in the coagulation cascade (5). Conventional hemostatic materials are introduced in this section. Table 2.1 shows the commercial hemostatic materials in the market. Figure 2.1 shows the chemical structure of conventional hemostatic materials.

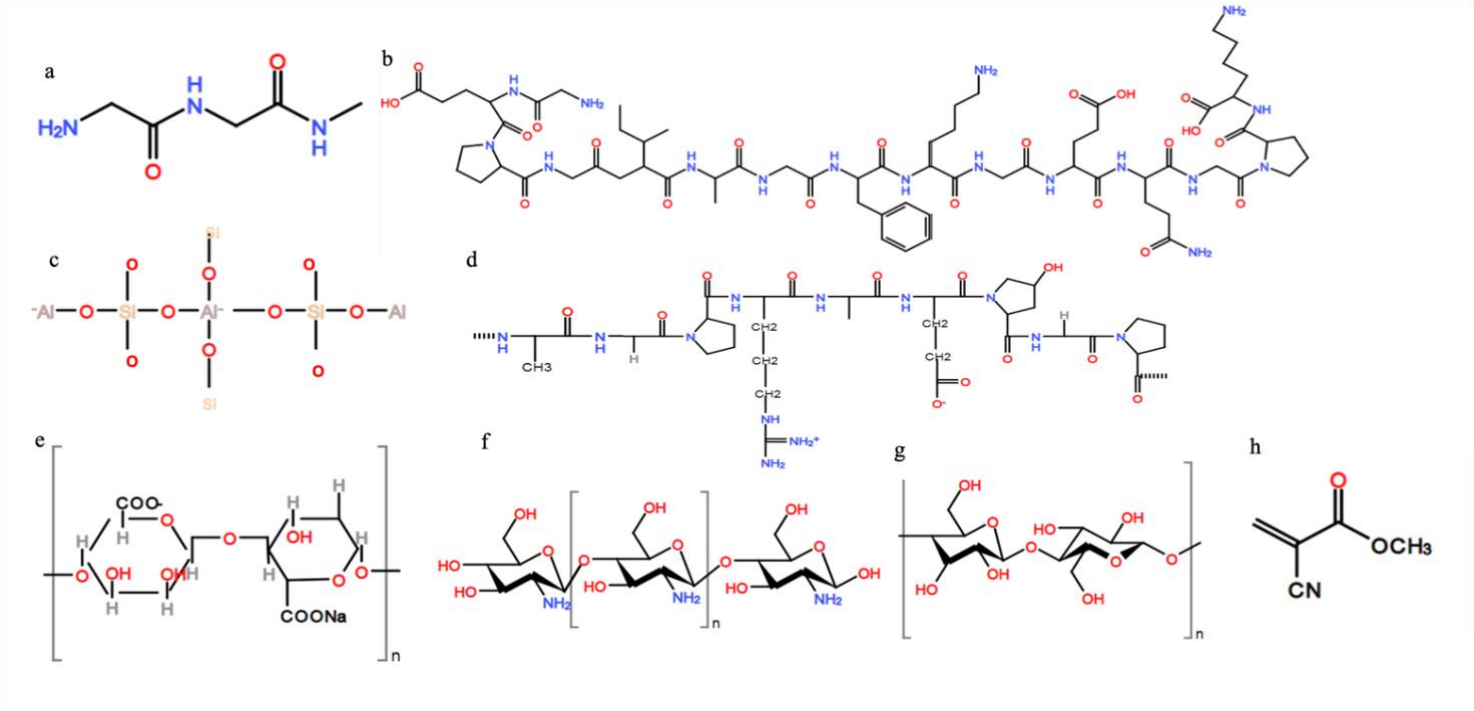

Figure 2.1. The chemical structures of fibrin (a), collagen(b), zeolite(c), gelatin(d), sodium alginate(e), chitosan(f), cellulose(g), and cyanoacrylate(h)

Table 2.1. Examples of commercial hemostatic materials

Materials	Brand name	Manufacturer	Pros (+) and Cons (-)
Fibrin sealant	Evicel®	OMRIX	+: easy to use; effectively hemostatic performance with heparin; -: may cause blood borne disease (43)
	Tisseel®	Baxter Healthcare	
	Crosseal®	Omrix	+: shorter hemostasis time; less postoperative complications; fewer blood loss (44) ; -: neurotoxicity (43)
	Quixil®	Omrix	
Oxidized cellulose	Surgicel Original®	Johnson & Johnson	+: antibacterial ability; easy to use and handle; -: lower pH cause inflammation and hemolysis (43,45)
	Surgicel Nu-Knit®		
	Surgicel Fibrillar®		
	Interceed®		

	Gelitacel®	Gelita Medical	
Gelatin	Surgifoam®	Johnson & Johnson	+: less complications; absorbed within 4-6 weeks; neutral pH; -: high swelling ability; foreign body reaction (43,45)
	Gelfoam®	Pfizer	
	Gelfilm®		
	Geli putty®	Gelita Medical	
	Gelita-spon®		
Collagen	Instat®	Johnson & Johnson	+: reducing blood loss; large surface area; stop bleeding within 2-5 min; -: less efficacy for patients with thrombocytopenia or coagulopathies; may cause neural pain or numbness (45)
	Helitene®	Integra	
	Helistat®		
	Avitene®	Davol	
	Avitene flour®		

	Avitene Ultrafoam®		
	Endo Avitene®		
	Avitene Ultrawrap®		
	Surgiflo®	Johnson & Johnson	
Cyanoacrylate adhesives	Dermabond®	Johnson & Johnson	+: rapidly stop bleeding; -: cytotoxicity
	Omnex®	Ethicon	
Polyethylene glycol	CoSeal®	Baxter Healthcare	+: degraded within 4 weeks; directly applied to the tissue surfaces; -: less swelling ability (up to 4 times) (45)
Zeolite	QuikClot®	Z-Medica	+: decreasing blood loss; -: exothermic reaction (24)

Chitosan	Celox	MedTrade Products Ltd	+: reduced compression time (1 minute) (46); -: cannot be used for long time (47).
	HemCon bandage	HemCon Medical Technologies Inc., Portland, OR	+: antibacterial property, useful on severe arterial hemorrhage (48); -: more expensive than Celox; longer treatment time (5 minutes) (48,49)

2.3.1 Blood-derived hemostatic materials--- Fibrin, thrombin and fibrinogen

Fibrin is one of the main components in hemostatic clot formation and can be derived from human plasma (3,35). In 1984, Rousou et al. (50) proved that fibrin glue is a simple, effective, and low-cost hemostatic agent for unsutured surgical bleeding. In 1990, Raccuia et al. (51) measured the hemostatic efficiency of oxidized cellulose, collagen, and fibrin glue in a rat kidney injury model and found that the fibrin glue has superior hemostatic ability compared to the other two materials. Delgado et al. (52) reported that, in a porcine grade V liver injury model, a fibrin patch effectively decreased the blood loss and increased the survival rate. Krishnan et al. (53) indicated that fibrin-based sheets can stop bleeding rapidly (about 3-5 seconds in a rabbit ear artery model and less than 3 minutes in a rat liver model) and be degraded within 15 days in rats. Because thrombin and fibrinogen are the major components of fibrin (54). Therefore, scientists also develop them as hemostatic materials. For example, Li et al.

prepared a thrombin/ graphene sponge that can block bleeding within 100 seconds in the rat tail injury, which is much faster than crosslinked graphene sponges (200 seconds) and gauze with thrombin (250 seconds); and even after 6 months of storage, it can block hemorrhage within 118 seconds (55). The immune response in pigs to the thrombin/fibrinogen wound dressings was investigated. The results demonstrated that, within 6 months, the immune response of swine was normal. Hence, thrombin and fibrinogen have been approved as safe in animals as hemostatic materials (56).

2.3.2 Collagen

Collagen is the most abundant protein in a mammal's body, constituting the extracellular matrix of most connective tissues (3,57). Collagen-based hemostatic materials can activate the intrinsic pathway of the secondary hemostatic process (45). The first commercial collagen-based hemostatic material was produced in the 1970s (45). In 1974, Morgenstern (58) reported the use of a microcrystalline collagen hemostat (Avitene®) to control splenic bleeding in a dog. The result showed that the material can stop bleeding within 5 minutes without any side effects and is degraded within 6 weeks. Cheng et al. (28) extracted collagen from jellyfish to prepare a collagen sponge for hemostasis. The results indicated that the non-cytotoxic collagen sponge can stop bleeding within 5 minutes, which is 10 minutes less than the medical gauze that was used as a control.

2.3.3 Zeolite and Kaolin

Zeolite and kaolin, which are microporous aluminosilicate minerals with large surface areas, have shown high hygroscopicity and excellent hemostatic performance. The hemostatic mechanism of zeolite is via the absorption of blood and the release of Ca^{2+} into the blood to spur the intrinsic path of the coagulation cascade (3,59). An example of a commercial zeolite-based hemostatic material is QuikClot®, which has been proved to have good hemostatic efficacy in different animal models, including a swine

groin injury model, a porcine grade V liver model, and a lethal rabbit groin injury model (3,60–63). Laurenti et al. (64) explored the hemostasis of zeolite-based procoagulant hemostatic agents, namely micro- and nanometric faujasite zeolites, and indicated that calcium ions exchanged nanometric faujasite zeolites (Nano-FAU/Ca) can enhance the hemostatic performance significantly.

Kaolin powder has also been used in hemostatic dressings. A sponge impregnated with kaolin and graphene was developed and shown to be non-cytotoxicity and biocompatible; it also blocked bleeding within 73 seconds in a rabbit injury model (59). As mentioned above, chitosan is a great hemostatic agent. Sun et al. (65) prepared a microsphere containing chitosan and kaolin and demonstrated that kaolin can improve the efficiency of hemostasis. The result shows that the time to hemostasis for composite microspheres (120 seconds and 99 seconds) was shorter than that of chitosan microspheres (183 seconds and 134 seconds) in the rat tail and liver models. Meanwhile, the chitosan/kaolin microspheres have lower blood loss than the chitosan microspheres in the rat model.

2.3.4 Gelatin

Gelatin is a water-soluble protein and is derived from collagen hydrolysis. Gelatin is highly absorbent and can absorb 5-10 times its dry weight in water (66,67). Gelatin and microbial transglutaminase were used to prepare in situ gel-forming adhesives that can form gels within 30 minutes under damp conditions and stop bleeding in 2.5 minutes in a rat liver and femoral artery injury model and 4 minutes in a porcine model (68). A novel chemical crosslinked gelatin sponge was prepared and used in a 12-year-old male patient who was suffering from bleeding of a pharyngeal angiofibroma. The result showed that the gelatin sponge can stop bleeding immediately and degrades after 2 weeks (29).

2.3.5 Alginate

Alginate, a natural polymer with negative ions, can be extracted from seaweed. Because of its biocompatibility and low cytotoxicity, it is commonly used for medicinal purposes, including in wound dressings. Alginate can form a gel or be crosslinked with divalent ions, such as Ca^{2+}. Alginate dressings are used to treat exuding wounds and may accelerate wound healing by creating a damp wound healing environment. It is also easy to remove the alginate dressing from a wound without causing additional injury (5,6,30). Thomas et al. also reported that alginate wound dressings can activate human macrophages to promote wound healing (30).

2.3.6 Chitosan

Chitosan is a natural cationic polysaccharide that is made from deacetylated chitin and is widely applied in different fields, such as the food industry and cosmetic industries (7,31). Because of its biocompatibility, biodegradability, non-cytotoxicity, and antibacterial properties, chitosan can be used in tissue engineering (5). Although the application of chitosan as a hemostatic material can be traced back to the early 1980s, the hemostatic mechanism of chitosan is still not well understood (7,69). Janvikul et al. (70) explored the *in vitro* hemostatic efficacy of chitin, chitosan, and their derivatives. Their results showed that chitosan derivatives, N, O-carboxymethyl chitosan (NOCC), can accelerate the hemostasis process *in vitro* and activate the platelets most effectively. Chitosan has also been used in combination with other chemicals and materials in developing hemostatic materials. For example, a team designed a chitosan-based wound dressing loaded with inorganic additives (aluminum chloride, iron (III) sulfate, and aluminum sulfate) and levofloxacin. In this system, inorganic additives can stop hemorrhage and levofloxacin can be released to provide the antibacterial ability for the material. The result showed that the chitosan-based materials with aluminum sulfate and levofloxacin had the highest blood absorption capacity and augmented the

hemostatic capacity in an *in vivo* mice injury model (71). Maevskaia et al. (72) prepared a chitosan-based wound dressing incorporated with chitin nanofibrils. Compared with two commercial hemostatic products (Surgicel and TachoComb), the chitosan sponges with 0.5% chitin nanofibrils demonstrated faster hemostatic ability in both rat femoral and vein artery injury models.

2.3.7 Cellulose-based materials

Cellulose is a linear biopolymer derived from delignified wood fibers (15). Recently, cellulose, especially nanocellulose and its derivatives have gained widespread attention in the biomedical field because of its biocompatibility, negative surface charges, high surface area, non-toxicity, and low cost (5,19). Oxidized cellulose is a popularly clinical hemostatic material that was first used in 1942. The first hemostatic product based on regenerated oxidized cellulose, Surgicel®, appeared in 1960 (45). However, compared to oxidized regenerated cellulose, oxidized non-regenerated cellulose showed better hemostatic efficacy due to its fiber structures, which are frayed and therefore provide a larger surface area (73).

2.3.8 Cyanoacrylate

Cyanoacrylate is a synthetic hemostatic polymer with good tissue-adhesive properties that has been used as a hemostatic material since 1942 (3,45). Cyanoacrylate has been commonly used as a clinical tissue adhesive due to its rapid hemostasis, reducing keloid formation, decreasing pain scores, and low cost (33,74). In recent years, the cyanoacrylate derivatives, 2-butyl cyanoacrylate, and 2-octyl cyanoacrylate have gained attention because they can improve the strength and flexibility of the cyanoacrylate-based materials. Jiang et al. (33) prepared a self-assembling 2-octyl cyanoacrylate film that can endure 147 mmHg of pressure and exhibits a rapid hemostatic ability (within 1 minute) in a pig liver model.

Although the materials mentioned above have good hemostatic performance, their shortcomings are also evident. For example, fibrin is extracted from the blood of pooled donors and may therefore pose a risk of viral infection. Nanofiltration can reduce the risk of viruses (such as human immunodeficiency virus (HIV), hepatitis B virus (HBV), hepatitis C virus (HCV), and hepatitis A virus (HAV)), but it may still be difficult to eliminate them (35,75). Swelling of collagen limits its usage in infected areas because it is likely to cause injuries in adjacent tissues and structures (76). Zeolite can absorb water and has exothermic reactions which can cause wound burn and inflammation (27,77). There is a report on a modified QuikClot that reduces the heat release. However, the temperature in the wound is still higher (40.3ºC) than the human body temperature (37ºC) (24). Cyanoacrylate-based hemostatic agents have been reported to be toxic and cause infection and tissue necrosis (35,74). Therefore, there has been an emergent need to develop high-performance hemostatic materials to satisfy the requirements of clinical applications.

2.4 High-performance hemostatic materials

The hemostatic process is complicated. Although the human body has its own hemostatic mechanism, it may not be sufficient for massive bleeding. Various methods, including cautery, suture, and lasers, have been developed to stop bleeding in surgery and on the battlefield; however, not all of them are efficient in all situations (75). Hemostatic agents have been used to improve the hemostatic efficiency and decrease the hemostasis time. Previous research illustrated that hemostatic agents can minimize blood loss and reduce the risk of surgical complications (78,79). High-performance hemostatic materials that promote hemostasis and wound healing will be discussed in this section.

2.4.1 Antibacterial hemostatic agents

Conventional hemostatic materials, such as medical gauze and fibrin, can transmit diseases and cause infections in hospitals and military camps or emergency situations, especially when a sterile environment is not available for traumatic patients (80,81). Antibiotics are used clinically to treat bacterial infections; however, overuse of antibiotics may lead to drug resistance problems (32). To minimize the usage of antibiotics, antibacterial agents have been used to endow hemostatic materials with antibacterial properties. Antibacterial agents include organic (i.e., quaternary ammonium salts) and inorganic agents (i.e., silver ions (81,82) and graphene oxide (83)) (32,84).

Chitosan has an intrinsic antibacterial efficacy which can be further enhanced by loading antibacterial agents, such as silver sulfadiazine (85). Li et al. (86) formulated chitosan/gelatin composite membranes loaded with ibuprofen. In the antibacterial experiments against *Staphylococcus aureus (S. aureus)* and *Escherichia coli (E. coli)*, the composite films displayed an excellent antimicrobial effect, especially against *Staphylococcus aureus*, and in a rabbit liver injury model, the ibuprofen-loaded chitosan/gelatin films displayed excellent hemostatic performance (86).

Metal ions, including silver (Ag^{+}), cooper (Cu^{2+}), and zinc ions (Zn^{2+}), also display antimicrobial properties because the positively charged metal ions can combine with the negatively charged bacterial membranes to interrupt normal bacterial functions and crush the structures, leading to cell death and achieving their antibacterial aims (87–93). Hu et al. (94) prepared a wound dressing containing nanoporous bioglass with silver that had a high surface area and water absorption rate. The hemostatic dressing exhibited a great antibacterial ratio (99% in 12 hours) against *E. coli*. A rabbit injury model showed that the hemostatic dressing has an outstanding hemostatic performance

and can reduce the hemorrhage time. Pourshahrestani et al. (95) proved that gallium ions have antibacterial abilities and can accelerate the hemostatic process.

Although inorganic antibacterial agents are more stable and have a longer shelf life than organic agents, inorganic nanoparticles can damage the human cardiovascular system (32,84). Therefore, organic antibacterial agents are also extensively used in studies. Polyhexamethylene biguanide (PHMB) is a polymeric antibacterial agent that has been used to disinfect swimming pools (32). PHMB was also integrated into electrospun nanofibers consisting of cellulose acetate (CA) and polyester urethane (PEU) to fabricate hemostatic nanofibrous films. *In vitro* antibacterial experiments showed that the films containing PHMB had a bacterial reduction rate of over 96% against *E. coli*. The diffusion speed of PHMB can be controlled at a sustained rate; hence, the films provide a long-term antibacterial property. An *in vivo* rat skin wound model indicated that the nanofibrous membranes have a good wound healing performance. Furthermore, poly(N, N-dimethylamino-2-ethyl methacrylate) (PDMAEMA) has been proved to have hemostatic and antimicrobial properties (96). In another study, poly(D-or L-)lactide with PDMAEMA was used to fabricate stereocomplex-based hemostatic materials (97). An *in vitro* blood adhesion experiment showed that mats containing PDMAEMA can absorb and adhere to human blood. However, PLA-b-PDMAEMA mats can adhere to a smaller number of *S. aureus* and *E. coli* cells.

Previous studies proved that oxidized regenerated cellulose (ORC) with metal ions showed great antimicrobial properties (98). An ORC gauze treated with chitosan and $NaOH/C_2H_5OH$ was reported (99). *In vivo* hemostatic experiments showed the minimum and maximum hemostasis times of the gauze were 145 seconds and 325 seconds in a rabbit liver injury model, respectively, and 155 seconds and 320 seconds in the rabbit ear artery injury model, respectively. The antibacterial experiments displayed that the antimicrobial efficiency against *S. aureus* and *E. coli* reached 99.9% for the ORC gauze.

2.4.2 Superhydrophobic or superhydrophilic hemostatic materials

Based on surface properties, materials can be categorized as hydrophobic or hydrophilic, which can be differentiated by their water contact angles. Water contact angles of hydrophobic surfaces are larger than 90º. When the angles are higher than 150º, the material is regarded as superhydrophobic. In contrast, a surface with a water contact angle smaller than 90º is hydrophilic, and if it is below 10º, it is superhydrophilic (100,101).

Superhydrophobic and superhydrophilic surfaces are common in nature and can be achieved by biomimetic designs. Superhydrophobic surfaces, for example, maybe inspired by duck feathers or lotus leaves, which are natural superhydrophobic materials (102,103). It has been found that the nanostructure of lotus leaves contributes to the high water contact angles on their surfaces (104). On the other hand, superhydrophilicity was initially discovered in human tears because they can spread and form a membrane to prevent any damage to the eyes; fish scales provided new inspiration for superhydrophilic surfaces (102,105). Generally superhydrophobic or superhydrophilic materials can be obtained by manipulating the roughness and microstructure of their surfaces (100,106), and have been applied in water collection, printing, self-cleaning, sensors, bio-adhesion, anti-fogging, liquid-liquid separation, liquid transport, anti-fouling, and water/oil separation (102,107,108).

The properties of superhydrophobicity and superhydrophilicity can also be used in hemostatic processes. Superhydrophobic surfaces may attract proteins and form a film on the wound to prevent further loss of blood (109,110). Hydrophilic materials, on the other hand, can extract water from the blood to speed up the blood coagulation process (110). Normally, the superhydrophobic material can be coated on the outside of the hydrophilic wound dressing to prevent blood loss. For instance, Cui et al. (111) designed a hyperbranched polymer (HBP) adhesive with a hydrophobic backbone and

a hydrophilic adhesive side chain. When the HBP comes in contact with liquid (such as blood or water), the hydrophobic backbone chains can self-aggregate rapidly and the hydrophilic groups can be exposed to water and adhere to different material surfaces under moist environments. The touch angles of HBP adhesives were all lesser than 90º (minimum 33.7º and maximum 51.4º). *In vivo* hemostatic experiments showed that the HBP adhesives have good hemostatic performances and can stop bleeding within 1.5 minutes in a rat femoral artery injury model and seal the wound within 4 seconds in a pig liver model.

Li et al. (112) synthesized a superhydrophobic hemostatic dressing by immobilizing carbon nanofibers (CNFs). The water contact angles of CNFs/ polytetrafluoroethylene Ti surface and CNFs/polydimethylsiloxane Ti surface are 162.1º and 154.9º, respectively. The superhydrophobic property of CNFs may alleviate blood loss and increase the bacteria reduction rate. In a rat injury model, compared to cotton gauze, the CNF gauze could control bleeding in 3 minutes and due to its superhydrophobic property, the CNF gauze is easy to peel without any wound tearing or hemorrhage.

Cotton gauze and paraffin were used to prepare a Janus fabric with superhydrophobic and superhydrophilic properties (110). Cotton gauze has an inherent hydrophilic property, with one side coated with paraffin to endow hydrophobic properties. Therefore, the two sides of the Janus fabric have different surface properties of superhydrophobicity and superhydrophilicity, respectively. The water contact angles for the two sides are 154º and 0º respectively. In rat injury models, compared with control groups, the Janus fabrics can reduce the blood loss (an average decrease of 64%) and prolong the survival time of rats (increased by 41%).

Dowling et al. (113) introduced a self-assembled amphiphilic biopolymer that was prepared by using a hydrophobically modified chitosan (hm-chitosan). Upon contact with the human blood, the polymer changed from a liquid state to a gel; the reversal of

the gelation was achieved by adding α-cyclodextrin because the hydrophobic polymers can be released from blood cells and inserted into cyclodextrin, and the internal structure of the gel was destroyed. In a rat femoral artery model, the material can reduce the hemostasis time by 90% compared with the control group. The hm-chitosan was attached to the wound in the pig femoral artery model and the wound was successfully clotted when the material was removed after 3 hours. Therefore, the potential for hm-chitosan to be used as a low-cost wound dressing with high hemostatic efficiency is encouraging.

2.4.3 Biomimetic hemostatic materials

Biomimetic materials research has a long history and is developing rapidly. Biomimetic materials are inspired by nature and examples include butterfly wings, bones, spider silks, and mussels (114,115). To design a biomimetic material, the structure and/or physical/chemical nature of the natural material are explored and imitated to duplicate the special function of the material (114). Recently, biomimetic materials have been applied in various fields, such as tissue engineering (116,117), myocardial tissue (118), actuator materials (119), drug delivery (120), and conductive film (121).

Most hemostatic adhesives may lose their efficiency underwater or in a wet environment because water molecules can impair the inter-surface physical adhesive forces and may change chemical bonds (122). Wound dressings with high hemostatic efficiency in the wet medium should be developed to meet such demands. Some marine organisms, such as mussels, have been found to have a natural ability to attach to different surfaces under the sea to gain necessary resources, avoid predators and improve genetic levels (123). Therefore, mussel-inspired hemostatic materials have been fabricated.

Mussel foot proteins contain 3,4-dihydroxyphenylalanine (DOPA), which can interact with substrates via strong covalent and noncovalent bonds; thus, the mussels have a

strong capacity to adhere to wet surfaces (124,125). Liu et al. (124) prepared a silica/ polydopamine nanoparticle (PDA/SiNP) via lyophilization, and PDA/SiNP can be degraded by 40% after 24 hours according to the *in vitro* degradation test. Compared with the commercial Celox®, the hemostasis time of PDA/SiNP decreased by 150 seconds in an *in vitro* experiment. In rat femoral artery and vein injuries models, the hemostasis time of PDA/SiNP was shorter than in the control groups. In a rat liver model, the PDA/SiNP stopped bleeding in 86 seconds, which was faster than in the Celox group (about 102 seconds). In addition, the material displayed a long-term antibacterial ability against *E. coli* even after 208 hours. Therefore, PDA/SiNP has the potential to serve as a rapid hemostatic dressing. Based on the adhesive mechanisms of mussels and the chitosan-based adhesives, chitosan-graft-polypeptides were polymerized by different initiators. The copolymers displayed high lap-shear adhesion strength, 195.97kPa on porcine skin, and high tensile adhesion strength, 642.7kPa on bone. In a rat skin injury and bone fracture models, the copolymer exhibited good hemostatic efficacy and shortened the healing period (1 day on skin wounds and 20 days on bone fracture) compared with the control group (14 days on skin wounds and 60 days on bone fracture) (126).

Gecko feet have thousands of setae (fibrils arrays) that can increase the adhesive force between gecko feet and various surfaces; therefore, gecko-like morphologies have been studied and used for developing hemostatic materials (127). Mahdavi et al. (128) modified the surface of poly(glycerol-co-sebacate acrylate) (PGSA) to imitate the morphology of gecko feet. Gecko-based PGSA has been coated with a layer of oxidized dextran (DXT) to promote tissue adhesion. The adhesive ability of this substance improved in an *in vitro* pig intestine tissue model and an *in vivo* mice abdomen subfascial tissue model relative to the unpatterned PGSA polymer. Therefore, the Gecko-based PGSA adhesives have a great potential to serve as a hemostatic material to seal wounds and replace sutures/staples.

2.4.4 Superelasticity

Superelasticity is used to describe an extraordinary capacity of materials in shape transformation (129). Superelastic materials can rapidly recover under a high compression (> 80%) and withstand a load of more than 50,000 times its weight; the elastic recovery of superelastic polymers is about 90% (130,131). Common superelastic materials include polymeric C_{60} (131), semicrystalline polymers (132), carbon nanofibers (133,134), and thermostable nanofibrous aerogels (135). Superelastic materials have been used in aerospace, soft robots, and supercapacitors (136).

On battlefields, the limbs and joints of soldiers are the body parts most likely to receive penetrating and deep traumatic injuries (17,137) that are difficult to be repaired or healed in a short time and may cause disability or death (138). To deal with such trauma, an injectable hemostatic material with superelastic properties may match the shapes of uncompressed wounds and promote wound healing. Zhao et al. (2) announced injectable antimicrobial conductive cryogels composed of carbon nanotube (CNT) and quaternized chitosan (QCSG). The cryogel can rapidly recover to its original shape upon contact with water (less than 1 second) and blood. The materials also have antimicrobial abilities, with 92%, 96%, and 95% inhibition rates for *S. aureus*, *E. coli*, and *Pseudomonas aeruginosa (P. aeruginosa)*, respectively. *In vitro* blood clotting tests demonstrated that incorporating carbon nanotube into QCSG can strengthen the blood clotting capacity and shorten the blood clotting index. *In vivo* hemostatic experiments in the mouse liver and tail amputation models and the rabbit liver volume injury model indicated that QCSG/CNT4 (cryogels with 4mg/mL CNT) has a better hemostatic ability compared with Tegaderm™ films, such as quick hemostasis, lower blood loss, and smaller wound surface.

Fan et al. (17) prepared an injectable antimicrobial aerogel composed of oxidized cellulose carboxyl nanofibers and chitosan. Because of the interlaced structure between

nanofibers and nanosheets, the aerogel has high compressive strength (maximum 75.4kPa) and a fast shape recovery capacity (recovery to its original shape within 30 seconds). An *in vitro* hemostatic performance test indicated the aerogel has excellent absorption and adhesion abilities for red blood cells and platelets.

Hydrogels can also be designed as a superelastic hemostatic material because of their high hemostatic performance and biocompatibility. A conductive self-healing hydrogel wound dressing was fabricated from chitosan-g-polyaniline (QCSP) and poly(ethylene glycol)-co-poly(glycerol sebacate) (PEGS-FA) (139). The hydrogels have a self-healing ability, and their gelation time is 86 seconds. QCSP3/PEGS-FA1.5 has comparable ionic conductivity to that of human skin and muscles. Hydrogel QCSP3/PEGS-FA1.5 can inhibit over 99% of *E. coli* and 100% of *S. aureus* within 2 hours. In a mouse liver model, relative to the control group (about 2025 mg of blood loss), the hydrogel effectively stopped bleeding and reduced blood loss (only 215mg). In a mouse skin lesion model, the hydrogel could repair the wound in 10 days, while the Tegaderm^{TM} film did not heal the wound even in 15 days. Therefore, the hydrogels can serve as an effective hemostatic dressing.

Shape memory polymers (SMPs) have a shape recovery ability and can also serve as effective hemostatic materials for uncompressed wounds. Jang et al. (140) designed a biodegradable SMP foam that is synthesized from triethanolamine (TEA) and hexamethylene diisocyanate (HDI). The SMP foams have a lower density (0.076g cm^3), high gel fraction (over 90%), and a thermo-responsive shape recovery ability (recover to its original shape in 37ºC water for 8 minutes). The degradation experiment showed that the ester-containing foams can be completely degraded at day 90. Thus, the biodegradable capacity can help patients to avoid secondary surgery. Due to their porous structure, the mechanical strength of SMP foams was increased. Biodegradable SMP foams with clinically relevant thermal properties and rapid expansion performance have exhibited promising potential as hemostatic materials.

2.4.5 High porosity (aerogel)

Aerogels have attracted numerous attention because of their outstanding properties, such as ultralow density, wide surface area, high mechanical properties, high porosity, and so forth (14,16,141). Various materials have been used to prepare the aerogels, including silica (142), polyurethane (143), cellulose (144), and carbon (145). The most common method for fabricating aerogels is direct freezing. In the freezing process, the microstructure of aerogels can be tuned by controlling external conditions like temperature. External forces can influence the microstructural growth of aerogels. Transverse magnetic fields, electrical fields, and ultrasonic waves can cause different microstructures, namely, lamellar walls and mineral bridges, lamellar walls with long alignment, and alternating complex rings, respectively (146). Studies have demonstrated that aerogels have a high water absorption rate, fast shape recovery ability, and high compressive mechanical strength (17). Therefore, aerogels have been broadly used in varied fields, such as energy applications (147), drug delivery systems (148), skeletal muscle regeneration (149), and 3D printing (150).

Due to their high porosity and broad surface areas, aerogels can be used in the hemostatic process and may have a similar hemostatic mechanism to ORC, that is, absorbing water when in contact with the blood, forming a barrier at the bleeding site, and serving as a matrix for clot formation (18). Mellado et al. (151) reported a composite aerogel, consisting of graphene oxide (GO) and poly(vinyl alcohol) (PVA), as a delivery system. The aerogel incorporates an extract from *Pai´s* grape seed (SD) and *Pai's* skin (SK) as the extract has abundant proanthocyanidins that have the potential to promote wound healing. The absorption capacity is about 60 times the dry weight for GO-PVA aerogels, 70 times for GO-PVA-SD aerogels, and 73 times for GO-PVA-SK aerogels. *In vitro* coagulant experiments showed that the GO-based aerogels started to coagulate from the beginning and that the aerogels with incorporated proanthocyanidins can completely coagulate the blood after 240 seconds. In the control

group, coagulation of the blood began at 60 seconds and the blood was not completely coagulated after 240 seconds. The aerogels released 20% of their extract in 3 hours to promote wound healing, suggesting that the GO-based aerogels are a promising hemostatic material and delivery system.

Another composite aerogel was prepared from dialdehyde nanocellulose fibers and collagen (152). The study reported that the aerogels have desirable properties, such as a density of 0.02g/cm^3, a water absorption rate of 4000%, and good biocompatibility. The average activity of L929 cells was 96.79% after culturing for five days, demonstrating that the aerogel can promote cell proliferation. The aerogels have higher porosity (95%) than the ideal porosity of hemostatic materials (at least 90%). Therefore, the nanocellulose fiber-based composite aerogels have a promising potential to act as hemostatic sponge materials and tissue engineering scaffolds.

2.4.6 Polypeptides

Polypeptides are compounds composed of 10 or more amino acids and peptide bonds. Polypeptides have various applications, including medications, such as Acthrel®, Xerecept® (153), and antimicrobial (154).

Polypeptides can also be used in hemostatic materials. Although different hemostatic materials, such as chitosan, collagen, cellulose nanofibers, and fibrin, have been developed and commercial hemostatic products based on these materials can be found on the market (Table 2.1), their limitations also remained for clinical and emergency situations. Therefore, materials containing self-assembled peptides become an effective and alternative method. Self-assembled peptides are a kind of peptides that can organize each component spontaneously into a structure with certain sequences without external intervention (155). Studies have demonstrated that self-assembling peptides can form nanofibers in solution to promote the coagulation process (156).

16-residue peptide RADARADARADARADA (RADA 16-1) is a self-assembled peptide that can be used for hemostasis (157). A layer-by-layer process was used to prepare a peptides-coated wound dressing. *In vitro* blood clotting experiments showed that RADA 16-1 and hemostatic materials (like gauze and gelatin sponge) coated with RADA 16-1 both can form nanofiber plugs in rabbit red blood cells. The porcine skin injury model indicated that peptide-coated gauze can stop bleeding within 2 minutes. Hemostatic bandages coated with RADA16-1 still release the active nanofibers formed by peptides for hemostasis upon being exposed to harsh conditions (-80 to 60ºC). Furthermore, Song et al. (158) evaluated the hemostatic ability of RADA16-1 in a rat kidney model. The results showed that, compared with Gelfoam (a commercial gelatin sponge), the blood loss in the RADA16-1 group was reduced and fewer histological responses occurred.

Kumar et al. (159) prepared self-assembled collagen mimetic peptides (KOD) to mimic the properties and structure of natural collagen for hemostasis. The platelet adhesion experiment indicated that KOD adheres to more platelets and forms larger clots compared with control groups. The soluble P-selectin secretion experiments demonstrated that KOD can activate platelets. These properties are similar to those of natural collagen. Therefore, the self-assembled KOD has the potential to serve as wound dressings.

2.5 Conclusion

Uncontrolled bleeding is a major cause of traumatic death. Hence, highly effective hemostats play an essential role in controlling hemorrhage and reducing the death rate in the prehospital stage. Commercial wound dressings, based on the traditional hemostatic materials, including fibrin, collagen, and zeolite, are available on the market. However, there are several disadvantages of these products, such as the risk of infection,

low tissue adhesion, and secondary damage. High-performance hemostatic materials are, therefore, in demand to overcome these problems.

In this thesis, we designed high-performance cellulose-based aerogels and hydrogels that can potentially be used as hemostatic materials. The developed aerogels have the antibacterial ability, lightweight, high-water absorption rate, excellent compressibility, and rapid water-induced shape memory capacity. The self-healing cellulose-based hydrogels with hydrophilicity, high water absorption rate, ultra-softness, tissue-adhesive ability, and injectability, were prepared by carboxymethylated cellulose (CMC), polyvinyl alcohol (PVA), and borax. The excellent properties of cellulose-based aerogels and hydrogels make them promising as hemostatic materials. Meanwhile, *in vitro* and *in vivo* tests on the developed aerogels demonstrated their outstanding hemostatic efficiency. This research is expected to provide new ideas for the use of cellulose-based materials as high-performance hemostatic materials.

Chapter 3 Nanocellulose fibers aerogels as hemostatic materials

3.1 Introduction

Hemorrhage is a critical cause of prehospital trauma death for military and civilian treatment. Around the world, over 30% of trauma death is caused by uncontrolled hemorrhage (2). Hemostasis has therefore become a major step for emergency treatment. As a result, it is critical to develop hemostatic materials that are cost-effective, efficient biocompatible, ultralight, stable, and easy for application (2,6,7). Recently, a number of materials have been widely used for hemostasis, such as collagen (Col), gelatin (GE), alginate (AE), chitosan (CS), oxidized cellulose, cyanoacrylic acid tissue adhesive, and porous zeolite (7,29–33). However, these hemostatic materials have both advantages and drawbacks. For example, collagen and gelatin are the main components of extracellular matrix and connective tissues, respectively. They can therefore facilitate the formation of fibrin. Alginate can also accelerate the formation of fibrin (5). However, collagen and gelatin have poor tissue adhesion and need a large number of platelets and clotting factors to achieve hemostatic efficiency. In addition, alginate dressings have poor chemical stability, and their structure degradation is unpredictable (5,6,17,23). Porous zeolite can adsorb water from blood, aggregate proteins, and cellular matrix to promote the formation of platelet plugs. However, porous zeolite undergoes exothermic reaction upon absorbing water from wounds and may cause wound burn and inflammation (17,24). New hemostatic techniques or materials have been developed, such as the XStat device, which is a syringe-like device that injects cellulose-based sponges coated with chitosan into penetrated wounds to absorb blood quickly (25). However, the preparation and synthesis of the new hemostatic materials are intricate and costly (2,17). Therefore, a hemostatic material that is cost effective, easy to prepare and use, and high in blood absorption capacity is highly demanded.

In this study, a lightweight, high porosity, injectable, water-induced shape memory and antibacterial carboxymethylated nanocellulose fibers (NCFs)-alginate aerogel was designed and prepared to promote wound healing. The NCFs-alginate aerogels with lightweight and high porosity have high water absorption rate. Besides, the NCFs-alginate aerogels with injectability and water-induced shape memory behaviour can be used in penetrated or uncompressed wound and fit the shapes of different wounds to accelerate penetrated wound healing. Additionally, NCFs-alginate aerogels with antibacterial property can reduce infection rate and increase patients' survival rate. Figure 3.1 illustrates the scheme of preparation of NCFs-alginate aerogel. Briefly, the carboxymethylated nanocellulose fibers were prepared firstly by high-speed mixing (7500rpm) and centrifugation twice. The first centrifugation (1400rpm) was to remove microfibers and the second one (4000rpm) was to extract nanofibers. Then, alginate, NCFs, and zinc chloride were mixed to prepare aerogels via the freeze-drying method. Among them, zinc chloride served as an antibacterial agent to prevent infection. Alginate provided a humid environment in the wound site to accelerate wound healing. Meanwhile, alginate as a natural polysaccharide was used to lock NCFs network and improve the water stability of NCFs network (141). The developed aerogel combined double networks, including an NCFs network and an alginate-zinc ions network. Herein, nanocellulose fibers as the substrate endow the aerogel with good mechanical properties and large surface area (160), and alginate and zinc ions can be used to maintain the wet stable of aerogels and reduce infection rate (141,161). The aerogel has water-induced shape memory ability and can recover to its original shape within 4s in water. As a result, the aerogel can be injected into uncompressed wounds to accelerate penetrated wound healing. The hemostatic materials can also reduce the infection rate of trauma patients due to the incorporation of an antibacterial agent, zinc chloride. *In vitro* and *in vivo* hemostatic assay also demonstrated that the NCFs-based aerogel has a good hemostatic ability (as Appendix1 showed). Table 3.1 compares the properties of NCFs-

based aerogels in previous works and this work, including density, water absorption, antibacterial ability, and shape recovery ability.

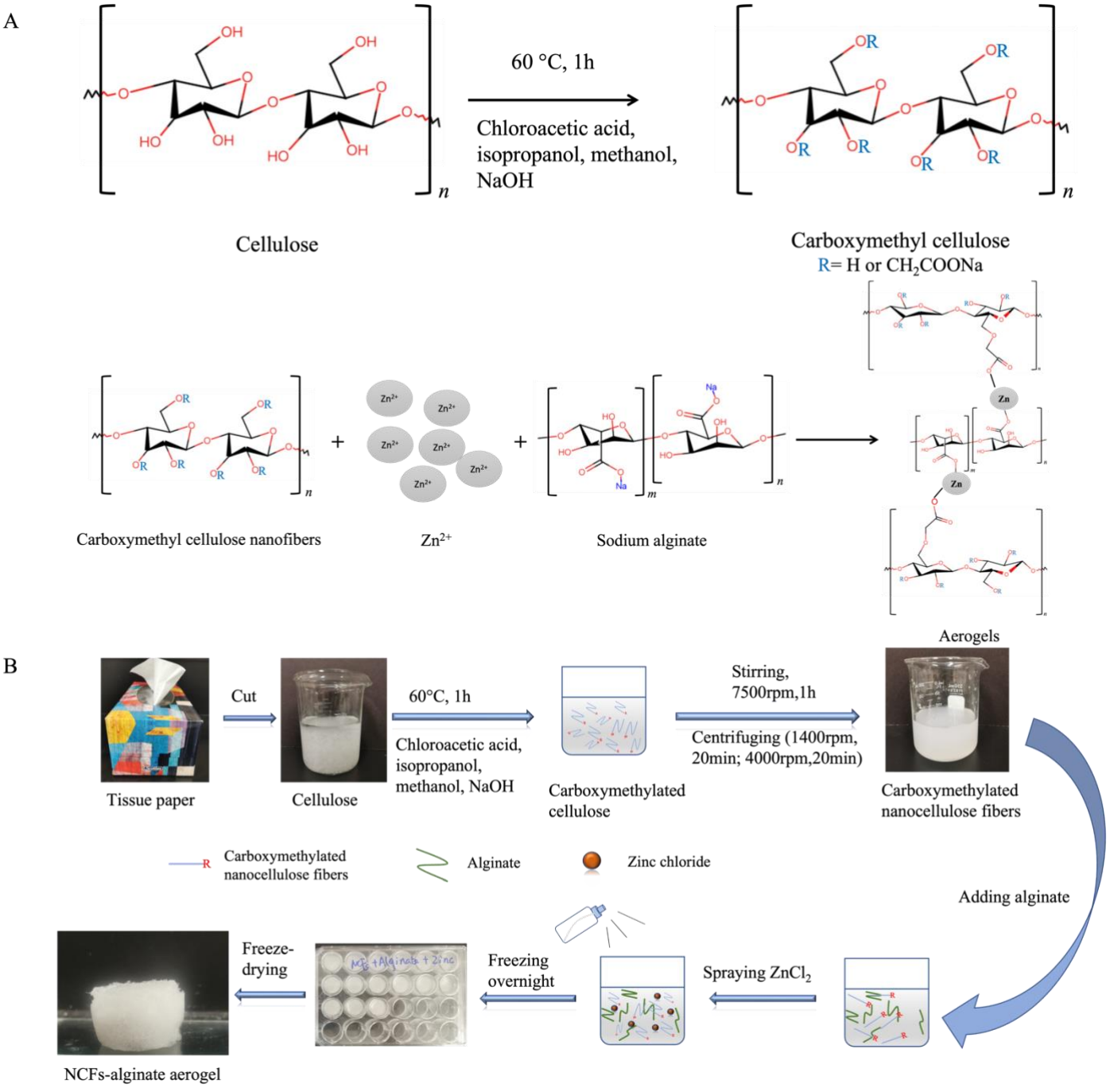

Figure 3.1. Scheme of preparation of NCFs-alginate aerogel. (A) The formula of synthetic carboxymethylated nanocellulose fibers and NCFs-alginate aerogel. (B)The process of preparing NCFs-alginate aerogels.

Table 3.1. Comparisons of cellulose fibers-based aerogels

Components	Density	Absorption rate	Antibacterial rate	Shape recovery time	Ref.
Cellulose nanofibers/alginate/$CaCl_2$	23-38mg/cm^3	-	-	-	(15)
Cellulose nanofibers/ chitosan	14.3-26.5mg/cm^3	39.1-53.7g/g	Yes	30s	(17)
Chitosan-based aerogel	80mg/cm^3	-	100% (*E. coli*)	-	(162)
Chitosan/mesoporous silica	120mg/cm^3	<3g/g(normal saline)	100% (*S. aureus* and *E. coli*)	-	(163)
Oxidized bacterial cellulose/ montmorillonite	-	29.32-33.3g/g	Yes (*S. aureus* and *E. coli*)	-	(164)
Cellulose nanocrystal	5.6mg/ cm^3	160g/g	-	85% (95%strain)	(165)

Carboxymethylated cellulose nanofibers/alginate/zinc chloride ($ZnCl_2$)	10.66-12.7mg/cm^3	37.8g/g (water)	89% (*E. coli*)	4s(wet condition)	This work

3.2 Materials and Methods

3.2.1 Materials

Tissue papers (Scotties Premium); alginic acid sodium salt was bought from Alfa Aesar. Zinc chloride was bought from Sangon Biotech, China. Hydrochloric acid (HCl) was bought from LabChem. Chloroacetic acid and isopropanol were bought from Sigma-Aldrich, NaOH and methanol were bought from VWR Chemicals, and acetic acid was bought from Fisher Scientific Canada. All materials were used in the received state.

3.2.2 Preparation of carboxymethylated nanocellulose fibers (NCFs)

The method of preparing carboxymethylated cellulose fibers was followed by previous research (166). Briefly, 2g of tissue paper were cut up and immersed in deionized water. Then, it was impregnated for 30min with a solution of 3g chloroacetic acid in 150mL isopropanol. These pieces were then added to a solution by mixing 0.972g NaOH, 30mL methanol, and 120mL isopropanol. The solution was heated to 60ºC in a beaker for 1h for reaction. Hereon, the carboxymethylation step was finished. After the carboxymethylation step, the pieces were washed in the three steps to remove residual solvent: firstly, washed with 50mL deionized water, then with 0.1M acetic acid, and finally with 50mL deionized water. Then, the pieces were then immersed in 0.01M NaOH solution for 30min. Finally, the fibers were washed in 100mL of deionized water.

The pieces with carboxymethylated group were homogenized by a shearing mixer (7500rpm) for 1h. Then, the obtained suspensions were centrifuged at 1400rpm for 20min to remove microfibers, and the supernatant was taken out for further centrifugation at 4000rpm for 20min. The precipitates were then carboxymethylated nanocellulose fibers. Finally, the obtained nanofibers were freeze-dried in a lyophilizer and prepared for the next steps.

3.2.3 Preparation of aerogels

Firstly, 100mM zinc chloride solution was prepared with 1.363g zinc chloride (anhydrous) and 100mL deionized water. After zinc chloride dissolved, 0.5mL 0.1M HCl was added to the above solution to inhibit the hydrolysis of zinc chloride. Then, the carboxymethylated nanocellulose fibers (NCFs) and alginate salt with different weight ratios, namely, 0:5, 1:4, 1:1, and 4:1, were mixed and cast into a 24-well plate. The concentrations of NCFs were 1mg/mL, 2mg/mL, 4mg/mL, and 6mg/mL. Then, 100mM zinc chloride (0.3mL) was added by a sprayer which can result in a more uniform incorporation of zinc ions into the solution. The mixed solution was frozen at -20 ºC and kept at this temperature overnight. After that, the 24-well plate with the solution was put into the lyophilizer overnight. Finally, the NCFs-based aerogels were obtained after moving the samples from the mold (24-well plate).

3.2.4 Materials Characterization

3.2.4.1 Density of aerogels

The aerogels were prepared by different concentrations of NCFs in the group of 1mg/mL, 2mg/mL, 4mg/mL, and 6mg/mL. The sample was cut to a diameter of 13mm and a thickness of 8mm. The diameter (d) and weight (m) were measured by a ruler and a balance. The density(ρ) of aerogel was calculated as:

$$\rho = \frac{m}{\pi h r^2} \quad (1)$$

where *m* is the mass of aerogel, *h* is the length of aerogel, and *r* is the radius of aerogel which is half of the diameter.

3.2.4.2 Fourier-transform Infrared (FTIR) Spectra Characterization

FTIR characterization of carboxymethylated cellulose nanofibers (NCFs) and NCFs-alginate aerogel was studied by an FTIR spectrometer (Bruker IFS 66v/s, German) within a wavenumber of 4500-500 cm^{-1}. The samples in FTIR test contained carboxymethylated nanocellulose fibers and NCFs-alginate aerogels.

3.2.4.3 Scanning Electron Microscope (SEM) Characterization

SEM characterization was carried out on a model of Quanta FEG 650 scanning electron microscope with an operation voltage of 5kV. The NCFs-based aerogel was lyophilized, sprayed with a layer of gold, and put on a metal holder to examine under the microscope.

3.2.5 Rheology test

The rheology of the aerogels was measured by the Discovery Hybrid Rheometer HR-1 (TA Instruments). The samples were cut to a diameter of 8 mm. Then, the freeze-dried aerogels immersed in 3mL water for 10min. The aerogels with different rates of NCFs and alginate (0:5, 1:1, 1:4, and 4:1) were prepared to optimize the parameters.

3.2.6 Compression test

Mechanical properties of aerogels were evaluated on the MTS Criterion Model 43 testing machine with a 1000N load cell. Compression tests were conducted on samples with different rates between NCFs and alginate (0:5, 1:1, 1:4, and 4:1). The concentration of zinc ions is consistent in all groups. The size of the samples was 13mm

in diameter and 8mm in thickness. All experiments were carried out at a steady speed of 10 mm/min. Five strains (10%, 20%, 30%, 40%, and 50%) were used to evaluate the compressive property of aerogels with different rates between NCFs and alginate. The slope of 10% strain was used to calculate Young's modulus of different aerogels. The energy loss coefficient was calculated by the hysteresis loop region enclosed by the loading-unloading curves:

$$Energy\ loss\ coefficient = \frac{\Delta U}{U} \times 100\%$$

Where $U=\int \sigma\, d\varepsilon$, and $\Delta U= \int \sigma_{loading}\, d\varepsilon - \int \sigma_{unloading}\, d\varepsilon$.

3.2.7 Injectable and Water-induced shape memory behaviour test

The samples with different ratios of NCFs and alginate were cut into a cylinder (8mm×13mm) and immersed in water for 30min to reach the saturated state. The aerogels will be put into syringes with a diameter of 2mm to explore the injectability of aerogels. Then, after the samples were injected into the water, the behaviour of the samples was observed whether they could return to their original shape.

3.2.8 Water-absorption test

The water absorption ability of aerogels will be measured by followed method (167). Firstly, the aerogel (the thickness of 8mm) was immersed in 10mL water and the weight of the aerogels was measured at specific intervals. The method of measurement is after removing the moisture from the aerogel surface, the obtained aerogel was weighted. The water absorption rate will be calculated as:

$$water\ absorption\ rate = \frac{m_s - m_0}{m_0}$$

Where m_s is the weight of saturated aerogel and m_0 is the weight of dry aerogel. The water absorption test was performed three times and the average value was obtained.

3.3 Results and Discussion

3.3.1 Density of aerogels

According to equation 1, the densities of aerogels with different concentrations of carboxymethylated cellulose were calculated. According to Figure 3.2A, the aerogel with 1mg/mL NCFs cannot form a regular shape while the other three samples can form a regular aerogel shape. The densities of aerogels with 2mg/mL, 4mg/mL, and 6mg/mL NCFs were 10.66mg/cm^3, 12.4mg/cm^3, and 12.7mg/cm^3, respectively (Figure 3.2B). Among them, aerogel with 2mg/mL NCFs has the lowest density which is lower than other light-weight cellulose fiber-based aerogels, as Table 3.1 shows.

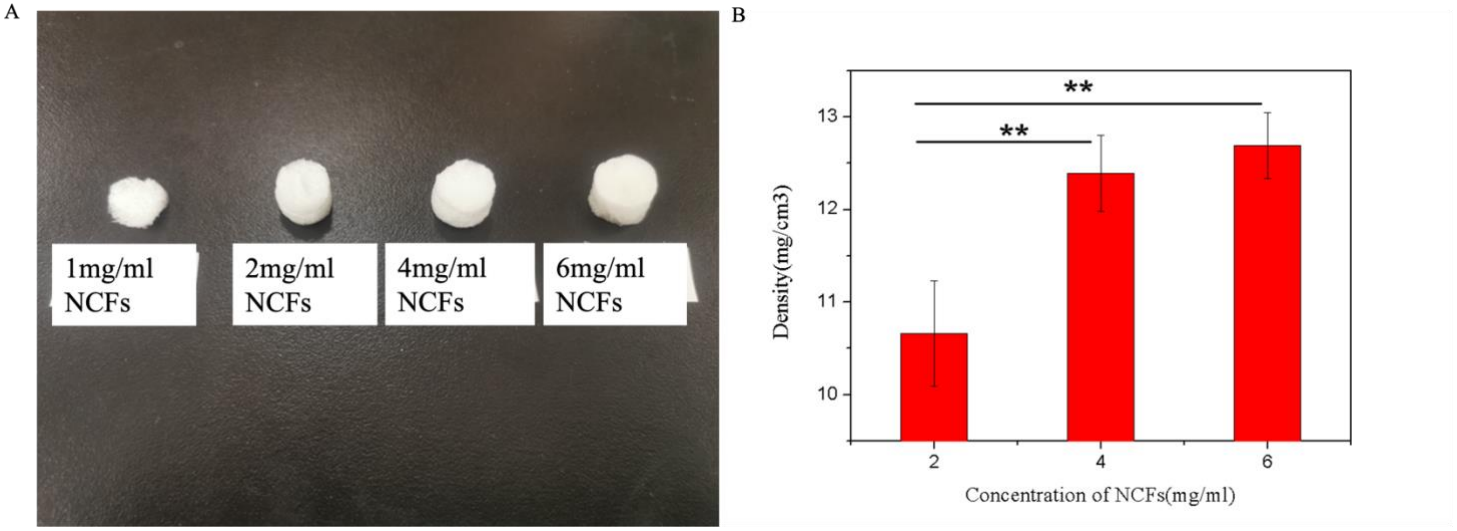

*Figure 3.2. Aerogels with different concentrations of NCFs. (A)Images of aerogels with different concentrations of carboxymethylated nanocellulose fibers. (B) Density of aerogels (n=3; **, p<0.05).*

3.3.2 Fourier-transform Infrared (FTIR) Spectra Characterization

As shown in Figure 3.3, the FTIR analysis of carboxymethylated nanocellulose fibers and NCFs-alginate aerogels was conducted. The dominant characteristic band at

3335cm^{-1} and 1031cm^{-1} are assigned to O-H and C-O-O stretching vibrations, respectively (160). The carboxymethyl group can be observed at the peak of 1631cm^{-1} and 1610 cm^{-1} (COO- stretching) (168). This indicated that the cellulose nanofibers were grafted with carboxymethyl group successfully. The absorption band at 2902cm^{-1} shows C-H stretching frequency (169). The 1425cm^{-1} and 1314cm^{-1} represent CH_2 scissoring and the C-H bending band, respectively (160,169,170).

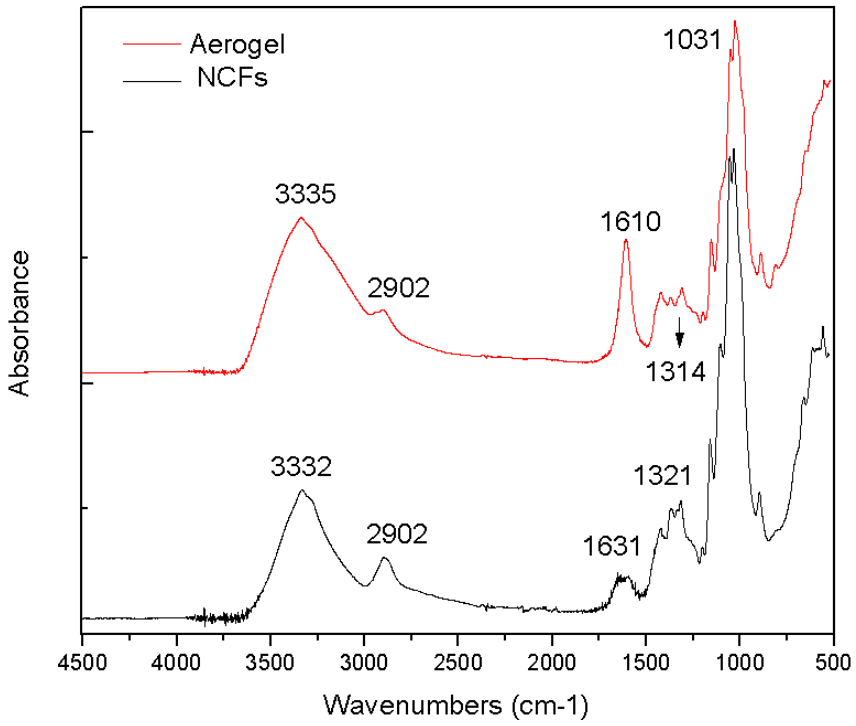

Figure 3.3. FTIR spectra of carboxymethylated nanocellulose fibers and NCFs-alginate aerogel

3.3.3 Scanning Electron Microscope (SEM) Characterization

The microstructure of aerogels was studied by scanning electron microscope (SEM). As Figure 3.4 illustration, the diameter obtained by carboxymethylated nanocellulose fibers is 83.8±20.85nm. The aerogels have a high interconnected porous 3D internal structure (Figure 3.5). A similar structure was also observed in previous cellulose-based aerogels (17). Compared with other groups, the surface of pristine alginate aerogel (0:5) was smoother since nanocellulose fibers were not contained in it (Figure 3.5A1-3).

NCFs-alginate aerogels have a more ordered internal structure (Figure 3.5B1, C1, and D1) since the crosslinking of alginate and Zn^{2+} can support the aerogel's network (171). The presence of fibers can be observed on the surface of NCFs-alginate aerogels (Figure 3.5B2, C2, and D2). Meanwhile, as the ratios between NCFs and alginate changed, the nanocellulose fibers content increased, and, from Figure 3.5B2 to D2, more fibers can be observed on the surface of the aerogels. Besides, the surface of NCFs-alginate aerogel (4:1) has larger aggregates (Figure 3.5D3) than the other two rates (1:1 and 1:4) (Figure 3.5C3 and D3). This is because aerogel (4:1) contain more nanofibers which can form fibrous aggregates. Besides, the macroporous structure of aerogels was constructed by ice crystals during the freeze-drying process (172).

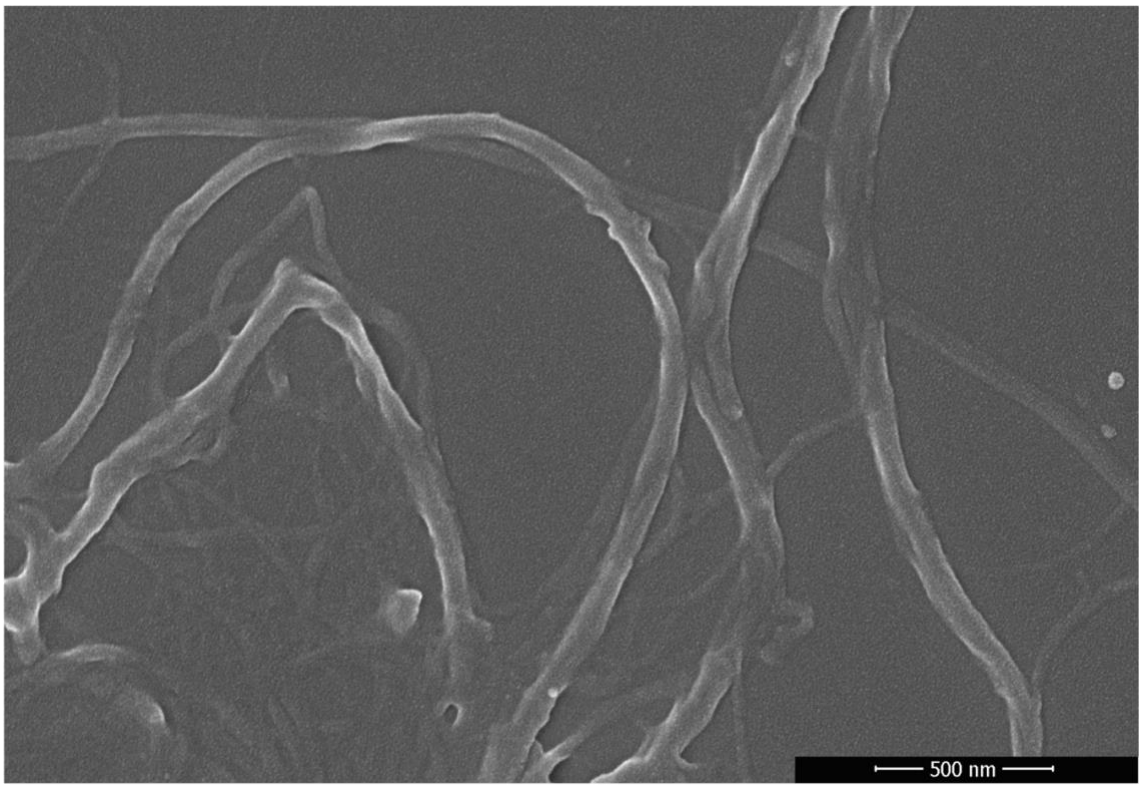

Figure 3.4. SEM image of carboxymethylated cellulose nanofibers

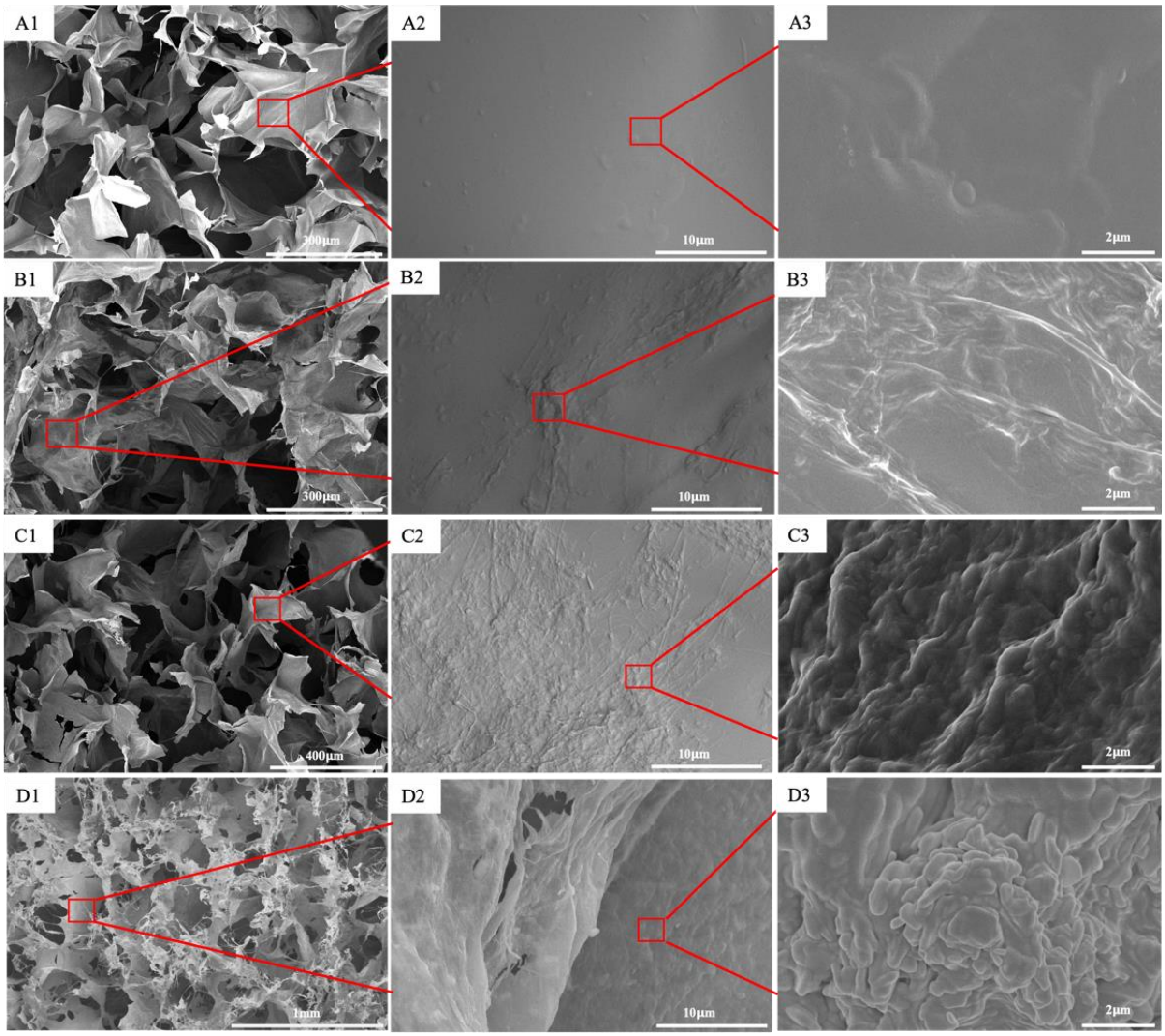

Figure 3.5. Scanning electron microscope (SEM)images of cross-section of NCFs-based aerogels with different ratios between NCFs and alginate: 0:5(A1-3), 1:1 (B1-3), 1:4 (C1-3), and 4:1 (D1-3).

3.3.4 Rheology assay

The mechanical properties of NCFs-based aerogels can be studied by rheology tests. As Figure 3.6 shows, the storage modulus (G') and loss modulus (G'') were tested at the constant strain (0.1%). In the whole angular frequency spectrum (0.1-100rad/s), the G' was higher than G'' which indicated that NCFs-based aerogels with different ratios of NCFs and alginate maintained a gel-like behaviour in the full angular frequency (Figure 3.6). As the fibers' content increased, the storage modulus (G') and loss modulus (G'') increased progressively, demonstrating the presence of nanocellulose

fibers enhanced the mechanical properties of aerogels. The modulus of NCFs-alginate (1:1) aerogel and NCFs-alginate (4:1) aerogel are very similar which may because the two groups have high NCFs content, and NCFs play a dominant role in the aerogel system, while the latter is slightly higher than the former. Therefore, among the four groups, the NCFs-alginate (4:1) aerogel has a higher modulus which illustrates the aerogel has greater elastic behavior and mechanical performance in wet conditions (173). Besides, the result indicated that the mechanical performance of alginate-based aerogel has been improved by the incorporation of NCFs which may be owing to the reinforcement effect of NCFs. A similar result was reported in previous research (174–176).

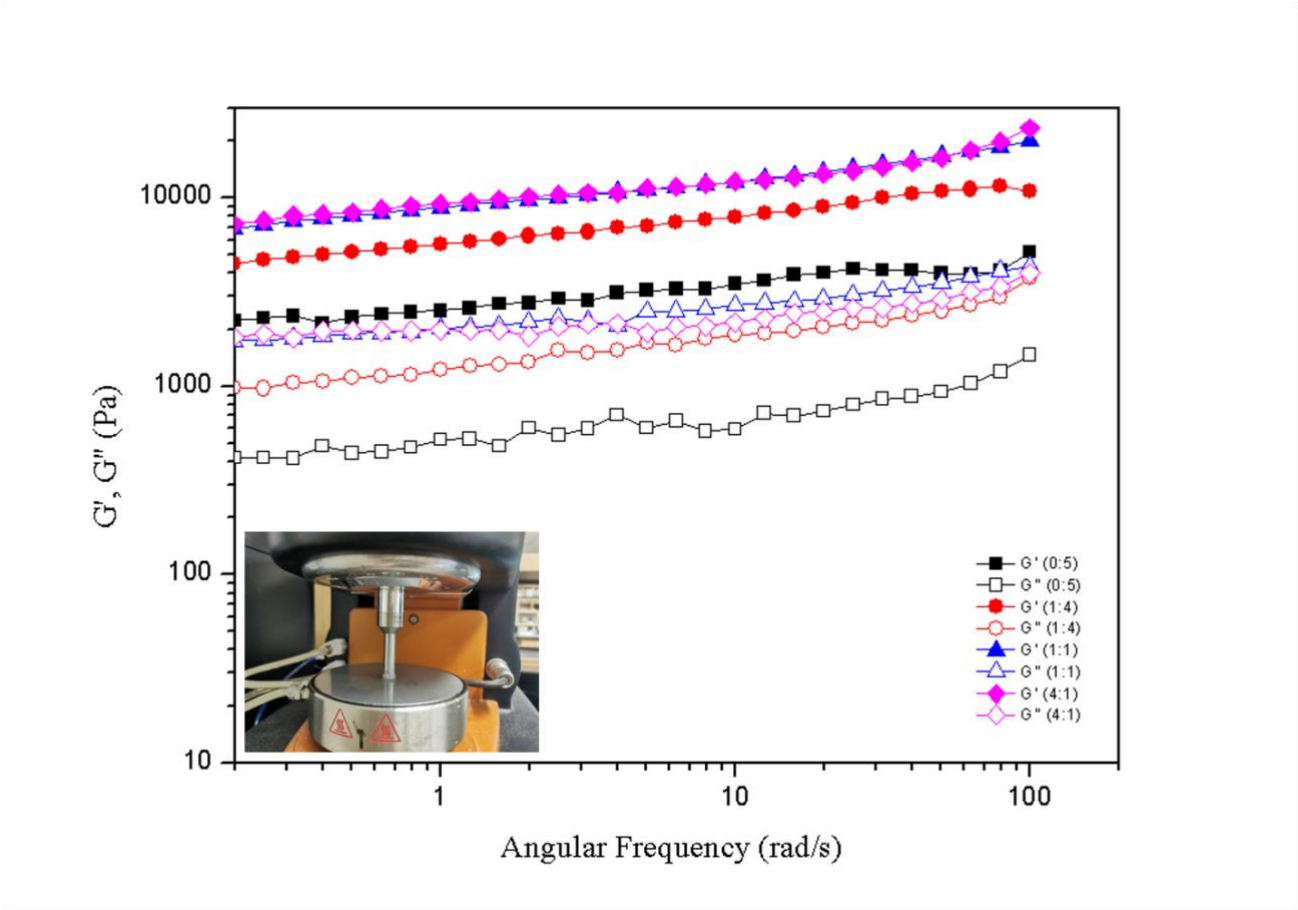

Figure 3.6. Rheology test for wet NCFs-based aerogels with different ratios of NCFs and alginate.

3.3.5 Compression test

To assess the mechanical properties of NCFs-based aerogels, compression tests were conducted, and the compressive stress-strain curves are shown in Figure 3.7. The process of the compression test is demonstrated in Figure 3.7A. In the compression test, the strains from 10% to 50% were used to calculate the curves. Figure 3.7B-E indicated the stress-strain plots of aerogels with different NCFs and alginate, namely 0:5, 1:4, 1:1, and 4:1. Meanwhile, three regions can be observed in the loading stress-strain curves of four groups: the Hookean region attributing to elastic bending deformation, a broad plateau relating to the collapse of the cell wall, and a densification region where the stress increases remarkably (15,177). A permanent residual deformation can be observed in the unloading curves after compression (149). Among the four groups, the aerogel (0:5), aerogel (1:4), and aerogel (1:1) have permanent residual deformation and loses its recoverability and elasticity from 10% strain (Figure 3.7B-D) (178,179). As Figure 3.7 E showed, the NCFs-alginate (4:1) aerogel has excellent compressibility and can completely recover back to its original shape at 30% strain. Other research also reported similar results (171). As Figure 3.7F indicates, in dry condition, the Young's modulus of NCFs-alginate (4:1) aerogel is much lower than aerogel (0:5) ($p<0.001$) and aerogel (1:4) ($p<0.001$), and has no significant difference with the aerogel (1:1), indicating the Yonge's modulus of NCFs-alginate aerogel decreases with increasing fibers content. Meanwhile, the tendency also proves that the aerogel (4:1) is softer than other groups because of the lower Young's modulus. The Young's modulus of aerogel (4:1) is similar with modulus of soft tissues, like livers, which can reduce the risk of stress shielding (180–182).

To further evaluate the recoverability and cyclic resilience properties of NCFs-alginate (4:1) aerogel, the compressive cycling test was carried out under 30% strain (Figure 3.7G). A hysteresis loop can be observed in the compressive stress-strain curves, which is similar to nanofiber-based aerogels (178,183). The loop of NCFs-alginate (4:1)

aerogel has shrunk after the first cycle, but it has remained largely constant after the fifth cycle (Figure 3.7G). The energy loss coefficient and maximum stress are assessed and demonstrated in Figure 3.7H. The value of maximum stress of the aerogel has not changed significantly since the first cycle and has remained at around 1.53kPa. However, the value of the energy loss coefficient of NCFs-alginate (4:1) aerogel is the highest one in the first cycle, then it starts to decrease, and roughly maintains at 33%. The final energy loss coefficient is similar to other studies (149,177–179).

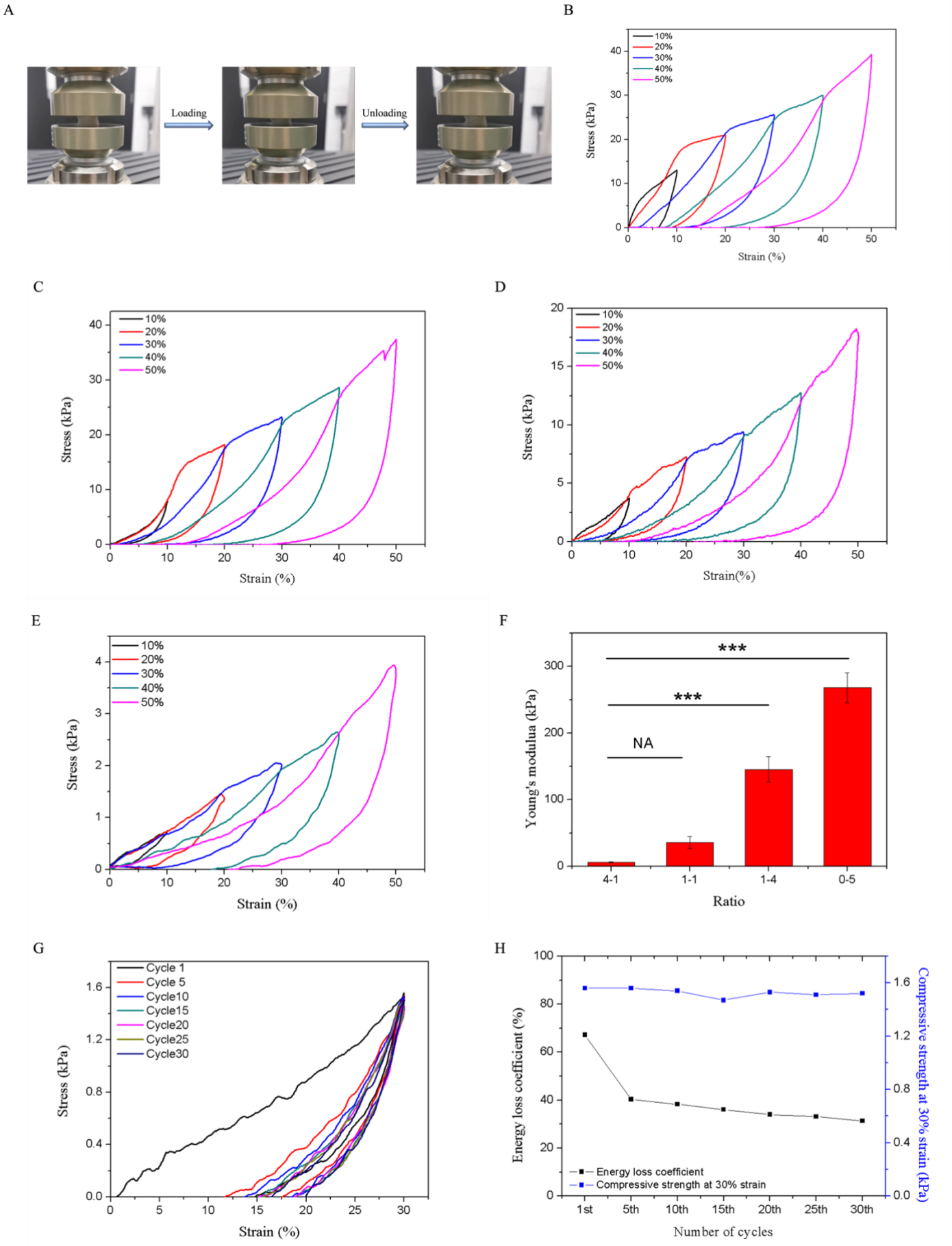
A
Loading
Unloading
B
10%
20%
30%
40%
50%
Stress (kPa)
Strain (%)
C
Stress (kPa)
Strain (%)
D
Stress (kPa)
Strain(%)
E
Stress (kPa)
Strain (%)
F
Young's modulua (kPa)
***
***
NA
4-1
1-1
1-4
0-5
Ratio
G
Cycle 1
Cycle 5
Cycle10
Cycle15
Cycle20
Cycle25
Cycle30
Stress (kPa)
Strain (%)
H
Energy loss coefficient (%)
Compressive strength at 30% strain (kPa)
Energy loss coefficient
Compressive strength at 30% strain
1st
5th
10th
15th
20th
25th
30th
Number of cycles

*Figure 3.7. Compression test of NCFs-alginate aerogels. (A) The loading-unloading process of NCFs-alginate (4:1) aerogel under 30% strain. The stress-strain curves during loading-unloading process under different compressive strains (10%, 20%, 30%, 40%, and 50%) for different rates between NCFs and alginate(n=3), (B) 0:5, (C) 1:4, (D) 1:1, and (E) 4:1. (F) Young's modulus of the four rates samples (n=3; ***, p<0.001). (G) 30 cycles compressive stress-strain curves of the aerogel (4:1) under 30% strain. (H) The energy loss coefficient and compressive stress at 30% strain for aerogel (4:1) during 30 compressive loading-unloading cycles in (G).*

3.3.6 Injectable and water-induced shape memory behaviours

The injectable ability and water-induced shape memory ability of aerogels have been indicated in Figure 3.8. As the images showed, the freeze-dried NCFs-alginate aerogels were squeezed to a certain shape and then put into tips with three designed diameters. The aerogels can be injected from the tips by a pipette and quickly back to their original shape within 4s when immersing in water. The shape recovery time of NCFs-alginate aerogel was consistent (167). The aerogels returned to their original state when squeezing out again, which can be repeated. The aerogels exhibited good water stability and structural stability due to freeze-dried NCFs and alginate-Zn^{2+} networks.

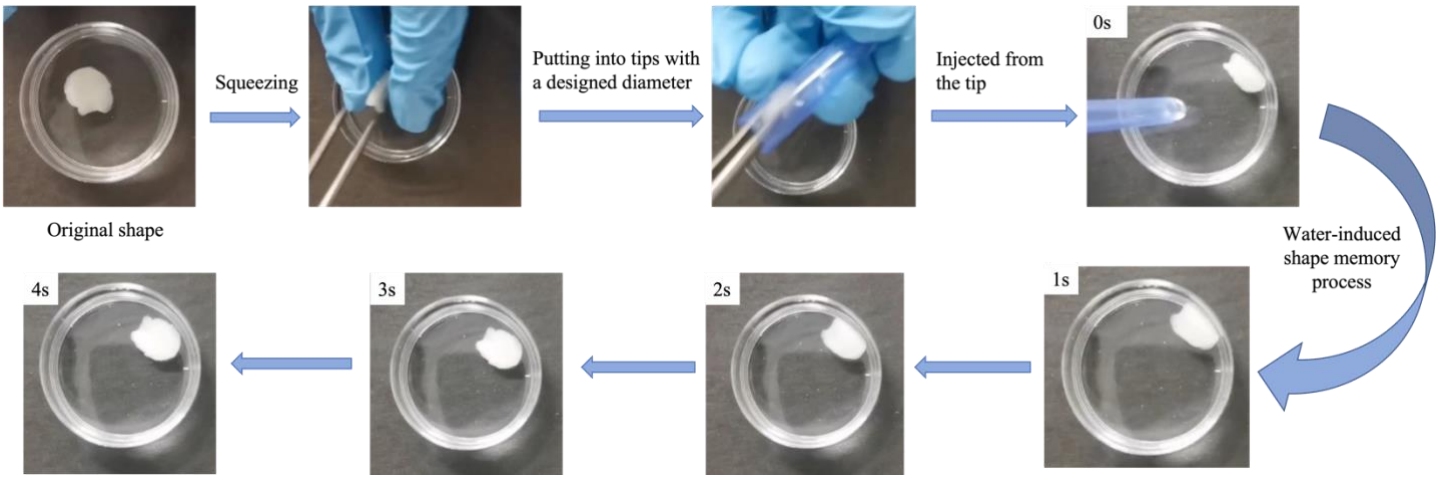

Figure 3.8. Images of NCFs-alginate aerogels with injectable and water-induced shape memory ability

3.3.7 Water absorption test

Because of its high porous, the NCFs-based aerogel has good water absorption ability. Figure 3.9A showed that in the first one minute, the water absorption of the aerogel (4:1) quickly increased to 36.28±2.23g/g. This means the water absorption of the aerogel reached 36 times its weight in the first one hour. After 1minute, the weight of aerogel (4:1) kept stable with slight fluctuation. The weight reached its peak at 1h, about 37.8±1.51g/g. The water absorption rates of the other three groups were higher than this aerogel (4:1). Among them, the aerogel (0:5) has a higher water absorption rate than other groups and the rate increased to 86.56 ± 22g/g within 30min. The water absorption of aerogel (0:5) was significantly higher than that of aerogel (0:4) ($p<0.01$) and was similar to that of aerogel (1:1) and aerogel (1:4) in 180min (Figure 3.9B). However, the weights of aerogel (0:5), aerogel (1:1), and aerogel (1:4) were decreased after their peak. This is because, in the three groups, the high proportion of alginate and the predominance of ionic bonds formed with zinc ions. Possibly, the ionic gel formed by alginate and zinc ions gradually dissolved, resulting in a decrease in the weight of the aerogels. On the contrary, the aerogel (4:1) maintain stably in water because of the high content of nanocellulose fibers. The water absorption ability of NCFs-alginate aerogel is much higher than methoxy polyethylene glycol/polycaprolactone nanofiber aerogels (24.11g/g) (184).

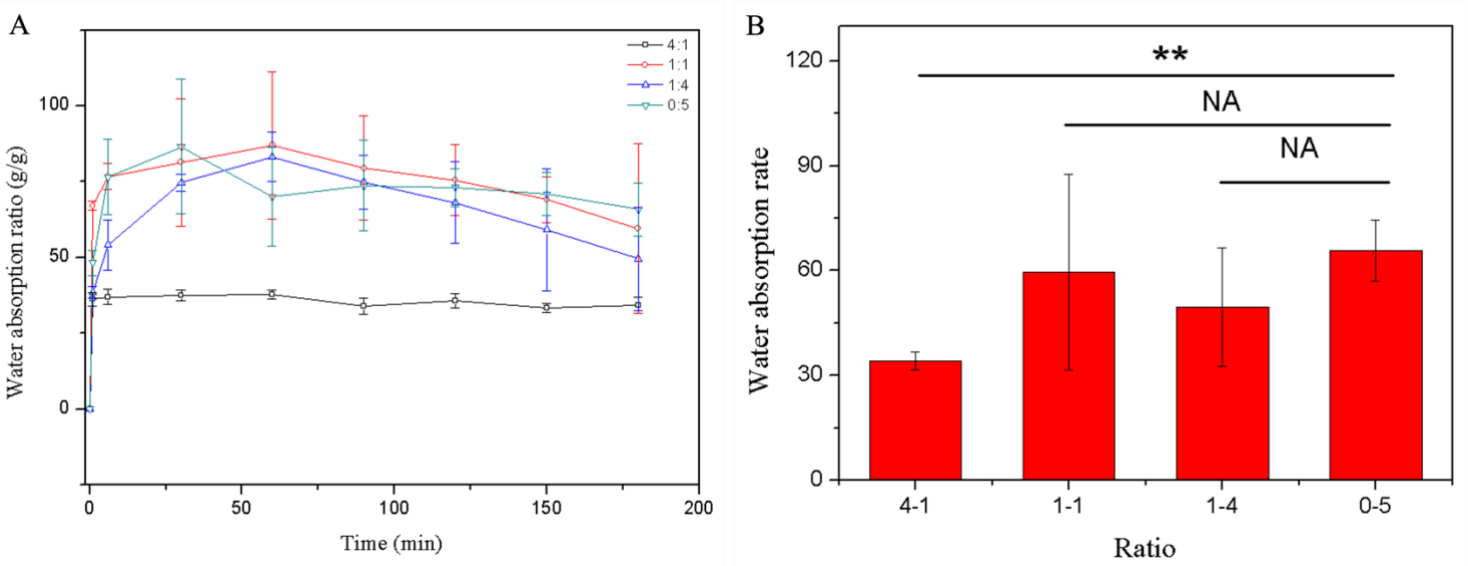

*Figure 3.9. Water absorption ability of NCFs-based aerogels with different rates between NCFs and alginate (n=3). (A) Water absorption of NCFs-based aerogels with time. (B) Statistical analysis of the water absorption of NCFs-based aerogels in 180min (**, p<0.01; NA, not significant. n=3).*

3.4 Conclusion

Overall, for NCFs-alginate aerogel, to improve the parameters in the manufacturing of aerogel, the impacts of the ratio between NCFs and alginate on the properties of aerogel, including water absorption, mechanical property in wet conditions, and compressive properties in dry conditions, were explored. It could be found that the ratio between NCFs and alginate can influence the water absorption ability and mechanical property of aerogels. The results indicated that the NCFs-alginate (4:1) aerogel has excellent mechanical properties in wet conditions and a stable water absorption rate, demonstrating the aerogel has great water stability and is insoluble in water, and good compressive properties in dry conditions, indicating the aerogel has extreme compressibility. Meanwhile, the NCFs-alginate (4:1) aerogel has a stable water absorption rate and rapid water-induced shape recovery capacity, which means the aerogel can be injected into uncompressed wounds and recover its shape and cover the wounds via absorbing blood in the wound site.

Chapter 4 Polyvinyl alcohol and carboxymethylated cellulose hydrogel as wound dressings

4.1 Introduction

Uncontrolled hemorrhage is a leading cause of trauma-related death on battlefields and in hospitals (1). Prolonged bleeding may cause such complications as hemorrhagic shock, hypothermia, and multiple organ failure (3,4). Thus, effective hemostatic methods are critical for increasing the survival rate of injured patients. The human body has a limited capacity for wound healing. Besides, the natural hemostasis mechanism of our body cannot timely control and stop massive bleeding in surgery and heavy trauma (5). Herein, hemostatic dressing and devices have been used to block bleeding and promote wound healing. These materials include dressings based on collagen (185), alginate (186), oxidized cellulose (20), zeolite (187), XStat (188), and sutures (189). Although these materials are common in the effective hemostasis, they still have limitations for severe bleeding. For example, collagen can block bleeding and promote tissue regeneration. However, collagen-based materials usually swell and may cause injury to neighbouring tissues (190,191). Besides, because of animal origin (like bovine and swine), collagen-based hemostatic materials can cause allergic reaction in people who are allergic to bovine and swine; meanwhile, thic can lead to severe diseases from animal and religious problems (54,192,193). Alginate-based hemostatic materials can absorb wound exude to decrease infectious rate and provide a humid environment for wounds to promote wound healing (194,195). Nevertheless, the chemical property and mechanical strength of alginate are poor which hamper its further applications (6,196). Oxidized cellulose has antibacterial ability but may hinder wound healing due to its production of acidic metabolites (197,198). Zeolite can produce heat when getting into contact with moisture in wounds, which may cause second tissue injury (198). XStat is a new hemostatic device that has been generally used for penetrating wounds; whereas, the cost of this

product is high (17,199). Sutures are a traditional hemostatic materials with a long history while they require surgical techniques to apply and are not for all types of wounds (191,200).

Hydrogels, a soft material with three-dimension network structures and tunable physical and chemical characteristics, has been widely used in different fields, including sensor, tissue engineering, biomaterials, and biomedical fields (8,9). In recent years, self-healing hydrogels have attracted researchers' attentions as they enable a structure or material to restore their mechanical properties and original integrity after being damaged. Thus, the lifetime of hydrogels can be prolonged, and their stability can be maintained (9–11). Additionally, self-healing hydrogels have obtained their potential as hemostatic materials and drug delivery carriers because of their self-recovery ability, high mechanical durability, high water content (max. to 99.5%), and long usage lifespan (12). Meanwhile, self-repairable hydrogels have been considered to be a preferred option for injectable materials (13). Therefore, self-healing hydrogels have an extensive potential as wound dressings where various physical scenarios are met in the wound area. Besides, conventionally, hydrogels with high toughness means lower tissue adhesion which cannot fix on wound sites (201). However, hemostatic materials with strong adhesive ability can cause secondary injury, additional bleeding and even severe infection when removing wound dressings (112). Therefore, it is a challenge to prepare one hydrogel with ultrasoft property, self-healing ability and low adhesion.

In this work, we designed a self-healing and ultrasoft hydrogel via a facile one-pot assembly. The MACMC-PVA hydrogels was prepared by MACMC, PVA, and borax with UV irradiation for 20 min. In here, the addition of CMC and low concentration of PVA can reduce the stiffness of hydrogels to prepare a ultrasoft hydrogel. The ultrasoft property allows conformable contact between the hydrogel and the wound site without gaps in the interface (202) which can reduce the contamination chance at the wound

site. Besides, the ultrasoft property allows the MACMC-PVA hydrogel can be molded into different shapes. Meanwhile, because of self-healing ability, the MACMC-PVA hydrogels can be directly injected in to wound sites with different shapes, especially penetrated wounds, and form a barrier to stop bleeding (203). In this project, the existing of dynamic complexation of didiol-borax bonds between PVA and borax endows the self-healing ability of MACMC-PVA hydrogels. In this system, borax, as a reversible crosslinker, can release boric acid and borate ions in water and the diol group on PVA can be crosslinked with borate ions to form didiol-borax complexation which is reversible (8). However, the stretchability of single-network hydrogel of PVA and borax is insufficient. Herein, MACMC can be introduced to modify PVA and improve toughness of the hydrogels (21,204). In this case, MACMC-PVA hydrogels contain the physical crosslinking network between PVA and borax, and the chemical crosslinking of MACMC. As Figure 4.1 illustrates, CMC was firstly grafted with double bonds by triethylamine and methacrylic anhydride to synthesize methacrylate carboxymethylated cellulose (MACMC). Then, MACMC was dissolved in water and mixed with photoinitiator (I2959) and PVA, followed by the addition of borax as the dynamic crosslinker for PVA. After that, ultraviolet (UV) light (365nm) was used to initiate the polymerization of double bonds in MACMC. The obtained MACMC-PVA hydrogel is highly stretchable, which allows the hydrogel to be used in wound sites with intensive movement, such as joints and hearts (205,206). Meanwhile, the tissue adhesion and self-healing ability lead the hydrogel to integrate with surrounding tissues. Table 4.1 compares the properties of PVA-based hydrogel in previous works and this work, including elongation, self-healing time, and water absorption ratio. Higher elongation, shorter self-healing time, and higher water absorption rate mean better tensile property, rapid self-healing ability, and higher porosity, respectively.

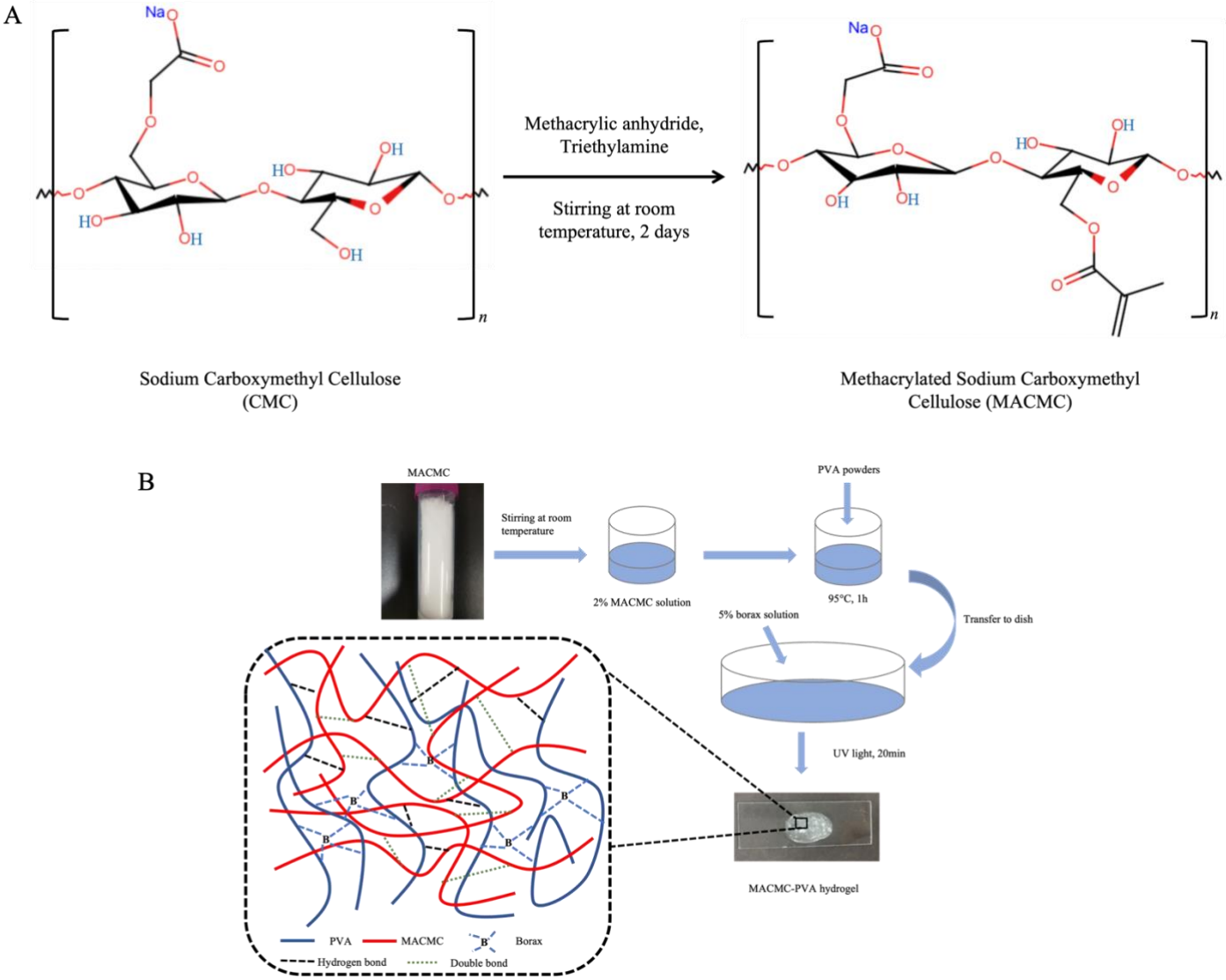

Figure 4.1. Scheme of preparation of MACMC (A) and MACMC-PVA hydrogel (B).

Table 4.1. Comparison of PVA-based self-healing time between previous research and this work

Materials	Elongation	Self-healing time	Water absorption rate	References
Microfibrillated cellulose/PVA/ borax	2900%	10min	-	(8)
PVA/kaolin	-	-	365%	(207)
PVA/alginate	-	-	274.6%	(208)
Sodium alginate / PVA	-	15s	-	(209)
Xylan/ PVA/borax	-	30s	-	(210)
Agar/PVA/graphene	-	10min	-	(211)
Bismuth oxide/ PVA	-	1min	-	(212)
Fe^{3+}/PVA	5 times	50min	-	(213)

Graphite oxide/ KCl/borax/PVA	273.3%	5min	-	(214)
nanofibrillated cellulose/ MnFe2O4 nanoparticles/polyaniline/ borax/PVA	900%	3min	-	(215)
Methacrylate carboxymethylated cellulose/ borax/PVA	2567%	8s	2356%	This work

4.2 Materials and methods

4.2.1 Materials

Polyvinyl alcohol (PVA, Mw: 20500) and carboxymethylated cellulose (CMC) were bought from Shanghai Aladdin Bio-Chem Technology Co., LTD; sodium tetraborate decahydrate was bought from VWR chemicals; triethylamine and methacrylic anhydride (MA) were bought from Sigma-Aldrich; and photoinitiator (I2959) was BASF corporation. All chemicals were used without any treatment.

4.2.2 Preparation of carboxymethylated cellulose with double bonds (MACMC)

Methacrylic anhydride (2 mL) and triethylamine (0.3 mL) were mixed with a 20 mL of 5% carboxymethylated cellulose (1g) aqueous solution with magnetic stirring (216). Among them, triethylamine served as a catalyst. The reaction occurred at room temperature. After 2 days, the solution was transferred to a dialysis tubing (MWCO:

3000D) for dialysis in deionized water for 5 days. The deionized water was changed once a day during dialysis. Then, the obtained MACMC aqueous solution was frozen at -20 ºC overnight and freeze-dried. The lyophilized MACMC was stored at -20 ºC.

4.2.3 Preparation of MACMC-PVA hydrogels

The MACMC-PVA hydrogels were synthesized by mixing the aqueous solution of MACMC, PVA, borax, and photoinitiator. Briefly, MACMC was dissolved in DI water to prepare a 2% MACMC solution. A certain amount of PVA powder (1.3%, 1.8%, and 2%) and 0.8% photoinitiator solution were dissolved in MACMC solution and magnetically stirred at 95 ºC for 1h. After that, borax solution (5wt%) was introduced into the mixed solution, and the final concentration of borax in the mixture was 0.75%. For 5% borax, the borax powder was added to the above solution directly. Then, the mixture was transferred to a glass slide and exposed under UV light (20 Watt) for 20 min.

4.2.4 Material Characterization

4.2.4.1 Fourier-transform Infrared (FTIR) Spectra Characterization

FTIR characterization was conducted using an FTIR spectrometer (Bruker IFS 66v/s, German) within a wavenumber of 4500-500 cm^{-1}. Freeze-dried samples were divided into four groups, including CMC, MACMC, and MACMC-PVA hydrogel, and were evaluated before UV and after UV exposure.

4.2.4.2 X-ray Photoelectron Spectroscopy (XPS) Characterization

MACMC-1.3%PVA hydrogels before and after UV irradiation were characterized by Kratos Axis Ultra X-ray Photoelecton Spectrometer in the range of 200-1200nm. The MACMC-PVA hydrogels before and after UV irradiation were air dried to prepare the samples of XPS.

4.2.4.3 Scanning Electron Microscope (SEM) Characterization

SEM characterization was carried out on a Quanta FEG 650 scanning electron microscope with an operation voltage of 15kV. MACMC-PVA hydrogels with 1.3%, 1.8%, and 2% PVA before and after UV were lyophilized, sprayed with a layer of gold, and put on a metal holder to examine under the microscope.

4.2.5 Water absorption

The water absorption of MACMC-PVA1.3% hydrogels was measured by followed method (167). Firstly, the hydrogels were cut into cylinders with a diameter of 0.8cm and height of 0.3cm and dried in an ambient environment overnight. Then, the dried hydrogels were immersed in 2mL water, and the weight of the hydrogels was measured at specific time intervals. The method of measurement is to remove the water from the surface of the hydrogels, and the obtained hydrogels were weighted. The water absorption ability will be calculated as:

$$water\ absorption\ ability = \frac{m_s - m_0}{m_0}$$

Where m_s is the weight of saturated hydrogel and m_0 is the weight of the dry hydrogel. The water absorption test was conducted three times to calculate the average value.

4.2.6 Adhesive test

The MACMC-PVA hydrogels before UV were placed between two coverslips and then irradiated by UV light for 20 min. The samples of MACMC-PVA hydrogels with 1.3%, 1.8%, and 2% PVA. The length and thickness of the overlap of the two coverslips were 22mm and 10mm, respectively. The adhesive ability was tested by an Instron 3366 Electronic Universal Testing Machine. The samples were tested at a crosshead speed

of 10mm/min at room temperature. The test was performed at least three times with the same protocol. Tensile stress(σ) was calculated as:

$$\sigma = \frac{F}{L_0 * T}$$

where F is the load, L_0 and T are the length and thickness of overlap of adhesive area.

4.2.7 Rheological test

The rheology of the aerogels was measured by a TA DHR-2 rheometer. The samples were cut to a cylindrical shape with diameter of 8 mm and thickness of 1mm. The MACMC-PVA hydrogels with different concentrations of PVA (before and after UV) were prepared to optimize parameters of mechanical properties. The hydrogels with 1.3%, 1.8%, and 2% PVA was synthesized for the rheology test to evaluate self-healing ability.

4.2.8 Self-healing property test

The obtained hydrogel was cut into two parts and then allowed the two parts to touch and heal on a glass slide. After healing, the healed hydrogel was observed under a microscope to check whether the cut line exist.

4.2.9 Water contact angles (CA)

Water contact angles of hydrogels were conducted with a goniometer (JY-PHA, Shanghai, China) at room temperature. The samples contained MACMC-PVA hydrogels containing 1.3%, 1.8%, and 2% PVA before and after UV light. The hydrogels were applied to glass slides and air-dried overnight to prepare MACMC-PVA film. Then, use the machine to measure the water contact angles of hydrogels. The water droplets (about 5μL) were dropped onto the hydrogels. The average values of contact angles were calculated at three different tests.

4.2.10 Rewet test

As-prepared hydrogels (before UV) were dried in an ambient environment overnight. After that, the dried hydrogels were cut into smaller pieces and DI water was then added to the small pieces. After rewetting for certain times, the rewetted hydrogels (with UV) were tested again for their rheology property. The rewet test can detect the effect of rewetting on the mechanical properties of MACMC-PVA hydrogels. In this case, inconspicuous difference between new and rewet hydrogels allows the hydrogel can be easily to transport and storage without any obvious loss of mechanical properties.

4.3 Results and discussion

4.3.1 Fourier-transform Infrared (FTIR) Spectra Characterization

MACMC-PVA hydrogels are expected to have excellent self-healing ability and good mechanical performance. To achieve the two properties, dynamic complexation of didiol-borax between PVA and borax, and UV-induced double-bond crosslink of MACMC were applied to the hydrogels. The network of PVA and borax endow self-healing ability to the hydrogels and the chemical network of MACMC improve the stretchability of the hydrogels. Chemical structures of CMC, MACMC, and MACMC-PVA hydrogel before UV and after UV are characterized by using FTIR (Figure 4.2). All the spectra indicated the characteristic peaks of carboxymethylated cellulose, including O-H stretching variation at 3353cm^{-1}, symmetric C-H stretching variation at 2916cm^{-1}, stretching bond of -COO- at 1601cm^{-1}(asymmetric stretching), 1420cm^{-1} and 1337cm^{-1}(symmetric stretching), and C-O-C stretching bond at 1020cm^{-1} (204). The stretching variation (1738cm^{-1}) assigned to the –C=O ester group was detected in MACMC, and MACMC-PVA hydrogel before and after UV FTIR spectra, respectively (217). This illustrated that the MACMC was grafted to the methacrylic group successfully. In the FTIR spectra of MACMC-PVA hydrogel, characteristic peaks of C-O-C, B-O-C, and B-O-B stretching frequency can be observed at 1250cm^{-1}, 1108cm^{-}

[1], and 664cm^{-1}, respectively (8,217). The appearance of B-O-C and B-O-B indicates the formation of didiol-borax complexation in hydrogels.

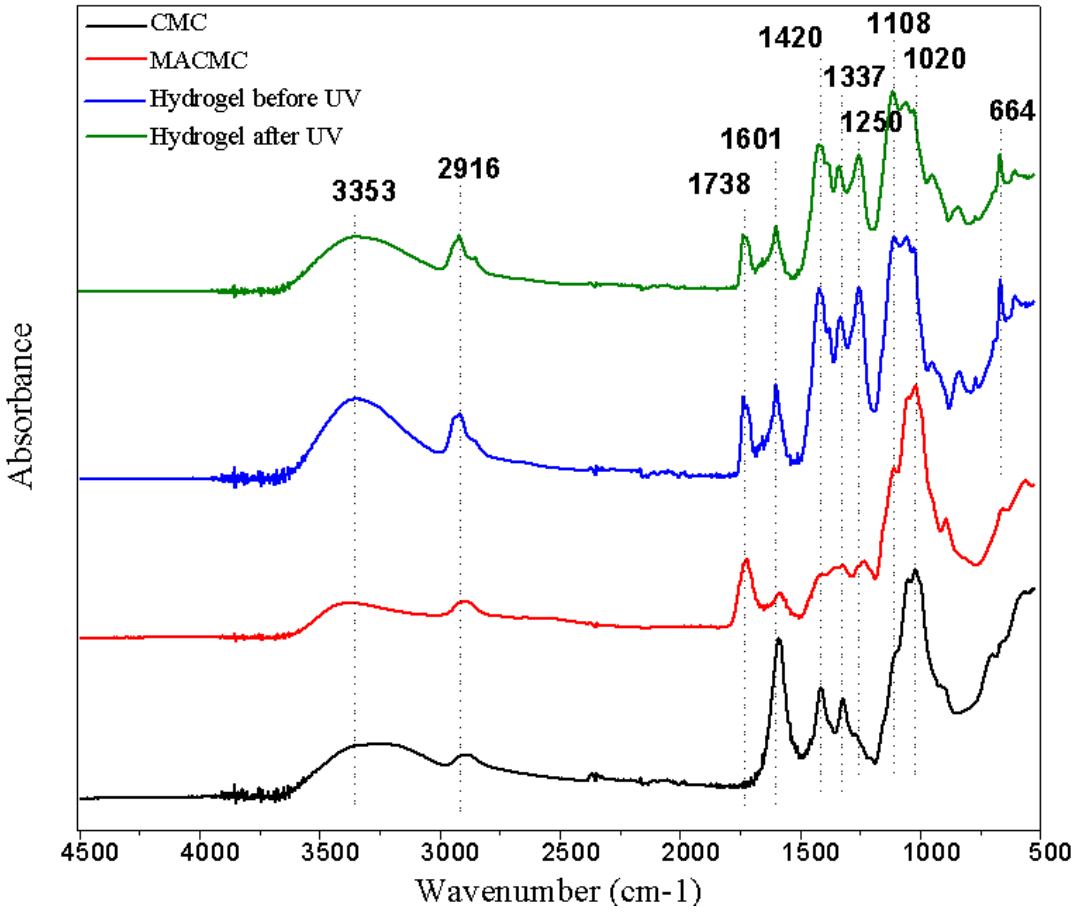

Figure 4.2. FTIR spectra of CMC, MACMC, MACMC-PVA hydrogel before UV and after UV

4.3.2 X-ray Photoelectron Spectroscopy (XPS) Characterization

XPS analysis can be used to detect the UV crosslinking mechanism of MACMC-PVA hydrogels. The XPS spectra of MACMC-PVA hydrogels before and after UV irradiation are illustrated in Figure 4.3. In XPS spectra, MACMC-PVA hydrogel before UV (Figure 4.3 A) has four peaks at 283.35, 284.97, 286.34, and 287.7eV corresponding to C=C double bond, C-C bond, C-OH, and O-C=O, respectively. For

MACMC-PVA hydrogel after UV, these four peaks can also be detected at the similar binding energy. The detection of C=C double bond indicates that the methacrylate group was grafted successfully to CMC, which agree with the result of FTIR spectra. Compared with MACMC-PVA hydrogels before UV irradiation, after UV irradiation, the ratio between C-C bond and C=C double bond increased and the conversion rate of C=C can reach 88.7%. This is because, in the crosslinking process, two C=C double bonds are broken to form two C-C bonds and one C=C double bond. Therefore, the XPS analysis proves that CMC was successfully grafted with methacrylate group and C=C double bond successfully crosslinked under UV irradiation.

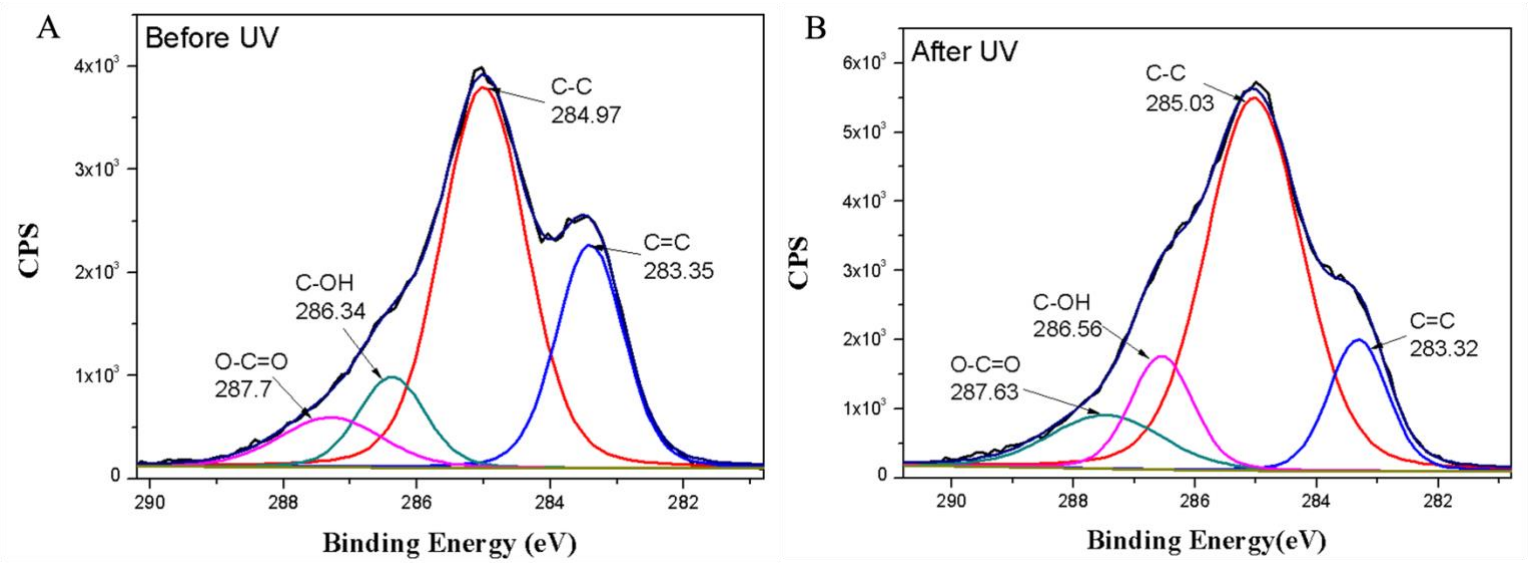

Figure 4.3 XPS spectra of MACMC-1.3% PVA hydrogels. (A) MACMC-1.3%PVA hydrogel before UV; (B) MACMC-1.3%PVA hydrogel after UV for 20min.

4.3.2 Scanning Electron Microscope (SEM) Characterization

As illustrated in Figure 4.4, the obtained MACMC-PVA hydrogels showed a three-dimension open porous structure with the pore size ranging from ten micrometers to a hundred micrometers. The compact internal morphology has been reported in a freeze-dried MACMC gel (172,216). The cross-sectional images of MACMC-PVA hydrogels before UV light indicate a decrease in pore size with increasing PVA concentrations

(Figure 4.4A1-C1) and the morphology of hydrogels after UV-irradiation shows a similar trend (Figure 4.4A2-C2). This trend may be explained by the fact that the addition of PVA concentration can crosslink with more borax. The microstructure of MACMC-PVA hydrogels can be influenced by UV irradiation. However, the morphology of hydrogels irradiated by UV (Figure 4.4A2-C2) is similar with those without UV (Figure 4.4A1-C1). Therefore, UV irradiation has minimal effect on the internal structure of these hydrogels. This showed that increasing PVA concentrations can enhance the mechanical strength of MACMC-PVA hydrogels. Ai et al. (210) also observed a similar pore cross-sectional structure in PVA-based hydrogels.

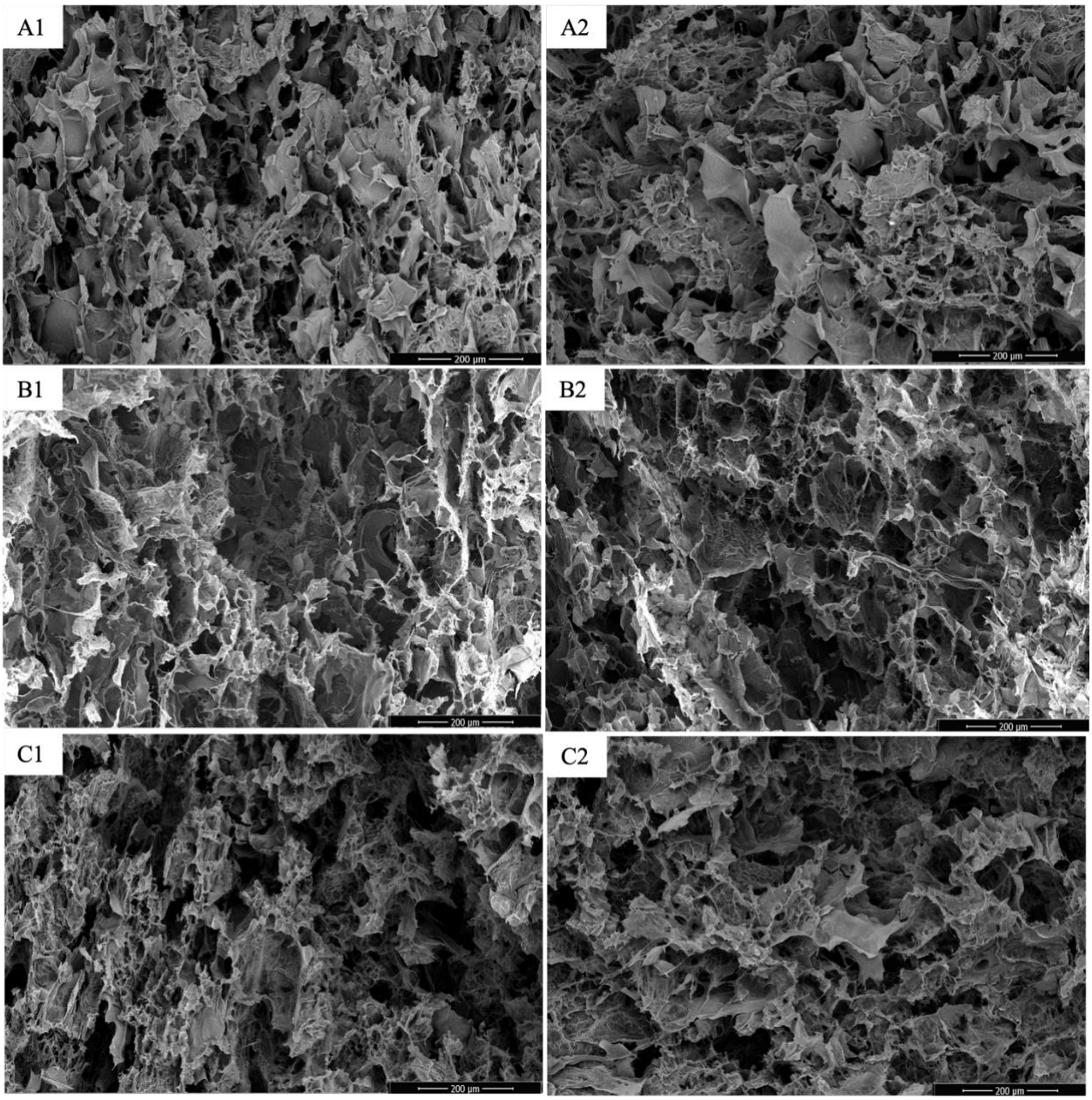

Figure 4.4. SEM images of cross-section of MACMC-PVA1.3% before UV(A1) and after UV(A2), MACMC-PVA1.8% before UV (B1) and after UV (B2), and MACMC-PVA2% before UV(C1) and after UV (C2).

4.3.3 Water absorption test

As shown in SEM images, the MACMC-PVA1.3% hydrogels have the highest porosity. Figure 4.5A showed that the water absorption of hydrogel increased dramatically within 40min, from 0 to 1881%. This means the hydrogel can absorb 19 times its own weight

of water. Then, the water absorption grew slightly and reach a plateau of about 2356% at 130min. Meanwhile, the water absorption rate of the groups of 1.8% and 2% PVA increases significantly within 17min, from 0 to 1821% and 1704%, respectively. The absorption profiles then rise slowly and arrive at the plateau of around 2000% at 130min. Among the three groups, the water absorption rate of MACMC-PVA1.3% hydrogel was higher than the other two groups, owing to the factor that the hydrogel with 1.3% PVA has the highest porosity, which agrees with SEM imaging. As Figure 4.5B shows, the water absorption rate of MACMC-PVA1.3% hydrogel has no significant difference with the groups of 1.8% and 2% PVA, which may be because of the difference in pore size among the three groups is not obvious. The developed MACMC-PVA hydrogels have a much higher water absorption ratio as compared to other similar materials including PVA/kaolin hydrogels (365%) and PVA/alginate hydrogels (274.6%) (207,208). Therefore, the MACMC-PVA hydrogels have an excellent water absorption ability and porous structure. Meanwhile, the high water absorption capacity of MACMC-PVA hydrogel can promote the proliferation of cells, absorption of wound exudate to prevent microbial infection and provide a moist environment to accelerate wound healing (207,218).

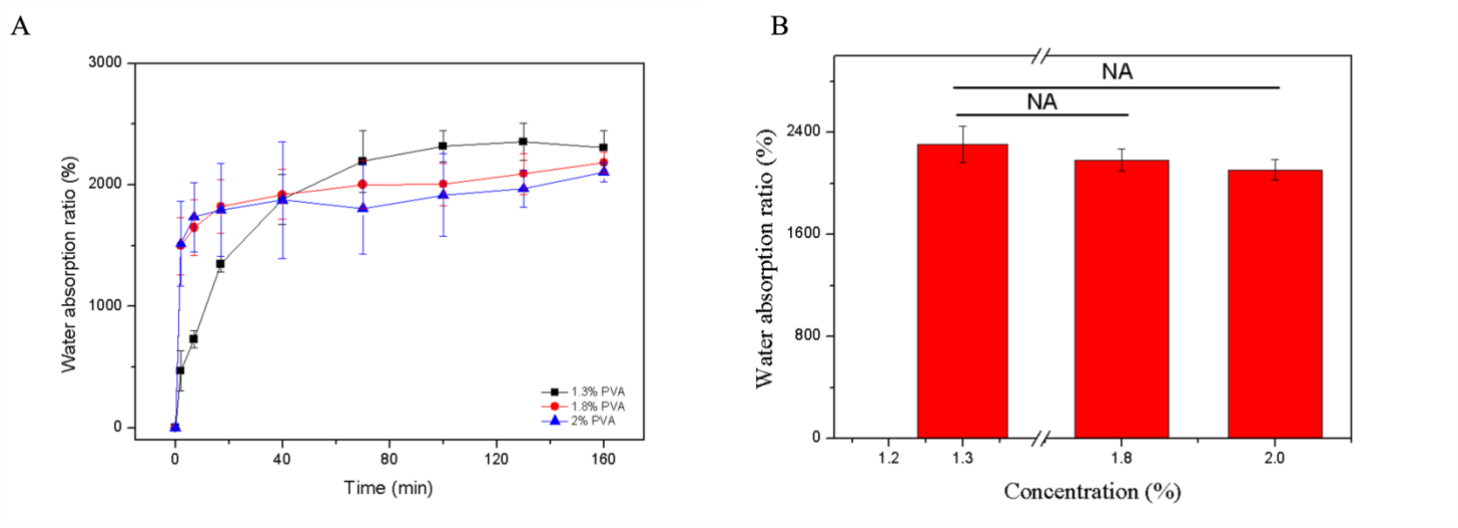

Figure 4.5. Water absorption of MACMC-PVA hydrogel (1.3%, 1.8%, and 2% PVA). (A) Water absorption ratio of MACMC-PVA hydrogels with time. (B) Statistical analysis of the water absorption ratio of MACMC-PVA hydrogels in 160min (NA, not significant).

4.3.4 Adhesive test

The adhesive property of MACMC-PVA hydrogels was evaluated by the Instron tester. The maximum adhesive stress of the MACMC-PVA hydrogel being peeled from a glass slide (Figure 4.6) was about 12kPa (MACMC-PVA1.8%hydrogel) which is similar to the stress of MACMC-PVA1.3% (11.4kPa). However, as the PVA concentration continues to increase to 2%, the adhesive stress decreased dramatically from 12kPa to 4kPa, which is a reduction of three times, indicating that excessively high PVA concentration can weaken the adhesive capacity of MACMC-PVA hydrogels.

To demonstrate the adhesive behavior of the MACMC-PVA1.3% hydrogel, the hydrogel was dyed yellow-green with a fluorescent dye. As illustrated in Figure 4.7, the hydrogel exhibits good adhesion to the surfaces of various materials, including rubber (Figure 4.7A), glass (Figure 4.7B), plastic (Figure 4.7C), and steel (Figure 4.7D). Most importantly, the hydrogel can directly adhere to the skin (fingers) and remain adhered to the bending fingers at different angles, like 30° (Figure 4.7E), 90° (Figure 4.7F), 120° (Figure 4.7G), and 180° (Figure 4.7H), indicating that the MACMC-

PVA1.3% hydrogel has a great tissue-adhesive capacity (219). Because of the existence of the carbonyl group and a large number of hydroxyl groups, the adhesive mechanisms of hydrogel include hydrogen bonding and hydrophobic interaction (rubber, glass, plastic, and skin), metal coordination (steel), and electrostatic effect (213,219). Additionally, the MACMC-PVA hydrogel has great potential as wound dressings owing to its tissue-adhesive property.

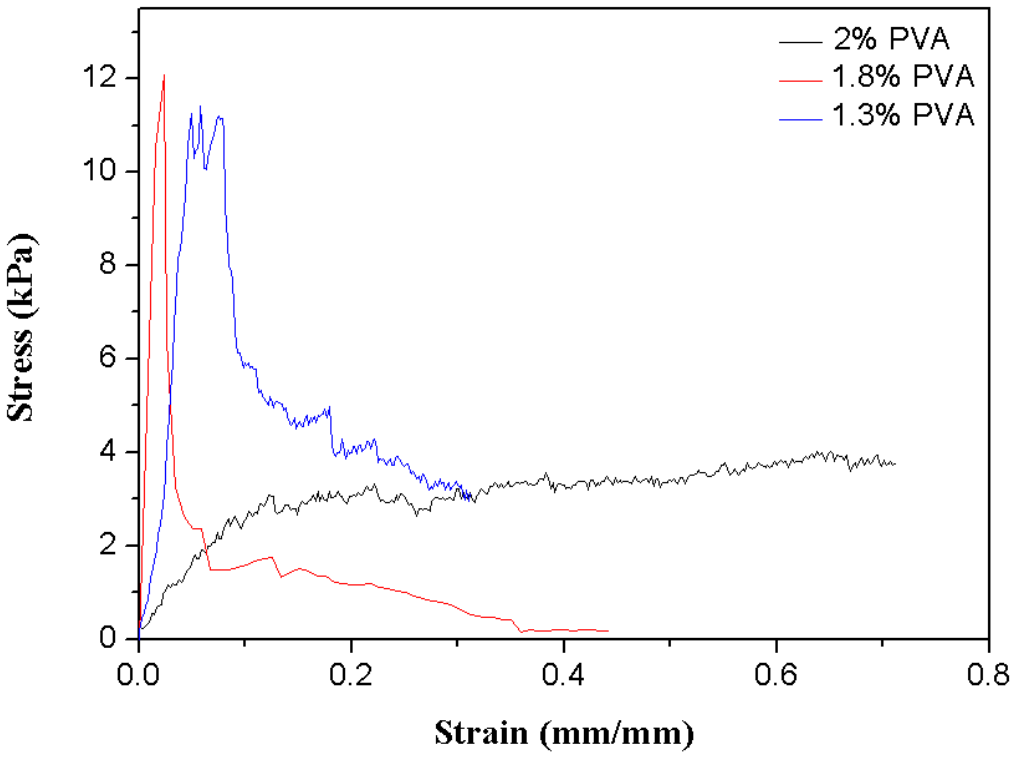

Figure 4.6. Adhesive property of MACMC-PVA hydrogel with different 1.3%, 1.8%, and 2% PVA concentrations

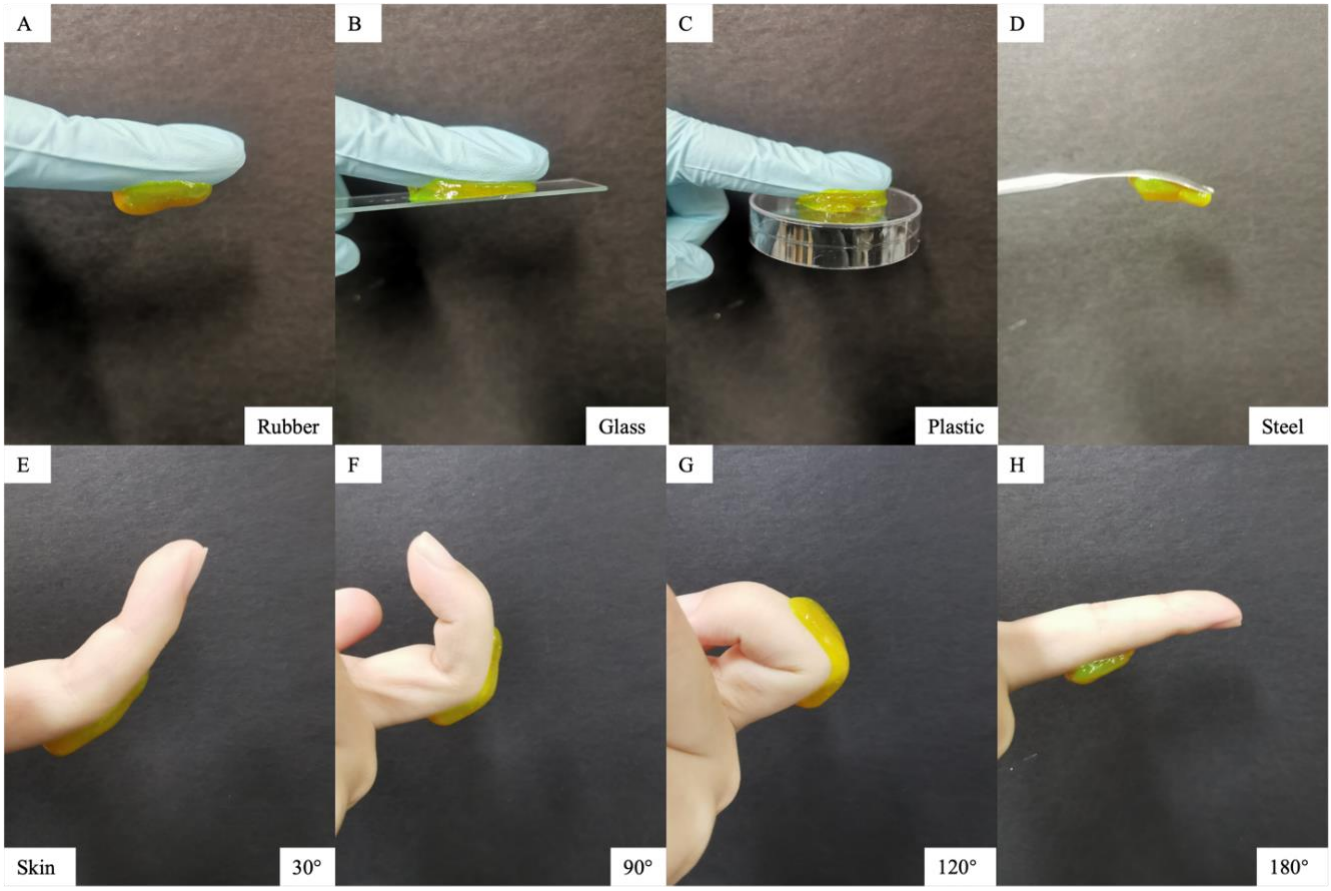

Figure 4.7. Adhesive ability of MACMC-PVA1.3% hydrogel on different surfaces, including rubber(A), glass(B), plastic (C), steel (D), and skin with different angles,30° (E), 90° (F), 120° (G), and 180°(H).

4.3.5 Rheological test and tensile property of MACMC-PVA hydrogel

Rheological tests were conducted to illustrate the influence of UV irradiation, borax, and PVA concentrations on the mechanical properties of PVA-MACMC hydrogels. The frequency-dependent sweep was performed within 0.1-100 rad/s to measure the storage modulus (G') and loss modulus (G'') at a fixed 0.1% strain. In Figure 4.8, the MACMC-PVA hydrogels showed a liquid-like behaviour at a lower angular frequency area (< 1 rad/s), where G'' was higher than G'. Then, with the increase of frequency, G' increased and exceeded G'' under a higher angular frequency area. Herein, the PVA-MACMC hydrogels showed a gel-like state. The modulus trend of Figure 4.8 was also observed in previous research (8,215). The behavior indicated that the crosslinked network of MACMC-PVA hydrogels is reversible (8). As shown in Figure 4.8A, the

storage modulus and loss modulus of MACMC-PVA hydrogels before UV irradiation increase with increasing PVA concentrations. Among them, the gap between the modulus of hydrogels with 1.8% PVA and 2% PVA is not large. Similarly, the modulus of MACMC-PVA hydrogels after UV irradiation also increases with the increase of PVA concentrations (Figure 4.8B). However, the modulus profiles of hydrogels with 1.8% PVA and 2% PVA overlap in the lower frequency, while the modulus of MACMC-PVA 2% hydrogel boosts higher than that of hydrogel with 1.8% PVA in the higher frequency. The modulus of MACMC-PVA1.3% hydrogel is lower than the other two groups in the whole angular frequency range. Overall, the hydrogels with higher PVA concentration have higher storage modulus and loss modulus, due to the entanglement and reversible network property of MACMC in the hydrogels (8). As shown in Figure 4.8C, Young's modulus of hydrogels exposed to UV light was higher than that without UV exposure. This is because the carboxymethylated cellulose was grafted with double bonds and UV irradiation can promote the chemical crosslink ratio of the hydrogel. To detect the impacts of borax content on rheological characteristics of hydrogels, MACMC-PVA 1.3% hydrogels with different borax contents were tested (Figure 4.8D). The results indicated that the lower the borax contents, the higher the modulus values, which is the opposite of the influence of PVA concentrations. Thus, using UV light, higher PVA contents, and lower borax ratios can increase Young's modulus of MACMC-PVA hydrogels and promote the crosslinking rate of the hydrogels, which agrees with the result of the SEM test.

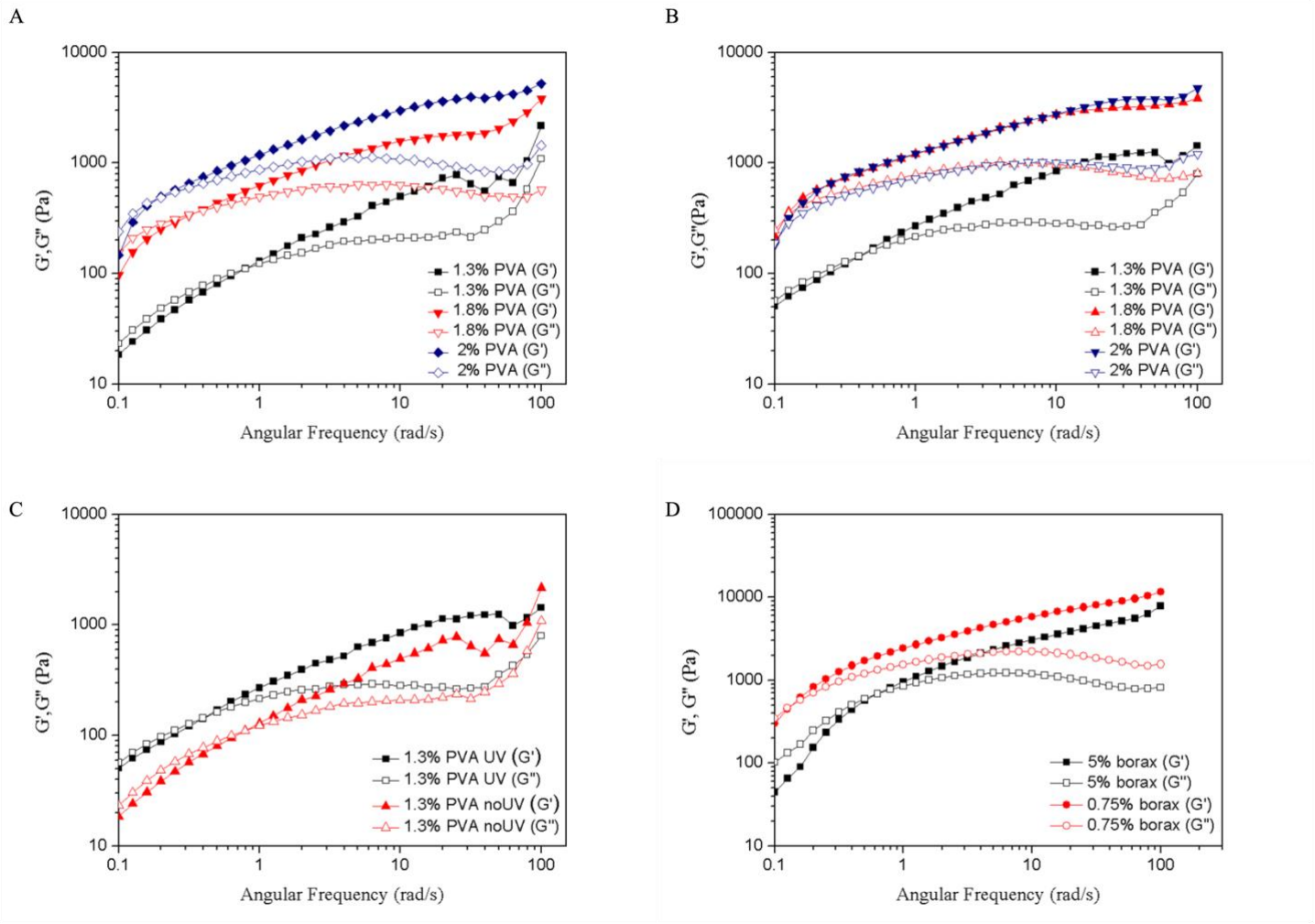

Figure 4.8. Rheological properties of MACMC-PVA hydrogels with different conditions. (A) MACMC-PVA hydrogels with different PVA concentrations before UV; (B) MACMC-PVA hydrogels with different PVA concentrations after UV; (C) Comparison between before and after UV irradiation; (D)MACMC-PVA hydrogels with different concentrations of borax (7.5% and 5%).

To evaluate the toughness and tensile properties of MACMC-PVA hydrogels, the tensile tests were conducted "by hand" since the hydrogels were too soft to be clamped on a tensile tester (215). Figure 4.9 indicates the toughness of MACMC-PVA1.3% hydrogel (Figure 4.9A, B) as compared to PVA hydrogel (Figure 4.9C, D). The MACMC-PVA1.3% hydrogel was dyed with fluorescent dyes (Fluorescein sodium salt). The original strength of the two samples is 1.5cm (Figure 4.9A, C). For MACMC-PVA1.3% hydrogel, about 40cm of elongation was observed without breakage (Figure 4.9B). The stretchable rate of MACMC-PVA1.3% hydrogel can reach 2567%.

However, the PVA hydrogel was easy to break during the process of stretching (Figure 4.9D). This demonstrated that the tensile strength of PVA hydrogel can be improved after the incorporation of MACMC, which maybe because of the crosslinking between PVA and MACMC. Previous studies also reported similar results (8,215). Liu et al. (215) improved the tensile property of PVA-borax hydrogel after the incorporation of the nanofibrillated cellulose (NFC).

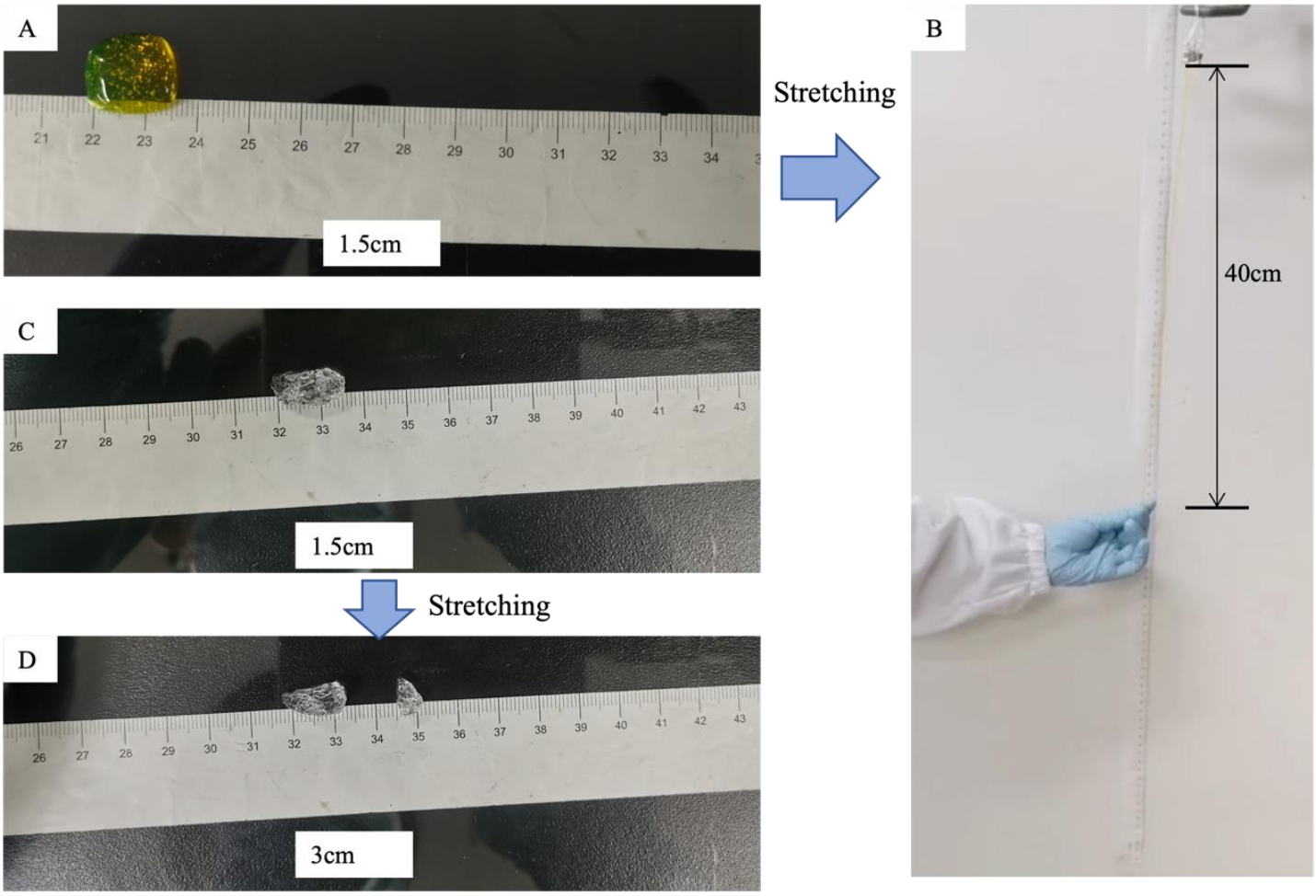

Figure 4.9. Tensile property of MACMC-PVA1.3% hydrogel and pure PVA hydrogel. (A) The original length and (B) stretched length of MACMC-PVA1.3% hydrogel. (C) Original length and (D) stretched length of pure PVA hydrogel.

4.3.6 Self-healing property test

The self-healing capacity of MACMC-PVA hydrogels is shown in Figure 4.10A. Herein, a hydrogel sample on a glass slide was cut in half and the two halves were put back together and healed into one after 8 seconds of contact. The healing time for the developed MACMC-PVA1.3% hydrogel is significantly shorter than those in similar research (Table 4.1), in which self-healing time range from 15s to 50min (209,213).

Additionally, step-strain measurements were conducted to evaluate the mechanical properties of hydrogels after self-healing. As shown in Figure 4.10B, the test was performed at a low oscillatory shear strain (1%) and a high one (400%). Each strain cycle was kept for 200 seconds with a constant angular frequency (10rad/s). In the low strain value (1%), the G' was higher than G'' which indicated a gel-like behaviour. However, when the strain was substantially increased to 400%, the modulus values were changed and the G'' value exceeded G', suggesting that the hydrogel was in a liquid-like state. The G' value decreased from 2200Pa to 200 Pa since the gel network was disrupted during the transition (10,138). When the 1% strain replaced the high strain, both G' and G'' returned to the original values within a few seconds. Meanwhile, the cycles can be performed multiple times (at least four times) without any significant loss of mechanical properties (Figure 4.10B). The rheology test proved that the MACMC-PVA hydrogel has an excellent self-healing ability which can back to its initial state after undergoing high strain.

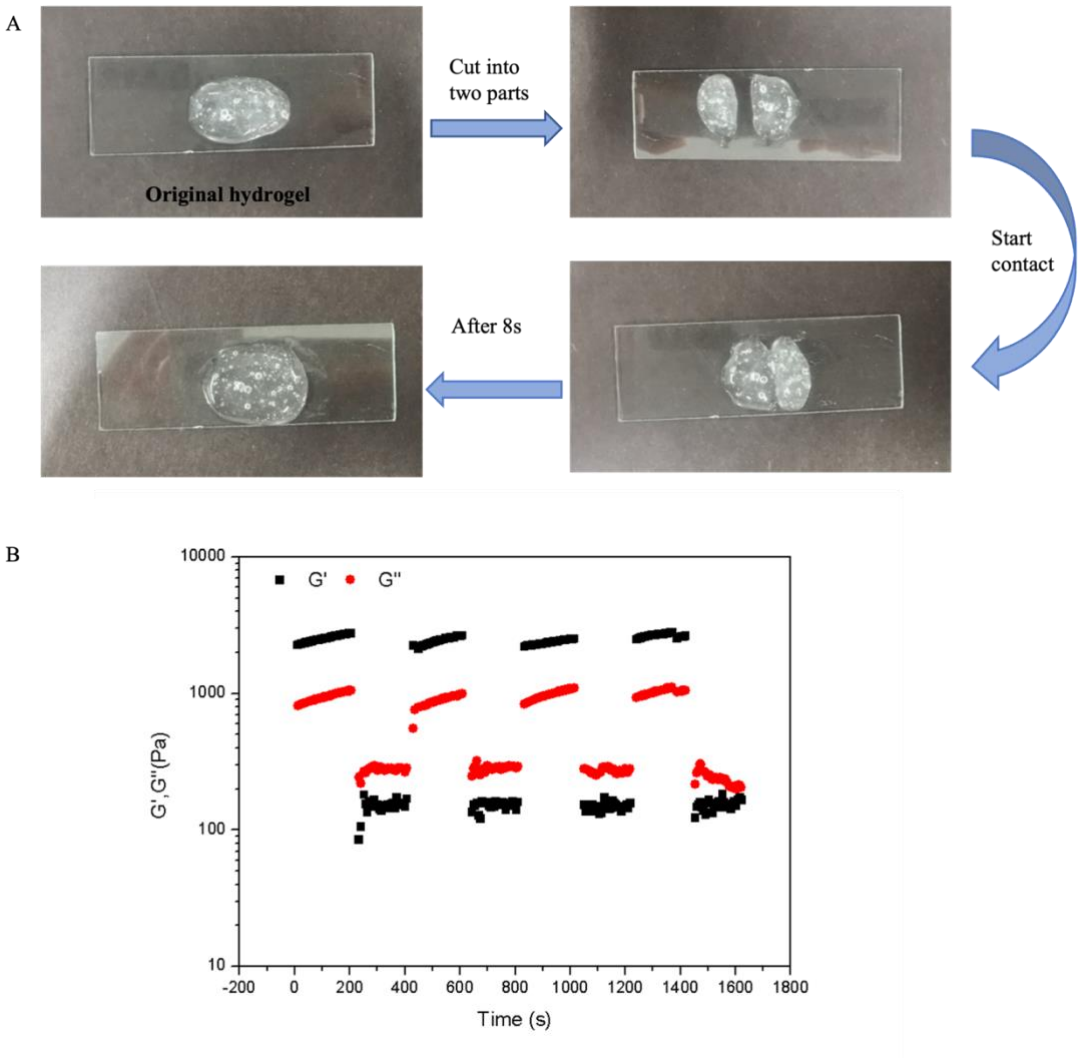

Figure 4.10. Self-healing performance of MACMC-PVA hydrogels. (A)Self-healing process of MACMC-PVA hydrogel; (B)Rheology test of hydrogel's self-healing property: step-strain measurements of MACMC-PVA hydrogel

4.3.7 Water contact angles

The surface hydrophilicity of MACMC-PVA hydrogel was measured by water contact angels. Figure 4.11A compares the water contact angles of MACMC-PVA hydrogels with different PVA concentrations before and after UV irradiation. The water contact angles of hydrogels after UV are increased with increasing PVA concentrations (Figure 4.11B, D, and F). This is probably due to the increased content of boronic ester bonds formed with the increase of the PVA concentration. According to previous research, boronic ester bonds can reversibly convert hydrophilicity to hydrophobicity (220). However, the contact angles of hydrogels before UV decrease from 1.3% (Figure 4.11C) to 1.8% (Figure 4.11E) and then increase when the PVA concentration increase to 2% (Figure 4.11G). The reduction of water contact angles from 1.3% PVA to 1.8% PVA may be influenced by hydroxyl group increases in PVA. Whereas the increase of water contact angle of MACMC-PVA2% hydrogel is due to boronic ester bonds and the effect of hydroxyl group is offset by boronic ester bonds. Additionally, the water contact angles of MACMC-PVA hydrogels after UV were higher than those of hydrogels before UV. This may be because part of the hydroxyl groups of PVA and MACMC form hydrogen bonds after UV irradiation. Herein, due to the reduction of hydroxyl groups, the hydrophilicity of MACMC-PVA hydrogel is correspondingly reduced. Thus, the introduction of PVA and UV irradiation can influence the water contact angle of PVA. However, the MACMC-PVA hydrogel still showed hydrophilicity.

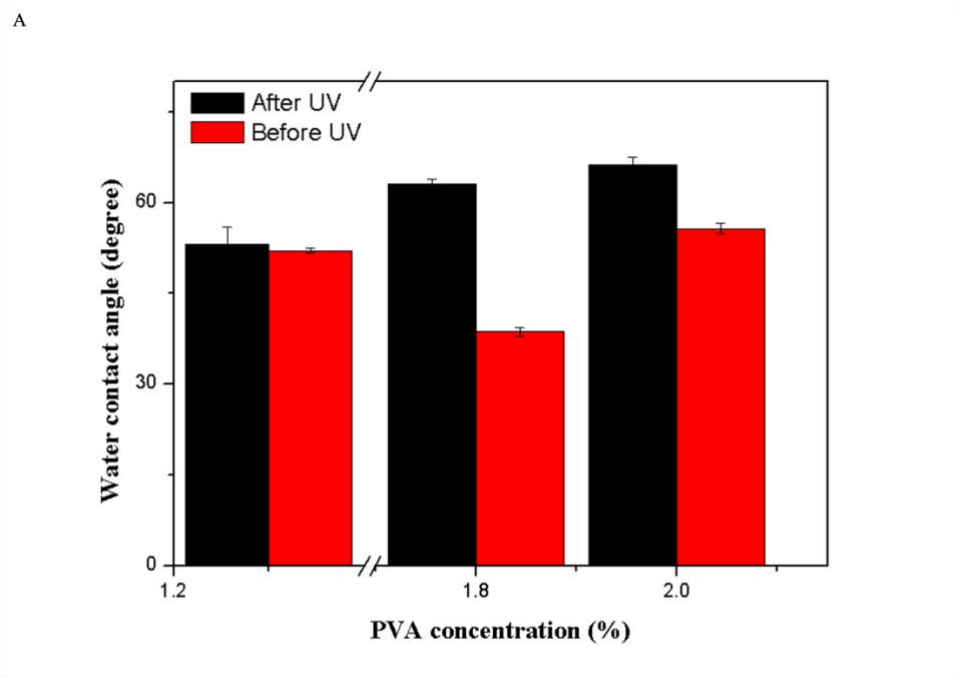
A
After UV
Before UV
Water contact angle (degree)
0
30
60
1.2
1.8
2.0
PVA concentration (%)

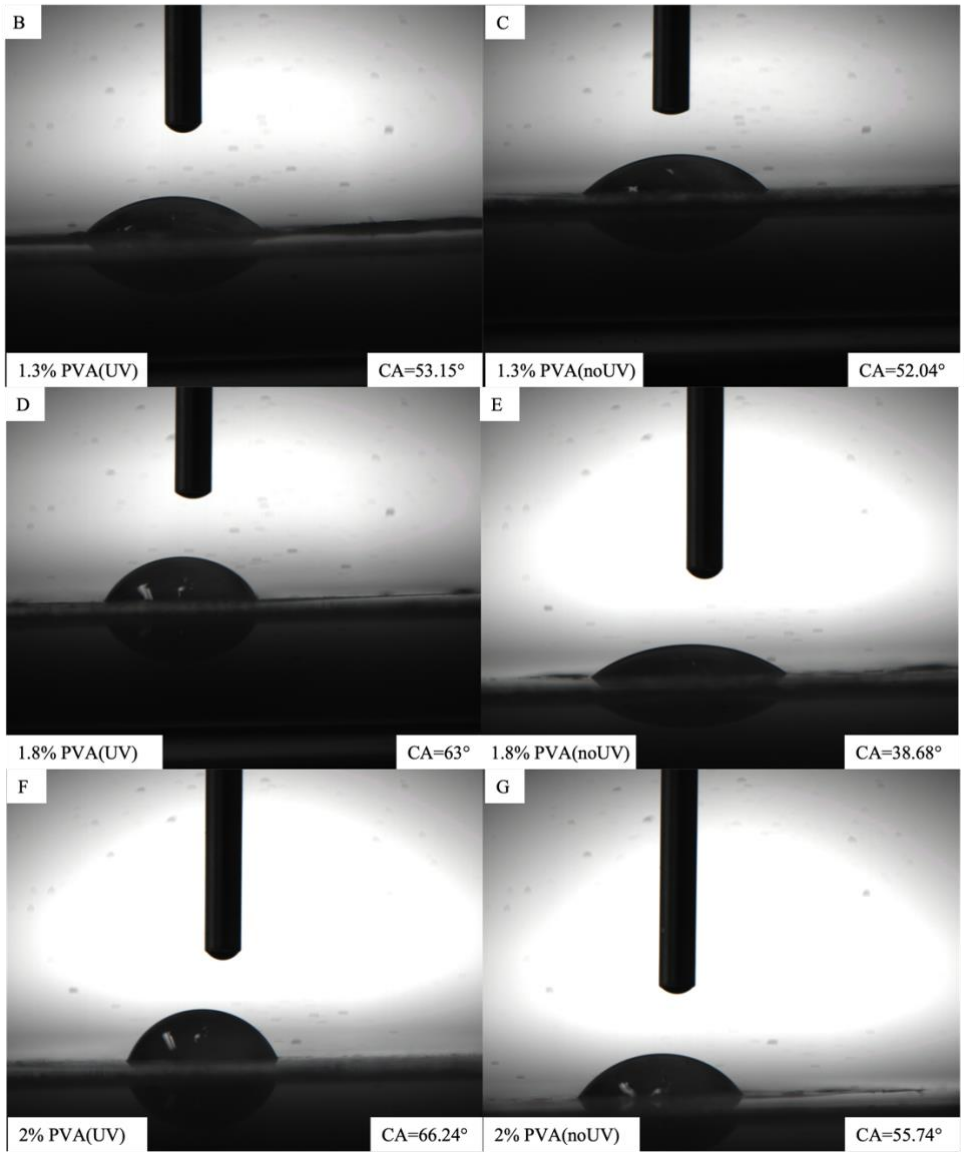
B
1.3% PVA(UV)
CA=53.15°
C
1.3% PVA(noUV)
CA=52.04°
D
1.8% PVA(UV)
CA=63°
E
1.8% PVA(noUV)
CA=38.68°
F
2% PVA(UV)
CA=66.24°
G
2% PVA(noUV)
CA=55.74°

Figure 4.11. Water contact angles of MACMC-PVA hydrogels. (A)Comparison between MACMC-PVA hydrogels with different PVA concentrations before and after UV. Images of water contact angles of different MACMC-PVA hydrogels: MACMC-PVA1.3% before UV (B) and after UV (C), MACMC-PVA 1.8% before UV (D)and after UV(E), and MACMC-PVA2% before UV (F) and after UV (G).

4.3.8 Rewet assay

To explore the mechanical property of rewet hydrogels, the rheology tests of new and rewet hydrogels were carried out. As indicated in Figure 4.12, the storage modulus of new hydrogel was higher than that of rewet one in low frequency. However, as the frequency increased, the gap between lines of storage modulus of two hydrogels was getting smaller and smaller; eventually, the gap disappeared after 31 rad/s. For loss modulus, the new hydrogel was higher than the rewet one from 0.1 to 100rad/s, whereas the gap between the two hydrogels was not much large. This test indicated that the MACMC-PVA hydrogel cannot lose much modulus after rewetting. Meanwhile, the mechanical property of rewet hydrogel is the same as the new one.

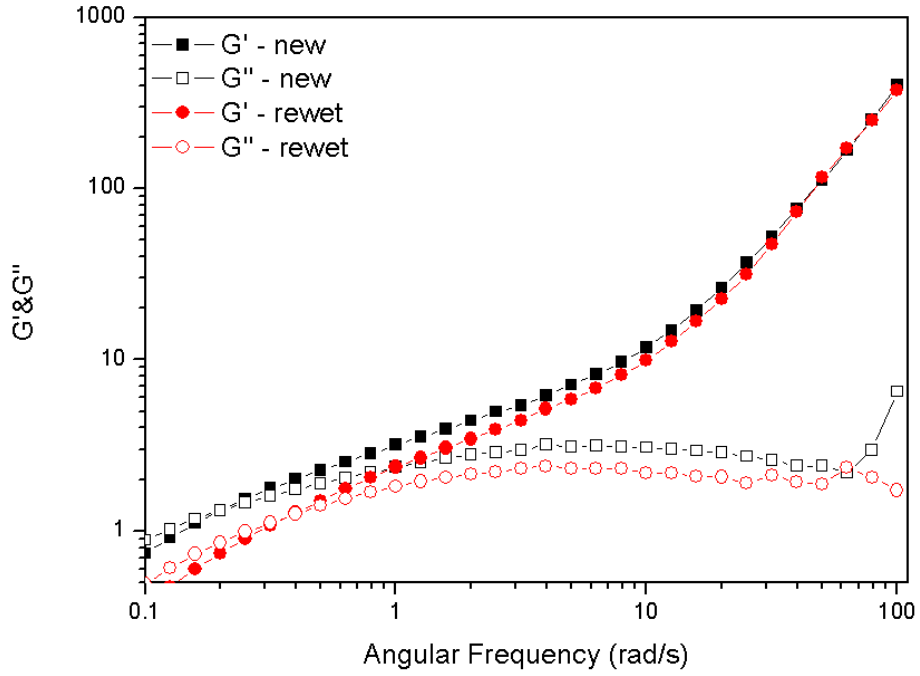

Figure 4.12. Rheologic property of new and rewet MACMC-PVA hydrogels.

4.4 Conclusion

In the MACMC-PVA hydrogel system, the existence of dynamic and reversible interactions containing hydrogen bonds and boron ester bonds endows its excellent self-healing capacity. This work investigated the factors, including PVA concentration, borax concentration, and UV light, affecting the microstructure and mechanical property of the hydrogels. The SEM images proved that the microstructure of MACMC-PVA hydrogel can be influenced by PVA concentrations and UV irradiation. The pore size of hydrogels decreased with increasing the PVA concentration and using UV irradiation, which was substantiated by water absorption tests. Meanwhile, the mechanical property of MACMC-PVA hydrogel can also be improved by increasing PVA concentration, reducing borax concentration, and UV irradiation. The MACMC-PVA hydrogels with hydrophilicity and higher water absorption can absorb blood quickly and provide a moisture environment to promote wound healing, the ultrasoft property and tissue adhesive ability can make the hydrogels stick to the skin surface better and reduce the gap between skin and the materials. Meanwhile, injectable hydrogels with self-healing ability can prolong their lifetime. Herein, the MACMC-PVA hydrogels showed promises to be used as high-performance wound dressings.

Chapter 5 Conclusion and future work

In this thesis, cellulose-based aerogels and hydrogels with double networks and good mechanical properties were prepared. For cellulose-based aerogels, NCFs and alginate have been used to accelerate hemostasis and promote wound healing and zinc ions can endow antibacterial ability to the aerogels to reduce infectious rate during wound healing. Similarly, cellulose-base hydrogels can provide a humid environment for wound sites to promote wound healing. Meanwhile, the hydrogels with self-healing ability can be injected into uncompressed wounds and have a longer lifespan. Therefore, the cellulose-based aerogels and hydrogels show great potential for hemostatic applications.

The improvement of mechanical property of cellulose-based aerogel and hydrogel is still an important topic in the biomedical field to expand or enhance their biomedical applications. For example, the compressibility and toughness of cellulose-based aerogel/ hydrogel can be improved by introducing reinforcement components, such as graphene oxide (GO), nanotubes (CNT) (221), hydroxyapatite (HAp) (222), and polypyrrole (PPy) (223). The performance of hemostatic materials based on the cellulose aerogels and/or hydrogels can be further enhanced by the incorporation of antibacterial agents, superhydrophobic/superhydrophilic materials, conductive materials, and polypeptide to endow additional advanced functions.

References

1. Shukla A, Fang JC, Puranam S, Jensen FR, Hammond PT. Hemostatic Multilayer Coatings. 2012;492–6.

2. Zhao X, Guo B, Wu H, Liang Y, Ma PX. Injectable antibacterial conductive nanocomposite cryogels with rapid shape recovery for noncompressible hemorrhage and wound healing. Nat Commun. 2018;9(1):1–17.

3. Hickman DSA, Pawlowski CL, Sekhon UDS, Marks J, Gupta A Sen. Biomaterials and Advanced Technologies for Hemostatic Management of Bleeding. Adv Mater. 2018;30(4):1–40.

4. Kauvar DS, Lefering R, Wade CE. Impact of hemorrhage on trauma outcome: An overview of epidemiology, clinical presentations, and therapeutic considerations. In: Journal of Trauma - Injury, Infection and Critical Care. 2006.

5. Yang X, Liu W, Li N, Wang M, Liang B, Ullah I, et al. Design and development of polysaccharide hemostatic materials and their hemostatic mechanism. Biomater Sci. 2017;5(12):2357–68.

6. Cheng F, Liu C, Wei X, Yan T, Li H, He J, et al. Preparation and Characterization of 2,2,6,6-Tetramethylpiperidine-1-oxyl (TEMPO)-Oxidized Cellulose Nanocrystal/Alginate Biodegradable Composite Dressing for Hemostasis Applications. ACS Sustain Chem Eng. 2017;5(5):3819–28.

7. Hu Z, Zhang DY, Lu ST, Li PW, Li SD. Chitosan-based composite materials for prospective hemostatic applications. Mar Drugs. 2018;16(8):1–25.

8. Lu B, Lin F, Jiang X, Cheng J, Lu Q, Song J, et al. One-Pot Assembly of Microfibrillated Cellulose Reinforced PVA-Borax Hydrogels with Self-Healing and pH-Responsive Properties. ACS Sustain Chem Eng. 2017 Jan 3;5(1):948–56.

9. Taylor DL, in het Panhuis M. Self-Healing Hydrogels. Vol. 28, Advanced Materials. Wiley-VCH Verlag; 2016. p. 9060–93.

10. Huang W, Wang Y, Chen Y, Zhao Y, Zhang Q, Zheng X, et al. Strong and Rapidly Self-Healing Hydrogels: Potential Hemostatic Materials. Adv Healthc Mater. 2016 Nov 9;5(21):2813–22.

11. Wei Z, Yang JH, Liu ZQ, Xu F, Zhou JX, Zrínyi M, et al. Novel biocompatible polysaccharide-based self-healing hydrogel. Adv Funct Mater. 2015 Mar 4;25(9):1352–9.

12. Zhang A, Liu Y, Qin D, Sun M, Wang T, Chen X. Research status of self-healing hydrogel for wound management: A review. Int J Biol Macromol [Internet]. 2020;164:2108–23. Available from: https://doi.org/10.1016/j.ijbiomac.2020.08.109

13. Zhang Y, Yang B, Zhang X, Xu L, Tao L, Li S, et al. A magnetic self-healing hydrogel. Chem Commun. 2012;48(74):9305–7.

14. De France KJ, Hoare T, Cranston ED. Review of Hydrogels and Aerogels Containing Nanocellulose. Chem Mater. 2017;29(11):4609–31.

15. Françon H, Wang Z, Marais A, Mystek K, Piper A, Granberg H, et al. Ambient-Dried, 3D-Printable and Electrically Conducting Cellulose Nanofiber Aerogels by Inclusion of Functional Polymers. Adv Funct Mater. 2020;

16. Wang D, Peng H, Yu B, Zhou K, Pan H, Zhang L, et al. Biomimetic structural cellulose nanofiber aerogels with exceptional mechanical, flame-retardant and thermal-insulating properties. Chem Eng J [Internet]. 2020;389(February):124449. Available from: https://doi.org/10.1016/j.cej.2020.124449

17. Fan X, Li Y, Li X, Wu Y, Tang K, Liu J, et al. Injectable antibacterial cellulose nanofiber/chitosan aerogel with rapid shape recovery for noncompressible hemorrhage. Int J Biol Macromol [Internet]. 2019;(xxxx). Available from: https://doi.org/10.1016/j.ijbiomac.2019.10.273

18. Hutchinson RW, George K, Johns D, Craven L, Zhang G, Shnoda P. Hemostatic efficacy and tissue reaction of oxidized regenerated cellulose hemostats. Cellulose. 2013;20(1):537–45.

19. Basu A, Hong J, Ferraz N. Hemocompatibility of Ca2+-Crosslinked Nanocellulose Hydrogels: Toward Efficient Management of Hemostasis. Macromol Biosci [Internet]. 2017 Nov 1 [cited 2020 Mar 25];17(11):1700236. Available from: http://doi.wiley.com/10.1002/mabi.201700236

20. Kanikireddy V, Varaprasad K, Jayaramudu T, Karthikeyan C, Sadiku R. Carboxymethyl cellulose-based materials for infection control and wound healing: A review. Vol. 164, International Journal of Biological Macromolecules. Elsevier B.V.; 2020. p. 963–75.

21. Nasibi S, Nargesi khoramabadi H, Arefian M, Hojjati M, Tajzad I, Mokhtarzade A, et al. A review of Polyvinyl alcohol / Carboxiy methyl cellulose (PVA/CMC) composites for various applications. J Compos Compd. 2020 May 1;2(3):68–75.

22. Vinklárková L, Masteiková R, Foltýnová G, Muselík J, Pavloková S, Bernatonienė J, et al. Film wound dressing with local anesthetic based on insoluble carboxymethycellulose matrix. J Appl Biomed. 2017 Nov 1;15(4):313–20.

23. Baik SH, Kim JH, Cho HH, Park SN, Kim YS, Suh H. Development and analysis of a collagen-based hemostatic adhesive. J Surg Res. 2010;164(2):221–8.

24. Arnaud F, Tomori T, Carr W, McKeague A, Teranishi K, Prusaczyk K, et al. Exothermic reaction in zeolite hemostatic dressings: QuikClot ACS and ACS+®. Ann Biomed Eng. 2008;36(10):1708–13.

25. Duong HM, Lim ZK, Nguyen TX, Gu B, Penefather MP, Phan-Thien N. Compressed hybrid cotton aerogels for stopping liquid leakage. Colloids Surfaces A Physicochem Eng Asp. 2018 Jan 20;537:502–7.

26. Hematology Glossary - Hematology.org [Internet]. [cited 2020 Apr 19]. Available from: https://www.hematology.org/education/patients/blood-basics

27. Behrens AM, Sikorski MJ, Kofinas P. Hemostatic strategies for traumatic and surgical bleeding. J Biomed Mater Res - Part A. 2014;102(11):4182–94.

28. Cheng X, Shao Z, Li C, Yu L, Raja MA, Liu C. Isolation , Characterization and Evaluation of Collagen from Jellyfish Rhopilema esculentum Kishinouye for Use in Hemostatic Applications. PLoS One. 2017;12(1):1–21.

29. Hajosch R, Suckfuell M, Oesser S, Ahlers M, Flechsenhar K. A novel gelatin sponge for accelerated hemostasis. J Biomed Mater Res Part B Appl Biomater. 2010;94(2):372–9.

30. Thomas A, Harding KG, Moore K. Alginates from wound dressings activate human macrophages to secrete tumour necrosis factor-α. Biomaterials. 2000;21(17):1797–802.

31. Lan G, Lu B, Wang T, Wang L, Chen J, Yu K, et al. Chitosan / gelatin composite sponge is an absorbable surgical hemostatic agent. Colloids surfaces B Biointerfaces. 2015;136:1026–34.

32. Liu X, Lin T, Gao Y, Xu Z, Huang C, Yao G, et al. Antimicrobial electrospun nanofibers of cellulose acetate and polyester urethane composite for wound dressing. J Biomed Mater Res - Part B Appl Biomater. 2012;100 B(6):1556–65.

33. Kai Jiang, Yun-Ze Long, Zhao-Jun Chen, Shu-Liang Liu, b Yuan-Yuan Huang XJ and Z-QH. Airflow-directed in situ electrospinning of a medical glue of cyanoacrylate for rapid hemostasis in liver resection. Nanoscale. 2014;6(14):7792–8.

34. Tomizawa Y. Clinical benefits and risk analysis of topical hemostats: A review. J Artif Organs. 2005;8(3):137–42.

35. Duarte AP, Coelho JF, Bordado JC, Cidade MT, Gil MH. Surgical adhesives: Systematic review of the main types and development forecast. Prog Polym Sci [Internet]. 2012;37(8):1031–50. Available from: http://dx.doi.org/10.1016/j.progpolymsci.2011.12.003

36. Ferreira1 CS, , Affonso Ferreira da Silva Caldas[2], Ana Paula Martinez de Abreu[2], Fábio Sartori[2] APF, Gustavo, Mendes Gomes[2], Kleber da Cunha Peixoto Jr.1 and André Maciel Crespilho1 2*. Evaluation of Nylon Cable Ties

as an Alternative Method of Preventive Hemostasis for Bovine Orchiectomy. Andrology-Open Access. 2015;04(02):2–5.

37. Itoi T, Yasuda I, Doi S, Mukai T, Kurihara T, Sofuni A. Endoscopic hemostasis using covered metallic stent placement for uncontrolled post-endoscopic sphincterotomy bleeding. Endoscopy. 2011;43(4):369–72.

38. Cho JH, Jun HS, Lee CN. Hemostatic suturing technique for uterine bleeding during cesarean delivery. Obstet Gynecol. 2000;96(1):129–31.

39. Maeda K, Maruta M, Utsumi T, Sato H, Aoyama H, Katsuno H, et al. Local correction of a transverse loop colostomy prolapse by means of a stapler device. Tech Coloproctol. 2004;8(1):45–6.

40. Annabi N, Tamayol A, Shin SR, Ghaemmaghami AM, Peppas NA, Khademhosseini A. Surgical materials: Current challenges and nano-enabled solutions. Nano Today [Internet]. 2014;9(5):574–89. Available from: http://dx.doi.org/10.1016/j.nantod.2014.09.006

41. Macario A, Dexter F, Sypal J, Cosgriff N, Heniford TB. Operative time and other outcomes of the electrothermal bipolar vessel sealing system (LigaSure™) versus other methods for surgical hemostasis: A meta-analysis. Surg Innov. 2008;15(4):284–91.

42. Shai, A. & Maibach HI. Wound Healing and Ulcers of the Skin. Vol. 53, Persepsi Masyarakat Terhadap Perawatan Ortodontik Yang Dilakukan Oleh Pihak Non Profesional. 2005. 1689–1699 p.

43. Dhillon S, De Boer MT, Papacharalabous EN, Schwartz M. Fibrin sealant (Evicel® [quixil®/crosseal™]): A review of its use as supportive treatment for haemostasis in surgery. Drugs. 2011;71(14):1893–915.

44. Schwartz M, Madariaga J, Hirose R, Shaver TR, Sher L, Chari R, et al. Comparison of a new fibrin sealant with standard topical hemostatic agents. Arch Surg. 2004;139(11):1148–54.

45. Bruno Monteiro Pereira, JoSé Benedito Bortoto1 GPF. Topical hemostatic agents in surgery: review and prospects. Rev Col Bras Cir. 2018;45(5):e1900–e1900.

46. The CELOX[tm] Advantage · Celox Hemostats [Internet]. [cited 2021 Mar 15]. Available from: https://www.celoxmedical.com/na/about-celox/

47. Otrocka-Domagała I, Jastrzębski P, Adamiak Z, Paździor-Czapula K, Gesek M, Mikiewicz M, et al. Safety of the long-term application of QuikClot Combat Gauze, ChitoGauze PRO and Celox Gauze in a femoral artery injury model in swine - A preliminary study. Pol J Vet Sci. 2016;19(2):337–43.

48. Product Introduction: The HemCon Bandage | Cath Lab Digest [Internet]. [cited 2021 Mar 15]. Available from: https://www.cathlabdigest.com/articles/Product-Introduction-The-HemCon-Bandage

49. Granville-Chapman J, Jacobs N, Midwinter MJ. Pre-hospital haemostatic dressings: A systematic review. Injury [Internet]. 2011;42(5):447–59. Available from: http://dx.doi.org/10.1016/j.injury.2010.09.037

50. Rousou JA, Engelman RM, Breyer RH. Fibrin Glue : An Effective Hemostatic Agent for Nonsuturable Intraoperative Bleeding. Ann Thorac Surg [Internet]. 1984;38(4):409–10. Available from: http://dx.doi.org/10.1016/S0003-4975(10)62297-7

51. Raccuia JS, Simonian G, Dardik M, Hallac D, Raccuia S V., Stahl R, et al. Comparative efficacy of topical hemostatic agents in a rat kidney model. Am J Surg. 1992;163(2):234–8.

52. Delgado A V, Kheirabadi BS, Fruchterman TM, Scherer M, Cortez D, Wade CE, et al. A Novel Biologic Hemostatic Dressing (Fibrin Patch) Reduces Blood Loss and Resuscitation Volume and Improves Survival in Hypothermic , Coagulopathic Swine With Grade V. J Trauma Acute Care Surg. 2008;64(1):75–80.

53. Krishnan LK, Mohanty M, Umashankar PR, Lal AV. Comparative evaluation of absorbable hemostats : advantages of fibrin-based sheets. 2004;25:5557–63.

54. Wheat JC, Wolf JS. Advances in Bioadhesives, Tissue Sealants, and Hemostatic Agents. Urol Clin North Am [Internet]. 2009;36(2):265–75. Available from: http://dx.doi.org/10.1016/j.ucl.2009.02.002

55. Li G, Quan K, Xu CC, Deng B, Wang X. Synergy in thrombin-graphene sponge for improved hemostatic efficacy and facile utilization. Colloids Surfaces B Biointerfaces [Internet]. 2018;161:27–34. Available from: http://dx.doi.org/10.1016/j.colsurfb.2017.10.021

56. Rothwell SW, Settle T, Wallace S, Dorsey J, Simpson D, Bowman JR, et al. The long term immunological response of swine after two exposures to a salmon thrombin and fibrinogen hemostatic bandage. Biologicals [Internet]. 2010;38(6):619–28. Available from: http://dx.doi.org/10.1016/j.biologicals.2010.07.001

57. Prockop DJ. Collagens: Molecular Biology, Diseases, and Potentials for Therapy. Annu Rev Biochem. 1995;64(1):403–34.

58. Morgenstern L. Microcrystalline Collagen Used in Experimental Splenic Injury. Arch Surg. 1974;109(1):44.

59. Liang Y, Xu C, Li G, Liu T, Liang JF, Wang X. Graphene-kaolin composite sponge for rapid and riskless hemostasis. Colloids Surfaces B Biointerfaces [Internet]. 2018;169(April 2008):168–75. Available from: https://doi.org/10.1016/j.colsurfb.2018.05.016

60. Li J, Cao W, Lv XX, Jiang L, Li YJ, Li WZ, et al. Zeolite-based hemostat QuikClot releases calcium into blood and promotes blood coagulation in vitro. Acta Pharmacol Sin. 2013;34(3):367–72.

61. Alam HB, Chen Z, Jaskille A, Querol RILC, Koustova E, Inocencio R, et al. Application of a zeolite hemostatic agent achieves 100% survival in a lethal model of complex groin injury in swine. J Trauma - Inj Infect Crit Care. 2004;56(5):974–83.

62. Pusateri AE, Delgado A V., Dick EJ, Martinez RS, Holcomb JB, Ryan KL. Application of a granular mineral-based hemostatic agent (QuikClot) to reduce blood loss after grade V liver injury in swine. J Trauma - Inj Infect Crit Care. 2004;57(3):555–62.

63. Li Y, Li H, Xiao L, Zhou L, Shentu J, Zhang X, et al. Hemostatic Efficiency and Wound Healing Properties of Natural Zeolite Granules in a Lethal Rabbit Model of Complex Groin Injury. 2012;2586–96.

64. Juliana Bergamasco L, Zazeri G, Paula A, Povinelli R, Fernandes M, Godoy D, et al. Enhanced pro-coagulant hemostatic agents based on nanometric zeolites. Microporous Mesoporous Mater. 2017;239:263–71.

65. Sun X, Tang Z, Pan M, Wang Z, Yang H, Liu H. Chitosan/kaolin composite porous microspheres with high hemostatic efficacy. Carbohydr Polym [Internet]. 2017;177(August):135–43. Available from: https://doi.org/10.1016/j.carbpol.2017.08.131

66. Fan L, Yang H, Yang J, Peng M, Hu J. Preparation and characterization of chitosan / gelatin / PVA hydrogel for wound dressings. Carbohydr Polym [Internet]. 2016;146:427–34. Available from: http://dx.doi.org/10.1016/j.carbpol.2016.03.002

67. Djagny KB, Wang Z, Xu S, Djagny KB, Wang Z, Xu S. Gelatin : A Valuable Protein for Food and Pharmaceutical Industries : Review. Crit Rev Food Sci Nutr ISSN. 2010;8398:481–92.

68. Liu Y, Kopelman D, Wu LQ, Hijji K, Attar I, Preiss-Bloom O, et al. Biomimetic sealant based on gelatin and microbial transglutaminase: An initial in vivo investigation. J Biomed Mater Res - Part B Appl Biomater. 2009;91(1):5–16.

69. Lena F. Hemostatic polymers: the concept, state of the art and perspectives. 2014;3567–77.

70. Janvikul W, Uppanan P, Thavornyutikarn B, Krewraing J, Prateepasen R. In Vitro Comparative Hemostatic Studies of Chitin , Chitosan , and Their Derivatives. 2006;

71. Koumentakou I, Terzopoulou Z, Michopoulou A, Kalafatakis I, Theodorakis K, Tzetzis D, et al. Chitosan dressings containing inorganic additives and levofloxacin as potential wound care products with enhanced hemostatic

properties. Int J Biol Macromol [Internet]. 2020;162:693–703. Available from: https://doi.org/10.1016/j.ijbiomac.2020.06.187

72. Maevskaia EN, Shabunin AS, Dresvyanina EN, Dobrovol'skaya IP, Yudin VE, Paneyah MB, et al. Influence of the introduced chitin nanofibrils on biomedical properties of chitosan-based materials. Nanomaterials. 2020;10(5).

73. Spazierer KMLD, Lin MDUL, Goppelt HRA. Comparison of regenerated and non-regenerated oxidized cellulose hemostatic agents. 2013;213–20.

74. Leggat PA, Smith DR, Kedjarune U. Surgical applications of cyanoacrylate adhesives: A review of toxicity. Vol. 77, ANZ Journal of Surgery. 2007. p. 209–13.

75. Emilia M, Luca S, Francesca B, Luca B, Paolo S, Giuseppe F, et al. Topical hemostatic agents in surgical practice. Transfus Apher Sci. 2011;45(3):305–11.

76. Spotnitz WD, Burks S. Hemostats, sealants, and adhesives: Components of the surgical toolbox. Transfusion. 2008;48(7):1502–16.

77. Gordy SD, Rhee P, Schreiber MA. Military applications of novel hemostatic devices. Expert Rev Med Devices. 2011;8(1):41–7.

78. Sundaram CP, Keenan AC. Evolution of hemostatic agents in surgical practice. Indian J Urol. 2010;26(3):374–8.

79. Vyas KS, Saha SP. Comparison of hemostatic agents used in vascular surgery. Expert Opin Biol Ther. 2013;13(12):1663–72.

80. Ibrahim NA, Abo-Shosha MH, Gaffar MA, Elshafei AM, Abdel-Fatah OM. Antibacterial properties of ester - Cross-linked cellulose-containing fabrics post-treated with metal salts. Polym - Plast Technol Eng. 2006;45(6):719–27.

81. Shin JU, Gwon J, Lee SY, Yoo HS. Silver-Incorporated Nanocellulose Fibers for Antibacterial Hydrogels. ACS Omega. 2018;3(11):16150–7.

82. Shi G, Wang Y, Derakhshanfar S, Xu K, Zhong W, Luo G, et al. Biomimicry of oil infused layer on 3D printed poly(dimethylsiloxane): Non-fouling, antibacterial and promoting infected wound healing. Mater Sci Eng C [Internet]. 2019;100(November 2017):915–27. Available from: https://doi.org/10.1016/j.msec.2019.03.058

83. Liu T, Liu Y, Liu M, Wang Y, He W, Shi G, et al. Synthesis of graphene oxide-quaternary ammonium nanocomposite with synergistic antibacterial activity to promote infected wound healing. Burn Trauma. 2018;6:1–23.

84. Bu-Peng Ding, Fang Wu, Si-Chong Chen, Yu-Zhong Wang J-BZ. Synthesis and characterization of polyurethane ionene/zinc chloride complex with antibacterial property. RSC Adcances [Internet]. 2015;5(16):12423–33. Available from: http://xlink.rsc.org/?DOI=C5TC02043C

85. Fajardo AR, Lopes LC, Caleare AO, Britta EA, Nakamura C V., Rubira AF, et al. Silver sulfadiazine loaded chitosan/chondroitin sulfate films for a potential wound dressing application. Mater Sci Eng C [Internet]. 2013;33(2):588–95. Available from: http://dx.doi.org/10.1016/j.msec.2012.09.025

86. Li H, Cheng F, Gao S, Wu Z, Dong L, Lin S, et al. Preparation, characterization, antibacterial properties, and hemostatic evaluation of

ibuprofen-loaded chitosan/gelatin composite films. J Appl Polym Sci. 2017;134(42):1–9.

87. Du WL, Niu SS, Xu YL, Xu ZR, Fan CL. Antibacterial activity of chitosan tripolyphosphate nanoparticles loaded with various metal ions. Carbohydr Polym [Internet]. 2009;75(3):385–9. Available from: http://dx.doi.org/10.1016/j.carbpol.2008.07.039

88. Hou Y, Xia Y, Pan Y, Tang S, Sun X, Xie Y, et al. Influences of mesoporous zinc-calcium silicate on water absorption , degradability , antibacterial efficacy , hemostatic performances and cell viability to microporous starch based hemostat. Mater Sci Eng C [Internet]. 2017;76:340–9. Available from: http://dx.doi.org/10.1016/j.msec.2017.03.094

89. Vaidya MY, McBain AJ, Butler JA, Banks CE, Whitehead KA. Antimicrobial Efficacy and Synergy of Metal Ions against Enterococcus faecium, Klebsiella pneumoniae and Acinetobacter baumannii in Planktonic and Biofilm Phenotypes. Sci Rep [Internet]. 2017;7(1):1–9. Available from: http://dx.doi.org/10.1038/s41598-017-05976-9

90. Kang J, Dietz MJ, Hughes K, Xing M, Li B. Silver nanoparticles present high intracellular and extracellular killing against Staphylococcus aureus. J Antimicrob Chemother. 2019;74(6):1578–85.

91. Liu M, Wang Y, Hu X, He W, Gong Y, Hu X, et al. Janus N,N-dimethylformamide as a solvent for a gradient porous wound dressing of poly(vinylidene fluoride) and as a reducer for in situ nano-silver production: anti-permeation, antibacterial and antifouling activities against multi-drug-resistant bacteria. RSC Adv. 2018;8(47):26626–39.

92. Chen G, Yu Y, Wu X, Wang G, Gu G, Wang F, et al. Microfluidic Electrospray Niacin Metal-Organic Frameworks Encapsulated Microcapsules for Wound Healing. Research. 2019;2019:1–11.

93. Xie T, Ding J, Han X, Jia H, Yang Y, Liang S, et al. Wound dressing change facilitated by spraying zinc ions. Mater Horizons [Internet]. 2020;7(2):605–14. Available from: http://dx.doi.org/10.1039/C9MH01255A

94. Bi D. Antibacterial hemostatic dressings with nanoporous bioglass containing silver. 2012;2613–20.

95. Pourshahrestani S, Zeimaran E, Kadri A, Gargiulo N, Towler MR. Gallium-containing mesoporous bioactive glass with potent hemostatic activity and antibacterial efficacy. 2016;71–86.

96. Guo-dong F, Fang Y, Zhigang L, Xinsong L. Solvent-resistant antibacterial microfibers of self-quaternized block copolymers from atom transfer radical polymerization and electrospinning. 2008;859–67.

97. Spasova M, Manolova N, Paneva D, Mincheva R, Dubois P, Rashkov I, et al. Polylactide stereocomplex-based electrospun materials possessing surface with antibacterial and hemostatic properties. Biomacromolecules. 2010;11(1):151–9.

98. Demirekin ZB, Sezer UA, Karatopuk DU, Sezer S. Development of Metal Ion Binded Oxidized Regenerated Cellulose Powder as Hemostatic Agent: A Comparative Study with in Vivo Performance. Ind Eng Chem Res. 2015;54(18):4906–14.

99. He JM, Wu YD, Wang FW, Cheng WL, Huang YD, Fu B. Hemostatic, antibacterial and degradable performance of the water-soluble chitosan-coated oxidized regenerated cellulose gauze. Fibers Polym. 2014;15(3):504–9.

100. Drelich J, Chibowski E. Superhydrophilic and superwetting surfaces: Definition and mechanisms of control. Langmuir. 2010;26(24):18621–3.

101. Lavieja C, Oriol L, Peña JI. Creation of superhydrophobic and superhydrophilic surfaces on ABS employing a nanosecond laser. Materials (Basel). 2018;11(12).

102. Si Y, Dong Z, Jiang L. Bioinspired Designs of Superhydrophobic and Superhydrophilic Materials. ACS Cent Sci. 2018;4(9):1102–12.

103. Barthlott W, Neinhuis C. Purity of the sacred lotus, or escape from contamination in biological surfaces. Planta. 1997;202(1):1–8.

104. Lin Feng, Shuhong Li, Yingshun Li, Huanjun Li, Lingjuan Zhang, Jin Zhai, Yanlin Song, Biqian Liu, Lei Jiang and DZ. Super-Hydrophobic Surfaces : From Natural to Artificial Super-Hydrophobic Surfaces : From Natural to Artificial **. 2002;(October):1857–60.

105. Liu M, Wang S, Wei Z, Song Y, Jiang L. Bioinspired design of a superoleophobic and low adhesive water/solid interface. Adv Mater. 2009;21(6):665–9.

106. Roach P, Shirtcliffe NJ, Newton MI. Progess in superhydrophobic surface development. Soft Matter. 2008;4(2):224.

107. Ueda E, Levkin PA. Emerging applications of superhydrophilic-superhydrophobic micropatterns. Adv Mater. 2013;25(9):1234–47.

108. Wang Y, Liu Y, Liu M, Qian W, Zhou D, Liu T, et al. Short fluorocarbon chains containing hydrophobic nanofibrous membranes with improved hemocompatibility, anticoagulation and anti-fouling performance. Colloids

Surfaces B Biointerfaces [Internet]. 2019;180(April 2018):49–57. Available from: https://doi.org/10.1016/j.colsurfb.2019.01.025

109. Fischer M, Sperling C, Werner C. Synergistic effect of hydrophobic and anionic surface groups triggers blood coagulation in vitro. J Mater Sci Mater Med. 2010;21(3):931–7.

110. Zhu T, Wu J, Zhao N, Cai C, Qian Z, Si F, et al. Superhydrophobic/Superhydrophilic Janus Fabrics Reducing Blood Loss. Adv Healthc Mater. 2018;7(7):1–7.

111. Cui C, Fan C, Wu Y, Xiao M, Wu T, Zhang D, et al. Water-Triggered Hyperbranched Polymer Universal Adhesives: From Strong Underwater Adhesion to Rapid Sealing Hemostasis. Adv Mater. 2019;31(49):1–9.

112. Li Z, Milionis A, Zheng Y, Yee M, Codispoti L, Tan F, et al. Superhydrophobic hemostatic nanofiber composites for fast clotting and minimal adhesion. Nat Commun. 2019;10(1).

113. Dowling MB, Kumar R, Keibler MA, Hess JR, Bochicchio G V., Raghavan SR. A self-assembling hydrophobically modified chitosan capable of reversible hemostatic action. Biomaterials [Internet]. 2011;32(13):3351–7. Available from: http://dx.doi.org/10.1016/j.biomaterials.2010.12.033

114. Aizenberg J, Fratzl P. Biological and biomimetic materials. Adv Mater. 2009;21(4):387–8.

115. Fratzl P. Biomimetic materials research: What can we really learn from nature's structural materials? J R Soc Interface. 2007;4(15):637–42.

116. Ma PX. Biomimetic materials for tissue engineering. Adv Drug Deliv Rev. 2008;60(2):184–98.

117. Shin H, Jo S, Mikos AG. Biomimetic materials for tissue engineering. Biomaterials. 2003;24(24):4353–64.

118. Silvestri A, Boffito M, Sartori S, Ciardelli G. Biomimetic materials and scaffolds for myocardial tissue regeneration. Macromol Biosci. 2013;13(8):984–1019.

119. Spinks GM. Advanced Actuator Materials Powered by Biomimetic Helical Fiber Topologies. Adv Mater. 2019;1904093:1–13.

120. Liu G, Zhao X, Zhang Y, Xu J, Xu J, Li Y, et al. Engineering Biomimetic Platesomes for pH-Responsive Drug Delivery and Enhanced Antitumor Activity. Adv Mater. 2019;31(32):1–12.

121. Jiang J, Huang Y, Wang Y, Xu H, Xing M, Zhong W. Mussel-inspired dopamine and carbon nanotube leading to a biocompatible self-rolling conductive hydrogel film. Materials (Basel). 2017;10(8).

122. Majumder A, Sharma A, Ghatak A. A bioinspired wet/dry microfluidic adhesive for aqueous environments. Langmuir. 2010;26(1):521–5.

123. Kamino K. Underwater Adhesive of Marine Organisms as the Vital Link Between Biological Science and Material Science. 2008. p. 111–21.

124. Liu C, Yao W, Tian M, Wei J, Song Q, Qiao W. Mussel-inspired degradable antibacterial polydopamine / silica nanoparticle for rapid hemostasis. Biomaterials [Internet]. 2018;179:83–95. Available from: https://doi.org/10.1016/j.biomaterials.2018.06.037

125. Akdogan Y, Wei W, Huang KY, Kageyama Y, Danner EW, Miller DR, et al. Intrinsic Surface-Drying Properties of Bioadhesive Proteins. Angew Chemie - Int Ed. 2014;53(42):11253–6.

126. Lu D, Wang H, Wang X, Li Y, Guo H, Sun S, et al. Biomimetic chitosan-graft-polypeptides for improved adhesion in tissue and metal. Carbohydr Polym [Internet]. 2019;215:20–8. Available from: https://doi.org/10.1016/j.carbpol.2019.03.065

127. Autumn K, Liang YA, Hsieh ST, Zesch W, Chan WP, Kenny TW, et al. Adhesive force of a single gecko foot-hair. Nature. 2000;405(6787):681–5.

128. Mahdavi A, Ferreira L, Sundback C, Nichol JW, Chan EP, Carter DJD, et al. A biodegradable and biocompatible gecko-inspired tissue adhesive. Proc Natl Acad Sci U S A. 2008;105(7):2307–12.

129. Moorleghem W Van, Chandrasekaran M, Reynaerts D, Peirs J, Brussel H Van. Shape memory and superelastic alloys : The new medical materials with growing demand. 1998;8:55–60.

130. Qiu L, Liu JZ, Chang SLY, Wu Y, Li D. Biomimetic superelastic graphene-based cellular monoliths. Nat Commun. 2012;3:1–7.

131. Talyzin A V., Dubrovinsky LS, Oden M, Jansson U. Superhard and superelastic films of polymeric C60. Diam Relat Mater. 2001;10(11):2044–8.

132. Auriemma F, De Rosa C, Esposito S, Mitchell GR. Polymorphic superelasticity in semicrystalline polymers. Angew Chemie - Int Ed. 2007;46(23):4325–8.

133. Yu ZL, Qin B, Ma ZY, Huang J, Li SC, Zhao HY, et al. Superelastic Hard Carbon Nanofiber Aerogels. Adv Mater. 2019;31(23):1–9.

134. Li C, Ding YW, Hu BC, Wu ZY, Gao HL, Liang HW, et al. Temperature-Invariant Superelastic and Fatigue Resistant Carbon Nanofiber Aerogels. Adv Mater. 2020;32(2):1–7.

135. Li Y, Cao L, Yin X, Si Y, Yu J, Ding B. Semi-Interpenetrating Polymer Network Biomimetic Structure Enables Superelastic and Thermostable Nanofibrous Aerogels for Cascade Filtration of PM2.5. Adv Funct Mater. 2020;30(14):1–11.

136. Zhang Z, Deng J, Li X, Yang Z, He S, Chen X, et al. Superelastic Supercapacitors with High Performances during Stretching. 2015;356–62.

137. Mathieu L, Bazile F, Barthélémy R, Duhamel P, Rigal S. Damage control orthopaedics in the context of battlefield injuries : The use of temporary external fixation on combat trauma soldiers. Orthop Traumatol Surg Res [Internet]. 2011;97(8):852–9. Available from: http://dx.doi.org/10.1016/j.otsr.2011.05.014

138. Sixiang Li, Le Wang, Wenfu Zheng, Guang Yang and XJ. Rapid Fabrication of Self-Healing, Conductive, and Injectable Gel as Dressings for Healing Wounds in Stretchable Parts of the Body. Adv Funct Mater. 2020;2002370.

139. Zhao X, Wu H, Guo B, Dong R, Qiu Y, Ma PX. Antibacterial anti-oxidant electroactive injectable hydrogel as self- healing wound dressing with hemostasis and adhesiveness for cutaneous wound healing. Biomaterials [Internet]. 2017;122:34–47. Available from: http://dx.doi.org/10.1016/j.biomaterials.2017.01.011

140. Jang LK, Fletcher GK, Monroe MBB, Maitland DJ. Biodegradable shape memory polymer foams with appropriate thermal properties for hemostatic applications. 2020;(May 2019):1281–94.

141. Françon H, Wang Z, Marais A, Mystek K, Piper A, Granberg H, et al. Ambient-Dried, 3D-Printable and Electrically Conducting Cellulose Nanofiber Aerogels by Inclusion of Functional Polymers. Adv Funct Mater. 2020;30(12).

142. Maleki H, Durães L, Portugal A. An overview on silica aerogels synthesis and different mechanical reinforcing strategies. J Non Cryst Solids [Internet]. 2014;385:55–74. Available from: http://dx.doi.org/10.1016/j.jnoncrysol.2013.10.017

143. Cui Y, Wang Y, Shao Z, Mao A, Gao W, Bai H. Smart Sponge for Fast Liquid Absorption and Thermal Responsive Self-Squeezing. Adv Mater. 2020;32(14):1–9.

144. Heath L, Thielemans W. Cellulose nanowhisker aerogels. Green Chem. 2010;12(8):1448–53.

145. Sun H, Xu Z, Gao C. Multifunctional, ultra-flyweight, synergistically assembled carbon aerogels. Adv Mater. 2013;25(18):2554–60.

146. Shao G, Hanaor DAH, Shen X, Gurlo A. Freeze Casting: From Low-Dimensional Building Blocks to Aligned Porous Structures—A Review of Novel Materials, Methods, and Applications. Adv Mater. 2020;1907176.

147. Biener J, Stadermann M, Suss M, Worsley MA, Biener MM, Rose KA, et al. Advanced carbon aerogels for energy applications. Energy Environ Sci. 2011;4(3):656–67.

148. García-González CA, Alnaief M, Smirnova I. Polysaccharide-based aerogels - Promising biodegradable carriers for drug delivery systems. Carbohydr Polym. 2011;86(4):1425–38.

149. Wang L, Zhang X, He Y, Wang Y, Zhong W, Mequanint K, et al. Ultralight Conductive and Elastic Aerogel for Skeletal Muscle Atrophy Regeneration. Adv Funct Mater. 2019;29(1):1–17.

150. Zhang Q, Zhang F, Medarametla SP, Li H, Zhou C, Lin D. 3D Printing of Graphene Aerogels. Small. 2016;12(13):1702–8.

151. Mellado C, Figueroa T, Ba R, Castillo R, Melendrez M, Schulz B, et al. Development of Graphene Oxide Composite Aerogel with Proanthocyanidins with Hemostatic Properties As a Delivery System. 2018;

152. Lu T, Li Q, Chen W, Yu H. Composite aerogels based on dialdehyde nanocellulose and collagen for potential applications as wound dressing and tissue engineering scaffold. Compos Sci Technol [Internet]. 2014;94:132–8. Available from: http://dx.doi.org/10.1016/j.compscitech.2014.01.020

153. Vlieghe P, Lisowski V, Martinez J, Khrestchatisky M. Synthetic therapeutic peptides : science and market. 2010;15(January).

154. Bahar AA, Ren D. Antimicrobial Peptides. 2013;1543–75.

155. Zhang S, Marini DM, Hwang W, Santoso S. Design of nanostructured biological materials through self-assembly of peptides and proteins. 2002;865–71.

156. Ellis-behnke R. At the nanoscale : nanohemostat , a new class of hemostatic agent. 2011;

157. Hsu BB, Conway W, Tschabrunn CM, Mehta M, Perez-Cuevas MB, Zhang S, et al. Clotting Mimicry from Robust Hemostatic Bandages Based on Self-Assembling Peptides. ACS Nano. 2015;9(9):9394–406.

158. Song H, Zhang L, Zhao X. Hemostatic Efficacy of Biological Self- Assembling Peptide Nanofibers in a Rat Kidney Model. 2010;33–9.

159. Kumar VA, Taylor NL, Jalan AA, Hwang LK, Wang BK, Hartgerink JD. A nanostructured synthetic collagen mimic for hemostasis. Biomacromolecules. 2014;15(4):1484–90.

160. Soni B, Hassan EB, Mahmoud B. Chemical isolation and characterization of different cellulose nanofibers from cotton stalks. Carbohydr Polym. 2015 Aug 24;134:581–9.

161. Fiedot-Toboła M, Ciesielska M, Maliszewska I, Rac-Rumijowska O, Suchorska-Woźniak P, Teterycz H, et al. Deposition of zinc oxide on different polymer textiles and their antibacterial properties. Materials (Basel). 2018 Apr 30;11(5).

162. Praglowska J, Piątkowski M, Janus Ł, Korniienko V, Husak E, Holubnycha V, et al. Chitosan-Based Bioactive Hemostatic Agents with Antibacterial Properties—Synthesis and Characterization. Molecules. 2019;24:17.

163. Wang Y, Yin M, Zheng X, Li W, Ren X. Chitosan/mesoporous silica hybrid aerogel with bactericidal properties as hemostatic material. Eur Polym J. 2021 Jan 5;142.

164. Cao S, Yang Y, Zhang S, Liu K, Chen J. Multifunctional dopamine modification of green antibacterial hemostatic sponge. Mater Sci Eng C

[Internet]. 2021;127(April):112227. Available from: https://doi.org/10.1016/j.msec.2021.112227

165. Yang X, Cranston ED. Chemically cross-linked cellulose nanocrystal aerogels with shape recovery and superabsorbent properties. Chem Mater. 2014;26(20):6016–25.

166. Wågberg L, Decher G, Norgren M, Lindström T, Ankerfors M, Axnäs K. The build-up of polyelectrolyte multilayers of microfibrillated cellulose and cationic polyelectrolytes. Langmuir. 2008;24(3):784–95.

167. Jiang F, Hsieh Y Lo. Super water absorbing and shape memory nanocellulose aerogels from TEMPO-oxidized cellulose nanofibrils via cyclic freezing-thawing. J Mater Chem A. 2014;2(2):350–9.

168. Ramli S, Ja'afar SM, Sisak MAA, Zainuddin N, Rahman IA. Formulation and physical characterization of microemulsions based carboxymethyl cellulose as vitamin c carrier. Malaysian J Anal Sci. 2015;19(1):275–83.

169. Onyianta AJ, Dorris M, Williams RL. Aqueous morpholine pre-treatment in cellulose nanofibril (CNF) production: comparison with carboxymethylation and TEMPO oxidisation pre-treatment methods. Cellulose. 2018 Feb 1;25(2):1047–64.

170. Maver T, Hribernik S, Mohan T, Smrke DM, Maver U, Stana-Kleinschek K. Functional wound dressing materials with highly tunable drug release properties. RSC Adv. 2015 Sep 9;5(95):77873–84.

171. Zhang A, Zou Y, Xi Y, Wang P, Zhang Y, Wu L, et al. Fabrication and characterization of bamboo shoot cellulose/sodium alginate composite aerogels for sustained release of curcumin. Int J Biol Macromol [Internet].

2021;192(October):904–12. Available from: https://doi.org/10.1016/j.ijbiomac.2021.10.027

172. Hossen MR, Dadoo N, Holomakoff DG, Co A, Gramlich WM, Mason MD. Wet stable and mechanically robust cellulose nanofibrils (CNF) based hydrogel. Polymer (Guildf). 2018 Aug 29;151:231–41.

173. Tajvidi M, Falk RH, Hermanson JC. Effect of natural fibers on thermal and mechanical properties of natural fiber polypropylene composites studied by dynamic mechanical analysis. J Appl Polym Sci. 2006;101(6):4341–9.

174. Ochbaum G, Davidovich-Pinhas M, Bitton R. Tuning the mechanical properties of alginate-peptide hydrogels. Soft Matter. 2018;14(21):4364–73.

175. Baniasadi M, Minary-Jolandan M. Alginate-collagen fibril composite hydrogel. Materials (Basel). 2015;8(2):799–814.

176. Pang L, Sun P, Dong X, Tang T, Chen Y, Liu Q, et al. Shear viscoelasticity of electrospinning PCL nanofibers reinforced alginate hydrogels. Mater Res Express. 2021;8(5).

177. Zhu C, Han TYJ, Duoss EB, Golobic AM, Kuntz JD, Spadaccini CM, et al. Highly compressible 3D periodic graphene aerogel microlattices. Nat Commun. 2015;6:1–8.

178. Wang H, Zhang X, Wang N, Li Y, Feng X, Huang Y, et al. Ceramic Nanofiber Sponges. Sci Adv. 2017;(June):1–10.

179. Si Y, Wang X, Dou L, Yu J, Ding B. Ultralight and fire-resistant ceramic nanofibrous aerogels with temperature-invariant superelasticity. Sci Adv. 2018;4(4).

180. Bai Y, Deng Y, Zheng Y, Li Y, Zhang R, Lv Y, et al. Characterization, corrosion behavior, cellular response and in vivo bone tissue compatibility of titanium-niobium alloy with low Young's modulus. Mater Sci Eng C [Internet]. 2016;59:565–76. Available from: http://dx.doi.org/10.1016/j.msec.2015.10.062

181. Zou Y, Liu PX, Cheng Q, Lai P, Li C. A New Deformation Model of Biological Tissue for Surgery Simulation. IEEE Trans Cybern. 2017;47(11):3494–503.

182. Kim HN, Kang DH, Kim MS, Jiao A, Kim DH, Suh KY. Patterning methods for polymers in cell and tissue engineering. Ann Biomed Eng. 2012;40(6):1339–55.

183. Yang J, Xia Y, Xu P, Chen B. Super-elastic and highly hydrophobic/superoleophilic sodium alginate/cellulose aerogel for oil/water separation. Cellulose [Internet]. 2018;25(6):3533–44. Available from: https://doi.org/10.1007/s10570-018-1801-8

184. Jia J, Wang C. A facile restructuring of 3D high water absorption aerogels from methoxy polyethylene glycol-polycaprolactone (mPEG-PCL) nanofibers. Mater Sci Eng C [Internet]. 2019;94(August 2017):965–75. Available from: https://doi.org/10.1016/j.msec.2018.10.044

185. Liu X, Hou M, Luo X, Zheng M, Wang X, Zhang H, et al. Thermoresponsive Hemostatic Hydrogel with a Biomimetic Nanostructure Constructed from Aggregated Collagen Nanofibers. Biomacromolecules. 2021 Feb 8;22(2):319–29.

186. Liu C, Shi Z, Sun H, Mujuni CJ, Zhao L, Wang X, et al. Preparation and characterization of tissue-factor-loaded alginate: Toward a bioactive hemostatic material. Carbohydr Polym. 2020 Dec 1;249.

187. Zhang W, Wu J, Yu L, Chen H, Li D, Shi C, et al. Paraffin-Coated Hydrophobic Hemostatic Zeolite Gauze for Rapid Coagulation with Minimal Adhesion. ACS Appl Mater Interfaces. 2021 Nov 10;13(44):52174–80.

188. Bonanno AM, Graham TL, Wilson LN, Ross JD. Novel use of XSTAT 30 for mitigation of lethal non-compressible torso hemorrhage in swine. PLoS One. 2020 Nov 1;15(11 November).

189. Morgan GJ, Waragai T, Eastaugh L, Chaturvedi RC, Lee KJ, Benson L. The fellows stitch: Large caliber venous hemostasis in pediatric practice. Catheter Cardiovasc Interv. 2012 Jul 1;80(1):79–82.

190. Luo J, Meng Y, Zheng L, Xu K, Li C. Fabrication and characterization of Chinese giant salamander skin composite collagen sponge as a high-strength rapid hemostatic material. J Biomater Sci Polym Ed. 2019;30(4):247–62.

191. Yu P, Zhong W. Hemostatic materials in wound care. Vol. 9, Burns and Trauma. Oxford University Press; 2021.

192. Emilia M, Luca S, Francesca B, Luca B, Paolo S, Giuseppe F, et al. Topical hemostatic agents in surgical practice. Transfus Apher Sci [Internet]. 2011;45(3):305–11. Available from: http://dx.doi.org/10.1016/j.transci.2011.10.013

193. Cheng X, Shao Z, Li C, Yu L, Raja MA, Liu C. Isolation, characterization and evaluation of collagen from jellyfish Rhopilema esculentum kishinouye for use in hemostatic applications. PLoS One. 2017;12(1).

194. Lee KY, Mooney DJ. Alginate: Properties and biomedical applications. Prog Polym Sci [Internet]. 2012;37(1):106–26. Available from: http://dx.doi.org/10.1016/j.progpolymsci.2011.06.003

195. Catanzano O, D'Esposito V, Acierno S, Ambrosio MR, De Caro C, Avagliano C, et al. Alginate-hyaluronan composite hydrogels accelerate wound healing process. Carbohydr Polym [Internet]. 2015;131:407–14. Available from: http://dx.doi.org/10.1016/j.carbpol.2015.05.081

196. Kaklamani G, Cheneler D, Grover LM, Adams MJ, Bowen J. Mechanical properties of alginate hydrogels manufactured using external gelation. J Mech Behav Biomed Mater. 2014;36:135–42.

197. Zhang S, Li J, Chen S, Zhang X, Ma J, He J. Oxidized cellulose-based hemostatic materials. Carbohydr Polym [Internet]. 2020;230(November 2019):115585. Available from: https://doi.org/10.1016/j.carbpol.2019.115585

198. Huang H, Chen H, Wang X, Qiu F, Liu H, Lu J, et al. Degradable and Bioadhesive Alginate-Based Composites: An Effective Hemostatic Agent. ACS Biomater Sci Eng. 2019;5(10):5498–505.

199. Beaman HT, Shepherd E, Satalin J, Blair S, Ramcharran H, Serinelli S, et al. Hemostatic shape memory polymer foams with improved survival in a lethal traumatic hemorrhage model. Acta Biomater. 2022;137:112–23.

200. Kohn J. Tissue Engineering: An Overview. MRS Bull. 1996;21(11):18–21.

201. Han L, Yan L, Wang K, Fang L, Zhang H, Tang Y, et al. Tough, self-healable and tissue-adhesive hydrogel with tunable multifunctionality. NPG Asia Mater. 2017;9(4).

202. Lim C, Hong YJ, Jung J, Shin Y, Sunwoo SH, Baik S, et al. Tissue-like skin-device interface for wearable bioelectronics by using ultrasoft, mass-permeable, and low-impedance hydrogels. Sci Adv. 2021;7(19):1–12.

203. Huang W, Wang Y, Chen Y, Zhao Y, Zhang Q, Zheng X, et al. Strong and Rapidly Self-Healing Hydrogels : Potential Hemostatic Materials. 2016;2813–22.

204. Taleb MFA, El-Mohdy HLA, El-Rehim HAA. Radiation preparation of PVA/CMC copolymers and their application in removal of dyes. J Hazard Mater. 2009 Aug 30;168(1):68–75.

205. Qu J, Zhao X, Liang Y, Zhang T, Ma PX, Guo B. Antibacterial adhesive injectable hydrogels with rapid self-healing, extensibility and compressibility as wound dressing for joints skin wound healing. Biomaterials [Internet]. 2018;183(August 2018):185–99. Available from: https://doi.org/10.1016/j.biomaterials.2018.08.044

206. Chen X. Making Electrodes Stretchable. Small Methods. 2017;1(4):1600029.

207. Tamer TM, Sabet MM, Omer AM, Abbas E, Eid AI, Mohy-Eldin MS, et al. Hemostatic and antibacterial PVA/Kaolin composite sponges loaded with penicillin–streptomycin for wound dressing applications. Sci Rep. 2021 Dec 1;11(1).

208. Golafshan N, Rezahasani R, Tarkesh Esfahani M, Kharaziha M, Khorasani SN. Nanohybrid hydrogels of laponite: PVA-Alginate as a potential wound healing material. Carbohydr Polym. 2017 Nov 15;176:392–401.

209. Wu G, Jin K, Liu L, Zhang H. A rapid self-healing hydrogel based on PVA and sodium alginate with conductive and cold-resistant properties. Soft Matter. 2020;16(13):3319–24.

210. Ai J, Li K, Li J, Yu F, Ma J. Super flexible, fatigue resistant, self-healing PVA/xylan/borax hydrogel with dual-crosslinked network. Int J Biol Macromol [Internet]. 2021;172:66–73. Available from: https://doi.org/10.1016/j.ijbiomac.2021.01.038

211. Samadi N, Sabzi M, Babaahmadi M. Self-healing and tough hydrogels with physically cross-linked triple networks based on Agar/PVA/Graphene. Int J Biol Macromol [Internet]. 2018;107:2291–7. Available from: http://dx.doi.org/10.1016/j.ijbiomac.2017.10.104

212. Tiamduangtawan P, Kamkaew C, Kuntonwatchara S, Wimolmala E, Saenboonruang K. Comparative mechanical, self-healing, and gamma attenuation properties of PVA hydrogels containing either nano- or micro-sized Bi2O3 for use as gamma-shielding materials. Radiat Phys Chem [Internet]. 2020;177(July):109164. Available from: https://doi.org/10.1016/j.radphyschem.2020.109164

213. Tie J, Liu H, Lv J, Wang B, Mao Z, Zhang L, et al. Multi-responsive, self-healing and adhesive PVA based hydrogels induced by the ultrafast complexation of Fe3+ ions. Soft Matter. 2019;15(37):7404–11.

214. Peng H, Lv Y, Wei G, Zhou J, Gao X, Sun K, et al. A flexible and self-healing hydrogel electrolyte for smart supercapacitor. J Power Sources [Internet]. 2019;431(May):210–9. Available from: https://doi.org/10.1016/j.jpowsour.2019.05.058

215. Liu K, Pan X, Chen L, Huang L, Ni Y, Liu J, et al. Ultrasoft Self-Healing Nanoparticle-Hydrogel Composites with Conductive and Magnetic Properties. ACS Sustain Chem Eng. 2018;6(5):6395–403.

216. Melilli G, Carmagnola I, Tonda-Turo C, Pirri F, Ciardelli G, Sangermano M, et al. DLP 3D printing meets lignocellulosic biopolymers: Carboxymethyl cellulose inks for 3D biocompatible hydrogels. Polymers (Basel). 2020 Aug 1;12(8).

217. Koysuren O, Karaman M, Dinc H. Preparation and characterization of polyvinyl borate/polyvinyl alcohol (PVB/PVA) blend nanofibers. J Appl Polym Sci. 2012 May;124(4):2736–41.

218. Cai J, Chen X, Wang X, Tan Y, Ye D, Jia Y, et al. High-water-absorbing calcium alginate fibrous scaffold fabricated by microfluidic spinning for use in chronic wound dressings. RSC Adv. 2018;8(69):39463–9.

219. Zhao L, Ren Z, Liu X, Ling Q, Li Z, Gu H. A Multifunctional, Self-Healing, Self-Adhesive, and Conductive Sodium Alginate/Poly(vinyl alcohol) Composite Hydrogel as a Flexible Strain Sensor. ACS Appl Mater Interfaces. 2021;13(9):11344–55.

220. Taleb S, Noyer E, Godeau G, Darmanin T, Guittard F. Switchable Surface Wettability by Using Boronic Ester Chemistry. ChemPhysChem. 2016;17(2):305–9.

221. Wang M, Anoshkin I V., Nasibulin AG, Korhonen JT, Seitsonen J, Pere J, et al. Modifying native nanocellulose aerogels with carbon nanotubes for mechanoresponsive conductivity and pressure sensing. Adv Mater. 2013;25(17):2428–32.

222. Silva TCF, Habibi Y, Colodette JL, Elder T, Lucia LA. A fundamental investigation of the microarchitecture and mechanical properties of tempo-oxidized nanofibrillated cellulose (NFC)-based aerogels. Cellulose. 2012;19(6):1945–56.

223. Carlsson DO, Nyström G, Zhou Q, Berglund LA, Nyholm L, Stromme M. Electroactive nanofibrillated cellulose aerogel composites with tunable structural and electrochemical properties. J Mater Chem. 2012;22(36):19014–24.

224. Hu J, Liu Z, Yu Q, Ma T. Preparation of reactive oxygen species-responsive antibacterial hydrogels for efficient anti-infection therapy. Mater Lett [Internet]. 2020;263:127254. Available from: https://doi.org/10.1016/j.matlet.2019.127254

225. Llor C, Bjerrum L. Antimicrobial resistance: Risk associated with antibiotic overuse and initiatives to reduce the problem. Ther Adv Drug Saf. 2014;5(6):229–41.

226. Friedman ND, Temkin E, Carmeli Y. The negative impact of antibiotic resistance. Clin Microbiol Infect [Internet]. 2016;22(5):416–22. Available from: http://dx.doi.org/10.1016/j.cmi.2015.12.002

227. Roca I, Akova M, Baquero F, Carlet J, Cavaleri M, Coenen S, et al. The global threat of antimicrobial resistance: Science for intervention. New Microbes New Infect [Internet]. 2015;6(January 2015):22–9. Available from: http://dx.doi.org/10.1016/j.nmni.2015.02.007

228. Ding BP, Wu F, Chen SC, Wang YZ, Zeng JB. Synthesis and characterization of a polyurethane ionene/zinc chloride complex with antibacterial properties. RSC Adv. 2015;5(16):12423–33.

229. Jin G, Cao H, Qiao Y, Meng F, Zhu H, Liu X. Osteogenic activity and antibacterial effect of zinc ion implanted titanium. Colloids Surfaces B Biointerfaces [Internet]. 2014;117:158–65. Available from: http://dx.doi.org/10.1016/j.colsurfb.2014.02.025

230. Cummins D. Zinc citrate/Triclosan: a new anti-plaque system for the control of plaque and the prevention of gingivitis: short-term clinical and mode of action studies. J Clin Periodontol. 1991;18(6):455–61.

231. Nouri S, Sharif MR, Tabatabaei F, Farokhi S. Investigating the Effect of Zinc Chloride to Control External Bleeding in Rats. Nurs Midwifery Stud. 2014;3(3).

232. Davis FE, Kenyon K, Kirk J. A Rapid Titrimetric Method for Determining the Water Content of Human Blood. Adv Sci. 1953;118(3062):276–7.

233. Dhahri M, Rodriguez-Ruiz V, Aid-Launais R, Ollivier V, Pavon-Djavid G, Journé C, et al. In vitro and in vivo hemocompatibility evaluation of a new dermatan sulfate-modified PET patch for vascular repair surgery. J Biomed Mater Res - Part B Appl Biomater. 2017 Oct 1;105(7):2001–9.

234. Wang Y, Liu Y, Liu M, Qian W, Zhou D, Liu T, et al. Short fluorocarbon chains containing hydrophobic nanofibrous membranes with improved hemocompatibility, anticoagulation and anti-fouling performance. Colloids Surfaces B Biointerfaces. 2019 Aug 1;180:49–57.

235. Reithofer MR, Lakshmanan A, Ping ATK, Chin JM, Hauser CAE. In situ synthesis of size-controlled, stable silver nanoparticles within ultrashort peptide hydrogels and their anti-bacterial properties. Biomaterials. 2014;35(26):7535–42.

236. Lu D, Wang H, Li T, Li Y, Dou F, Sun S, et al. Mussel-Inspired Thermoresponsive Polypeptide-Pluronic Copolymers for Versatile Surgical Adhesives and Hemostasis. ACS Appl Mater Interfaces. 2017;9(20):16756–66.

237. Hong Y, Zhou F, Hua Y, Zhang X, Ni C, Pan D, et al. A strongly adhesive hemostatic hydrogel for the repair of arterial and heart bleeds. Nat Commun [Internet]. 2019;10(1):1–11. Available from: http://dx.doi.org/10.1038/s41467-019-10004-7

238. Wang Y, Zhao Y, Qiao L, Zou F, Xie Y, Zheng Y, et al. Cellulose fibers-reinforced self-expanding porous composite with multiple hemostatic efficacy and shape adaptability for uncontrollable massive hemorrhage treatment. Bioact Mater [Internet]. 2021;6(7):2089–104. Available from: https://doi.org/10.1016/j.bioactmat.2020.12.014

239. Quan K, Li G, Luan D, Yuan Q, Tao L, Wang X. Black hemostatic sponge based on facile prepared cross-linked graphene. Colloids Surfaces B Biointerfaces [Internet]. 2015;132:27–33. Available from: http://dx.doi.org/10.1016/j.colsurfb.2015.04.067

Appendix I. Nanocellulose fibers aerogels as hemostatic materials

Abstract

Effective management of haemorrhage, including the use of hemostatic materials, is essential in reducing casualty in hospital and battlefields. Aerogels are becoming promising hemostatic materials due to its large specific surface aera, high absorption, low density, and biocompatibility. In this study, aerogels with lightweight, injectability, antibacterial capacity, and water-induced shape memory properties were prepared from carboxymethylated nanocellulose fibers (NCFs), sodium alginate and zinc chloride. In this design, NCFs served as a substrate of the aerogel, alginate can promote wound healing, and zinc chloride was used as the antibacterial agent to endow the aerogels with antibacterial ability. The density of the developed aerogels can be as low as 10.66mg/cm^3. The water absorption of the NCFs-based aerogels can reach 36.28±2.23g/g. Aerogels have rapid shape recovery ability in water and can restore its original shape within 4 seconds. This NCFs-alginate aerogel possesses good mechanical property in wet condition and opportune Young's modulus in dry condition. In vitro hemostatic test showed that the aerogels have great hemocompatibility and excellent coagulation ability in the whole-blood test. In vivo hemostatic tests indicated that the NCFs-alginate aerogels can reduce the blood loss (0.124±0.1g) in a rat liver model and quickly stop bleeding within 31s in the rat heart model. All of the foregoing results indicated that the NCFs-alginate aerogel has great potential as a non-cytotoxic and efficient hemostatic wound dressing.

1 Introduction

Hemorrhage is a critical cause of prehospital trauma death for military and civilian treatment. Around the world, over 30% of trauma death is caused by uncontrolled hemorrhage(1). Hemostasis has therefore become a major step for emergency treatment.

As a result, it is critical to develop hemostatic materials that are cost-effective, efficient biocompatible, ultralight, stable, and easy for application (1–3). Recently, a number of materials have been widely used for hemostasis, such as collagen (Col), gelatin (GE), alginate (AE), chitosan (CS), oxidized cellulose, cyanoacrylic acid tissue adhesive, and porous zeolite(3–9). However, these hemostatic materials have both advantages and drawbacks. For example, collagen and gelatin are the main components of extracellular matrix and connective tissues, respectively. They can therefore facilitate the formation of fibrin. Alginate can also accelerate the formation of fibrin(10). However, collagen and gelatin have poor tissue adhesion because they need ample platelets to form clots. In addition, alginate dressings have poor chemical stability, and their structure degradation is unpredictable(2,10–12). Porous zeolite can adsorb water from blood, aggregate proteins, and cellular matrix to promote the formation of platelet plugs. However, porous zeolite undergoes exothermic reaction upon absorbing water from wounds and may cause wound burn and inflammation (11,13). New hemostatic techniques or materials have been developed, such as the XStat device, which is a syringe-like device that injects cellulose-based sponges coated with chitosan into penetrated wounds to absorb blood quickly(14). However, the preparation and synthesis of the new hemostatic materials are intricate and costly(1,11). Therefore, a hemostatic material that is cost effective, easy to prepare and use, and high in blood absorption capacity is highly demanded.

Hemostatic materials, particularly textile fibers, can cause infection(15). Microorganisms (i.e., bacteria and virus) may cause infection and hinder wound healing, and may enter human body through the wounds to infect host tissue and cause disease (i.e., sepsis) and/or death(15,16). Antibiotic therapies have been commonly used to treat bacterial infections. However, antibiotics overuse can cause antibiotic resistance which can reduce the effectiveness of the treatment, increase mortality and complications risks, produce drug-resistance bacteria and increase infection rate, and cause environmental pollution (17–20). To reducing the abuse of antibiotics, antibacterial hemostatic

materials have been developed by incorporation of antibacterial agents, including inorganic antibacterial agents like silver ion, nanoparticles, and organic antibacterial agents like quaternary ammonium salts(21). Compared with organic antibacterial agents, inorganic antibacterial agents are more stable and have longer shelf life(21). Studies showed that zinc ion can prohibit multiple bacterial activities including transmembrane proton translocation(22) and inhibit glucose uptake(23). Zinc chloride is a low-cost antibacterial agent has been suggested to provide the most potent antibacterial activity among metal compounds like zinc acetate, zinc chloride, zinc sulfate, cupric acetate, cupric chloride, cupric sulfate, and nickel sulfate(15,21). Zinc chloride has also been used in dental surgeries as a hemostatic material to control local hemorrhage. Moreover, zinc chloride has been used in water purifications as a protein coagulant, which can be an add-on feature for hemostasis since blood have a large number of proteins(24).

In recently years, natural polymers have gained much attention in the development of biomaterials due to their biocompatibility and sustainability. Alginate, a natural biocompatibility polymer extracted from seaweed, has been widely used in biomedical applications, including wound dressings. Alginate dressings have been used to treat exuding wounds and can accelerate wound healing by providing a moist environment. Besides, it is easy to remove the alginate dressing from wounds without causing additional injuries(2,6). Nanocellulose fibers is another natural polymer that can be obtained from various sources, such as bacteria, algae, and wood, among which the wood based nanocellulose fibers (NCFs) have been mostly studied due to their great environmental and industrial importance(25). Nanocellulose is a linear natural polymer with highly ordered, long, and thin nanostructure(26). NCFs have the advantages of natural abundance, biodegradation, low thermal conductivity, light weight, and high strength, therefore, is becoming a promising material for wound care applications(25,27). Nanocellulose has abundant active hydroxyl groups, which can be chemically modified into functional groups, such as carboxymethyl. Some recent

studies showed promising results for NCFs-based wound dressings for wound healing(25).

Aerogel is an ultralight material with a highly porous structure produced by sublimating the liquid component from a hydrogel via freezing-drying or critical point drying(26,28). Aerogels show the merits of low density, large specific surface area, high porosity, and low thermal conductivity(27). Compared with other aerogel building blocks, nanocellulose aerogels offer tunable interfacial chemistry, excellent mechanical property, extremely high specific surface area, and beneficial renewable origins(28). Aerogels have high water absorption, great mechanical property, and rapid shape recovery ability, making it a promising hemostatic material(11). Because of the large specific surface area and high porosity, aerogels can adsorb liquid upon contact with the blood and swell to provide a haemostat in a bleeding site: Aerogels can entangle proteins, platelets and red blood cells to form a "barrier" which prevents the flow of blood, and serves as a matrix for fibrin to form the solid fibrin clot(29).

In this study, a lightweight, high porosity, injectable, water-induced shape memory and antibacterial carboxymethylated nanocellulose fibers (NCFs)-alginate aerogel was designed and prepared to promote wound healing. The NCFs-alginate aerogels with lightweight and high porosity have high water absorption rate. Besides, the NCFs-alginate aerogels with injectability and water-induced shape memory behaviour can be used in penetrated or uncompressed wound and fit the shapes of different wounds to accelerate penetrated wound healing. Additionally, NCFs-alginate aerogels with antibacterial property can reduce infection rate and increase patients' survival rate. Figure 1 illustrates the scheme of preparation of NCFs-alginate aerogel. Briefly, the carboxymethylated nanocellulose fibers were prepared firstly by high-speed mixing (7500rpm) and centrifugation twice. The first centrifugation (1400rpm) was to remove microfibers and the second one (4000rpm) was to extract nanofibers. Then, alginate, NCFs, and zinc chloride were mixed to prepare aerogels via the freeze-drying method.

Among them, zinc chloride served as an antibacterial agent to prevent infection. Alginate provided a humid environment in the wound site to accelerate wound healing. Meanwhile, alginate as a natural polysaccharide was used to lock NCFs network and improve the water stability of NCFs network (31). The developed aerogel combined double networks, including an NCFs network and an alginate-zinc ions network. Herein, nanocellulose fibers as the substrate endow the aerogel with good mechanical properties and large surface area (32), and alginate and zinc ions can be used to maintain the wet stable of aerogels and reduce infection rate(31,33). The aerogel has water-induced shape memory ability and can recover to its original shape within 4s in water. As a result, the aerogel can be injected into uncompressed wounds to accelerate penetrated wound healing. The hemostatic materials can also reduce the infection rate of trauma patients due to the incorporation of an antibacterial agent, zinc chloride. *In vitro* and *in vivo* hemostatic assay also demonstrated that the NCFs-based aerogel has a good hemostatic ability. Table 1 compares the properties of NCFs-based aerogels in previous works and this work, including density, water absorption, antibacterial ability, and shape recovery ability.

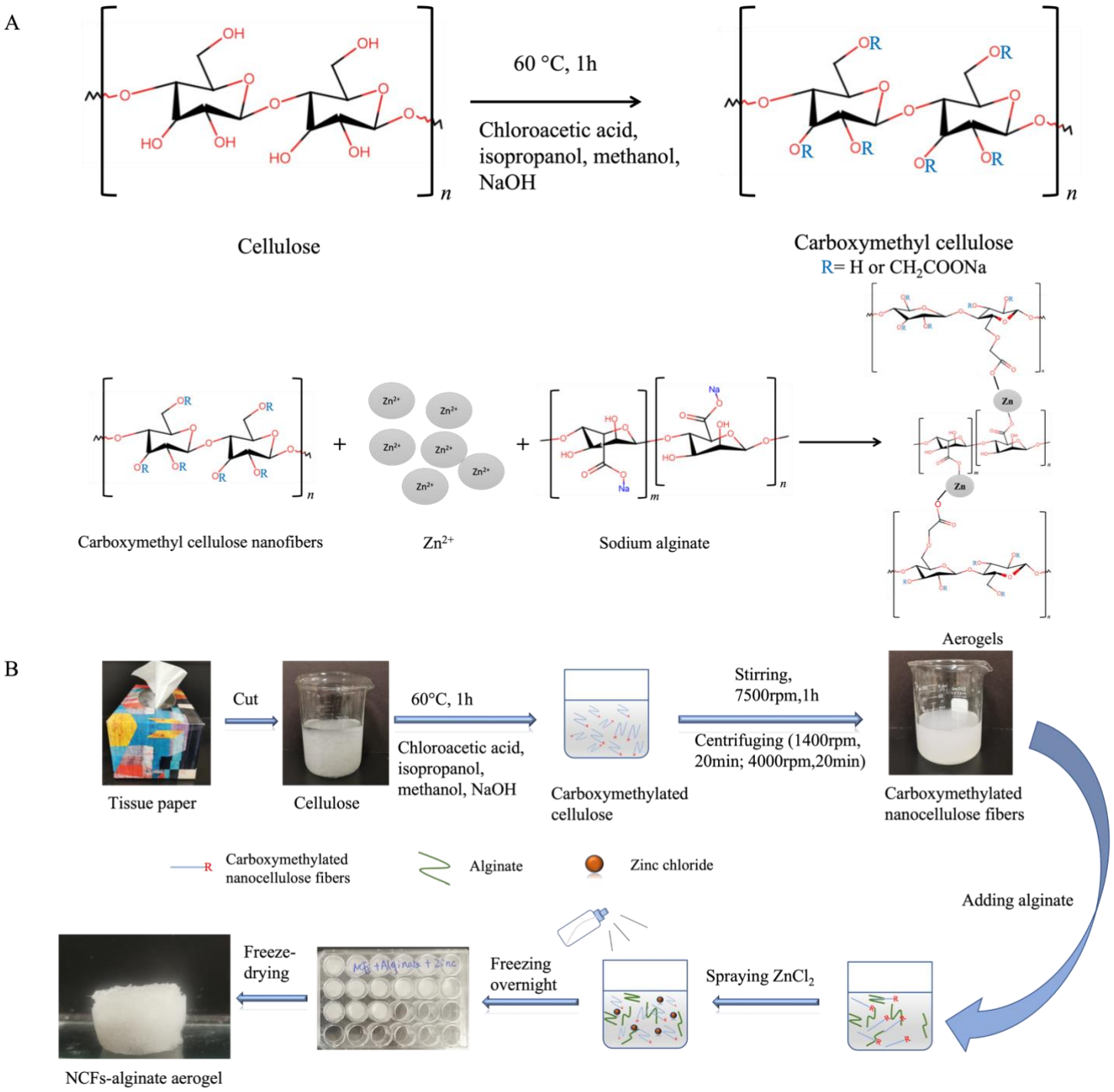

Figure 1. Scheme of preparation of NCFs-alginate aerogel. (A) The formula of synthetic carboxymethylated nanocellulose fibers and NCFs-alginate aerogel. (B)The process of preparing NCFs-alginate aerogels.

Table 1. Comparisons of density of cellulose fibers-based aerogels

Components	Density	Absorption rate	Antibacterial rate	Shape recovery time	Ref.
Cellulose nanofibers/alginate/$CaCl_2$	23-38mg/cm^3	-	-	-	(26)
Cellulose nanofibers/ chitosan	14.3-26.5mg/cm^3	39.1-53.7g/g	Yes	30s	(11)
Chitosan-based aerogel	80mg/cm^3	-	100% (*E. coli*)	-	(34)
Chitosan/mesoporous silica	120mg/cm^3	<3g/g(normal saline)	100% (*S. aureus* and *E. coli*)	-	(35)
Oxidized bacterial cellulose/ montmorillonite	-	29.32-33.3g/g	Yes (*S. aureus* and *E. coli*)	-	(36)
Cellulose nanocrystal	5.6mg/ cm^3	160g/g	-	85% (95%strain)	(37)
Carboxymethylated cellulose nanofibers/alginate/zinc chloride ($ZnCl_2$)	10.66-12.7mg/cm^3	37.8g/g (water)	89% (*E. coli*)	4s	This work

2. Materials and Methods

2.1 Materials

Tissue papers (Scotties Premium), alginic acid sodium salt was bought from Alfa Aesar. Zinc chloride was bought from Sangon Biotech, China. Hydrochloric acid (HCl) was bought from LabChem. Chloroacetic acid and isopropanol were bought from Sigma-Aldrich, NaOH and methanol were bought from VWR Chemicals, and acetic acid was bought from Fisher Scientific Canada. All materials were used as received state.

2.2 Preparation of carboxymethylated nanocellulose fibers (NCFs)

The method of preparing carboxymethylated cellulose fibers was followed by previous research(38). Briefly, 2g tissue papers were cut up and immersed into deionized water. Then, it was impregnated for 30min with a solution of 3g chloroacetic acid in 150ml isopropanol. These pieces were added in a solution of mixing 0.972g NaOH, 30ml methanol, and 120ml isopropanol. The solution was heated to 60ºC in a beaker for 1h for reaction. Hereon, the carboxymethylation step was finished. After the carboxymethylation step, the pieces were washed in the three steps to remove residual solvent: firstly, washed with 50mL deionized water, then with 0.1M acetic acid, and finally with 50mL deionized water. Then, the pieces were then immersed in 0.01M NaOH solution for 30min.Finally, the fibers were washed in 100ml deionized water.

The pieces with carboxymethylated group were homogenized by a shearing mixer (7500rpm) for 1h. Then, the obtained suspensions were centrifuged at 1400rpm for 20min to remove microfibers, and the supernatant was taken out for further centrifugation at 4000rpm for 20min. The precipitates were then carboxymethylated nanocellulose fibers. Finally, the obtained nanofibers were freeze-dried in a lyophilizer and prepared for the next steps.

2.3 Preparation of aerogels

Firstly, 100mM zinc chloride solution was prepared with 1.363g zinc chloride (anhydrous) and 100mL deionized water. After zinc chloride dissolved, 0.5ml 0.1M HCl was added into above solution to inhibit the hydrolysis of zinc chloride. Then, the carboxymethylated nanocellulose fibers (NCFs) and alginate salt with different ratios, namely, 0:5, 1:4, 1:1, and 4:1, were mixed and cast into the 24-well plate. The concentrations of NCFs were 1mg/ml, 2mg/ml, 4mg/ml, and 6mg/ml. Then, 100mM zinc chloride (0.3mL) was added by a sprayer which can result in a more uniform incorporation of zinc ions into the solution. The mixed solution was frozen at -20 ºC and kept at this temperature overnight. After that, the 24-well plate with the solution was put into the lyophilizer overnight. Finally, the NCFs-based aerogels were obtained after moving the samples from the mold (24-well plate).

2.4 Materials Characterization

2.4.1 Density of aerogels

The aerogels were prepared by different concentrations of NCFs in the group of 1mg/ml, 2mg/ml, 4mg/ml, and 6mg/ml. The sample was cut to a diameter of 13mm and a thickness of 8mm. The diameter (*d*) and weight (*m*) were measured by a ruler and a balance. The density(ρ) of aerogel was calculated as:

$$\rho = \frac{m}{\pi h r^2} \quad (1)$$

where *m* is the mass of aerogel, *h* is the length of aerogel, and *r* is radius of aerogel which is half of the diameter.

2.4.2 Fourier-transform Infrared (FTIR) Spectra Characterization

FTIR characterization of carboxymethylated cellulose nanofibers (NCFs) and NCFs-alginate aerogel was studied by a FTIR spectrometer (Bruker IFS 66v/s, German) within wavenumber of 4500-500 cm $^{-1}$. The samples in FTIR test contained carboxymethylated nanocellulose fibers and NCFs-alginate aerogels.

2.4.3 Scanning Electron Microscope (SEM) Characterization

SEM characterization was carried out on a model of Quanta FEG 650 scanning electron microscope with an operation voltage of 5kV. The NCFs-based aerogel was lyophilized, sprayed with a layer of gold, and put on a metal holder to exam under the microscope.

2.5 Rheology assay

Rheology of the aerogels was measured by the Discovery Hybrid Rheometer HR-1 (TA Instruments). The samples were cut to a diameter of 8 mm. Then, the freeze-dried aerogels immersed in 3mL water for 10min. The aerogels with different rates of NCFs and alginate (0:5, 1:1, 1:4, and 4:1) were prepared to optimise parameters.

2.6 Compression test

Mechanical properties of aerogels were evaluated on the MTS Criterion Model 43 testing machine with a 1000N load cell. Compression tests were conducted on samples with different rates between NCFs and alginate (0:5, 1:1, 1:4, and 4:1). The concentration of zinc ions is consistent in all groups. The size of samples was 13mm in diameter and 8mm in thickness. All experiments were carried out at a steady speed of 10 mm/min. Five strains (10%, 20%, 30%, 40%, and 50%) were used to evaluate the compressive property of aerogels with different rates between NCFs and alginate. The slope of 10% strain was used to calculate the Young's modulus of different aerogels. The energy loss coefficient was calculated by the hysteresis loop region enclosed by the loading-unloading curves:

$$Energy\ loss\ coefficient = \frac{\Delta U}{U} \times 100\% \quad (2)$$

Where $U=\int \sigma\, d\varepsilon$, and $\Delta U= \int \sigma_{loading}\, d\varepsilon - \int \sigma_{unloading}\, d\varepsilon$.

2.7 Injectable and Water-induced shape memory behaviour test

The samples with different ratios of NCFs and alginate were cut into a cylinder (8mm×13mm) and immersed in water for 30min to reach the saturated state. The aerogels will be put into syringes with a diameter of 2mm to explore the injectability of aerogels. Then, after the samples were injected into the water, the behaviour of the samples was observed whether they could return to their original shape.

2.8 Water-absorption test

The water absorption ability of aerogels will be measured by followed method(39). Firstly, the aerogel (the thickness of 8mm) was immersed in 10mL water and the weight of the aerogels was measured at specific intervals. The method of measurement is after removing the moisture from the aerogel surface, the obtained aerogel was weighted. The water absorption rate will be calculated as:

$$water\ absorption\ rate = \frac{m_s - m_0}{m_0} \quad (3)$$

Where m_s is the weight of saturated aerogel and m_0 is the weight of dry aerogel. The water absorption test was performed three times and the average value was obtained.

2.9 In vitro Hemolysis assay

The degree of hemolysis represents the amount of the red blood cells broken by the sample in contact with blood. Briefly, the diluted blood sample was prepared by mixing 2 mL of the anticoagulated Sprague Dawley rat whole blood with 2.5 mL 0.9% NaCl solution (8:10). In 10ml Centrifuge tube, NCFs aerogel and NCFs-alginate groups were

incubated at 37°C in 5ml of 0.9% NaCl solution for 30 min. Before the tests, all the materials were sterilized by UV irradiation for 30 min. After then, 0.2 mL of diluted blood sample was added. After 60 min of incubation at 37°C, the whole system was subjected to centrifugation at 1500 rpm for 10 min. The upper clear solution of the blood mixture was characterized by the absorption spectrum(545nm). The mixture of 5 mL 0.9% NaCl and 0.2 mL diluted blood sample was used as negative control. Positive control was prepared by mixing 5 mL of distilled water with 0.2 mL blood sample. The HR was calculated according to the following formula:

$$HR\% = \frac{OD_s - OD_n}{OD_p - OD_n} \times 100 \quad (4)$$

OD_s, OD_n, OD_p were the corresponding OD values of the sample, negative control, and positive control groups, and repeated three times for each group(40,41).

2.10 Whole blood agglutination test

Sprague Dawley rat Citrate anticoagulated whole blood used in this test. NCFs aerogel, NCFs-alginate aerogel, and gelatin hemostatic sponge was put in a 24-well plate, and 100 μL of anticoagulated whole blood was then added. At 5 min, each well was added with 2ml distilled water to halt clotting. The group without added material is the positive control group. Hemoglobin released from uncoagulated blood is detected with a microplate reader (at 545nm). For SEM, samples were fixed in 2% glutaraldehyde for 12 h, gradient dehydrated in ethanol and tert-butanol, sputter coated with gold-palladium, and then examined by SEM.

2.11 Antibacterial assay

An *Escherichia coli colony* was inoculated overnight in 5 mL of LuriaeBertani (LB) medium, with constant shaking at 220 rpm for 37 °C. The log-phase bacterial solution was then diluted in LB medium to obtain an O.D. of 0.07 (at 600 nm). This was used

as the starting bacterial solution (0 h reading) and 2 mL of the solution was dispensed into each well of the 24-well plate containing the aerogel. Bacteria-only solutions served as the positive controls. Before the tests, all the materials were sterilized by UV irradiation for 30 min. The plates were placed at 37 °C under 50 rpm rotation in a shaker incubator for 24 h. For the OD readings, at 4h,12h, and 24h, 100 μL of the bacterial solution was transferred into a 96-well plate just before measurement. The assay was performed in triplicates(42).

2.12 Cytocompatibility

3T3 and Huvec cell line were cultured routine in a 5% CO_2 incubator at 37 °C. The 3T3 and HUuvec cells were seeded in 96-well plates at $3x10^3$ /100 μL per well. The culture medium was replaced with the leach liquor extracting from each group after 6 h, and untreated medium was used as a blank control. The cells in 96-well plates was assessed using cell counting kit (CCK-8, Dojindo,Kyushu, Japan) test on 24 and 74 hours after seeding. In brief, at each time point, the medium was replaced with RIPM, and 10 μL of CCK-8 solution was added to each well, followed by incubation at 37 °C for 2 h. The mean optical density (OD) value was determined at 450 nm using Microplate reader (Thermo Varioskan Flash, USA), and the cell viability (%) was expressed in percentage relative to a control group. The cells on 24 and 72h was tested by Cell LIVE/DEAD kit (Invitrogen, USA). The relevant reagent added to incubation at 37°C for 20 min, and the resultant images were observed under Whole slide scanning system (Olympus, VS200, Japan) (41,43).

$$Cell\ viability\ (\%) = \frac{OD_s - OD_n}{OD_c - OD_n} \times 100\% \quad (5)$$

OD_s, OD_n, OD_c were the corresponding OD values of the sample, negative control, and positive control groups, and repeated three times for each group.

2.13 In vivo hemostatic assay

Male Sprague−Dawley rats (180−200 g) were obtained from the Animal Center at the Army Medical University. Animals were housed in standard rat/mouse cages under conditions of optimum light and temperature at 20 ± 1 °C, with normal water and food. Animal care and experiments were carried out in accordance with procedures approved by Animal Care and Use Committees of Army Medical University (AMUWEC20203021)

2.13.1 In vivo hemostasis in a liver injury model in rats

Sprague−Dawley rats (180−200 g) were anesthetized, and the abdomen was opened in the rostral-to-caudal direction to expose the liver. Injury of 2 mm deep into the left lobe of the liver, with a length of 0.5 cm, was cut using a syringe needle, separating the two halves of the lobe transversely. Subsequently, hemostatic NCFs-alginate aerogel (8 mm x 13 mm) as experimental group was applied to the site of injury and gently press it tightly. In the control group, NCFs aerogel (8mm x 13mm) was applied to the injured site. In the blank groups, nothing was applied to the injured site. In the positive groups, gelatin hemostatic sponge was applied to the injured site (5,6). All the procedures were performed by the same operator blinded to the treatment groups. The volume and time for blood after completely blocking bleeding (no blood flow within 10 s) was recorded in three independent experiments by the same researcher. For SEM, samples were fixed in 2% glutaraldehyde for 12 h, gradient dehydrated in ethanol and tert-butanol, sputter coated with gold-palladium, and then examined by SEM.

2.13.2 In vivo hemostasis in a heart injury model in rats

Sprague−Dawley rats (180−200 g) were anesthetized and a needle with a diameter of 6mm was used to puncture the ventriculus sinister of rat hearts. For the experimental group, the NCFs-alginate aerogel (8 mm x 13 mm) was applied to the wound site and

gently press it tightly. For the control group, NCFs aerogel (8 mm x 13 mm) was applied to the site of wound and gently press it. For the blank groups, nothing was applied to the wound site. For the positive groups, gelatin hemostatic sponge was applied to the injured site(44). The same researcher observes blood flow.

3 Results and Discussion

3.1 Density of aerogels

According to equation 1, the densities of aerogels with different concentrations of carboxymethylated cellulose were calculated. According to Figure 2A, the aerogel with 1mg/ml NCFs cannot form a regular shape while other three samples can form a regular aerogel shape. The densities of aerogels with 2mg/ml, 4mg/ml, and 6mg/ml NCFs were 10.66mg/cm^3, 12.4mg/cm^3, and 12.7mg/cm^3, respectively (Figure 2B). Among them, aerogel with 2mg/ml NCFs has the lowest density which is lower than other light-weight cellulose fiber-based aerogels, as Table 1 shows.

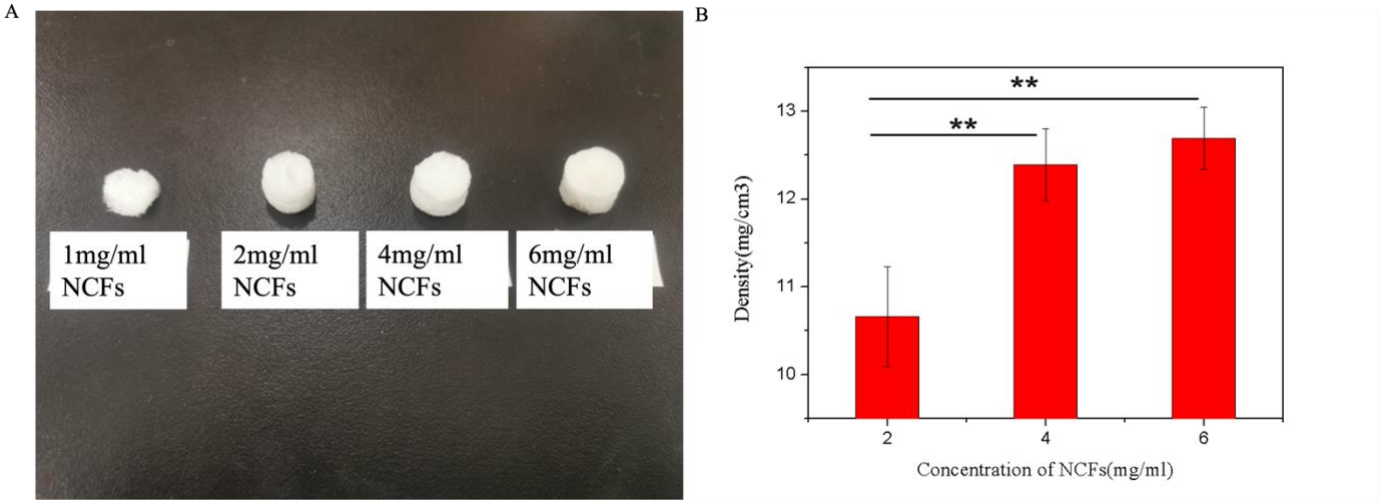

*Figure 2. Aerogels with different concentrations of NCFs. (A)Images of aerogels with different concentrations of carboxymethylated nanocellulose fibers. (B) Density of aerogels (n=3; **, p<0.05).*

3.2 Fourier-transform Infrared (FTIR) Spectra Characterization

As shown in Figure 3, the FTIR analysis of carboxymethylated nanocellulose fibers and NCFs-alginate aerogels were conducted. The dominant characteristic band at 3335cm^{-1} and 1031cm^{-1} are assigning to O-H and C-O-O stretching vibrations, respectively(32). The carboxymethyl group can be observed at the peak of 1631cm^{-1} and 1610 cm^{-1} (COO- stretching)(45). This indicated that the cellulose nanofibers were grafted with carboxymethyl group successfully. The absorption band at 2902cm^{-1} shows C-H stretching frequency(46). The 1425cm^{-1} and 1314cm^{-1} represent to CH_2 scissoring and C-H bending band, respectively(32,46,47).

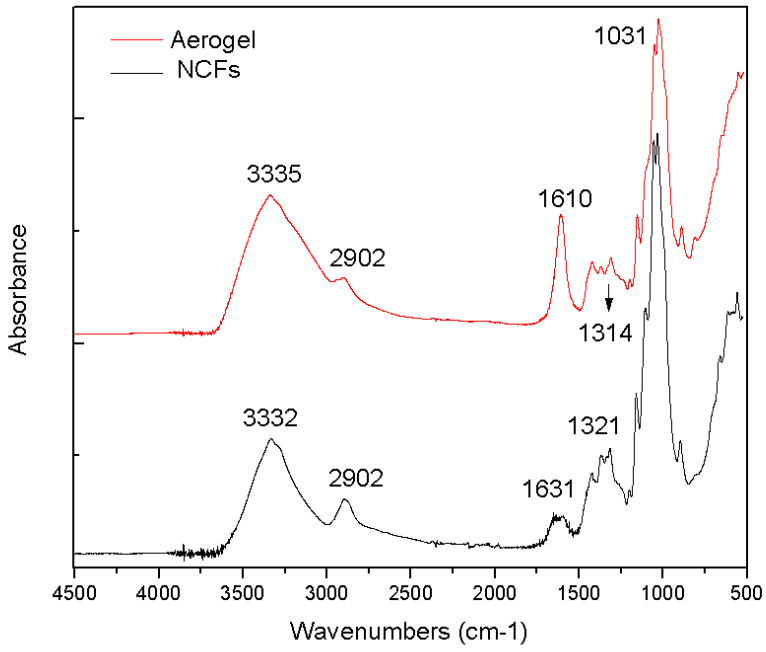

Figure 3. FTIR spectra of carboxymethylated nanocellulose fibers and NCFs-alginate aerogel

3.3 Scanning Electron Microscope (SEM) Characterization

The microstructure of aerogels was studied by scanning electron microscope (SEM). As Figure 4 illustration, the diameter obtained by carboxymethylated nanocellulose fibers is 83.8±20.85nm. The aerogels have a high interconnected porous 3D internal

structure (Figure 5). A similar structure was also observed in previous cellulose-based aerogels (11). Compared with other groups, the surface of pristine alginate aerogel (0:5) was smoother since nanocellulose fibers were not contained in it (Figure 5A1-3). NCFs-alginate aerogels have a more ordered internal structure (Figure 5B1, C1, and D1) since the crosslinking of alginate and Zn^{2+} can support the aerogel's network (48). The presence of fibers can be observed on the surface of NCFs-alginate aerogels (Figure 5B2, C2, and D2). Meanwhile, as the ratios between NCFs and alginate changed, the nanocellulose fibers content increased, and, from Figure 5B2 to D2, more fibers can be observed on the surface of the aerogels. Besides, the surface of NCFs-alginate aerogel (4:1) has larger aggregates (Figure 5D3) than the other two rates (1:1 and 1:4) (Figure 5C3 and D3). This is because aerogel (4:1) contain more nanofibers which can form fibrous aggregates. Besides, the macroporous structure of aerogels was constructed by ice crystals during the freeze-drying process (49).

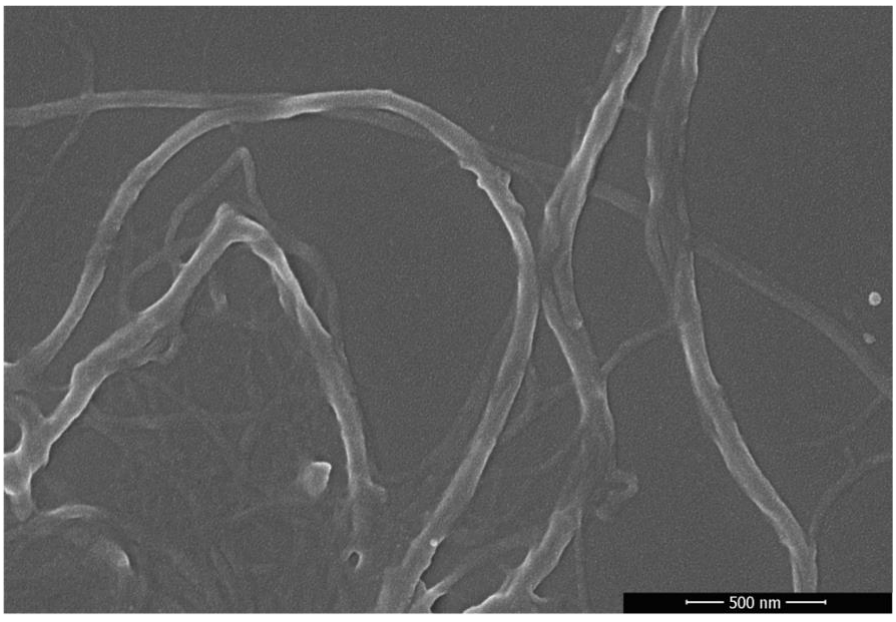

Figure 4. SEM image of carboxymethylated cellulose nanofibers

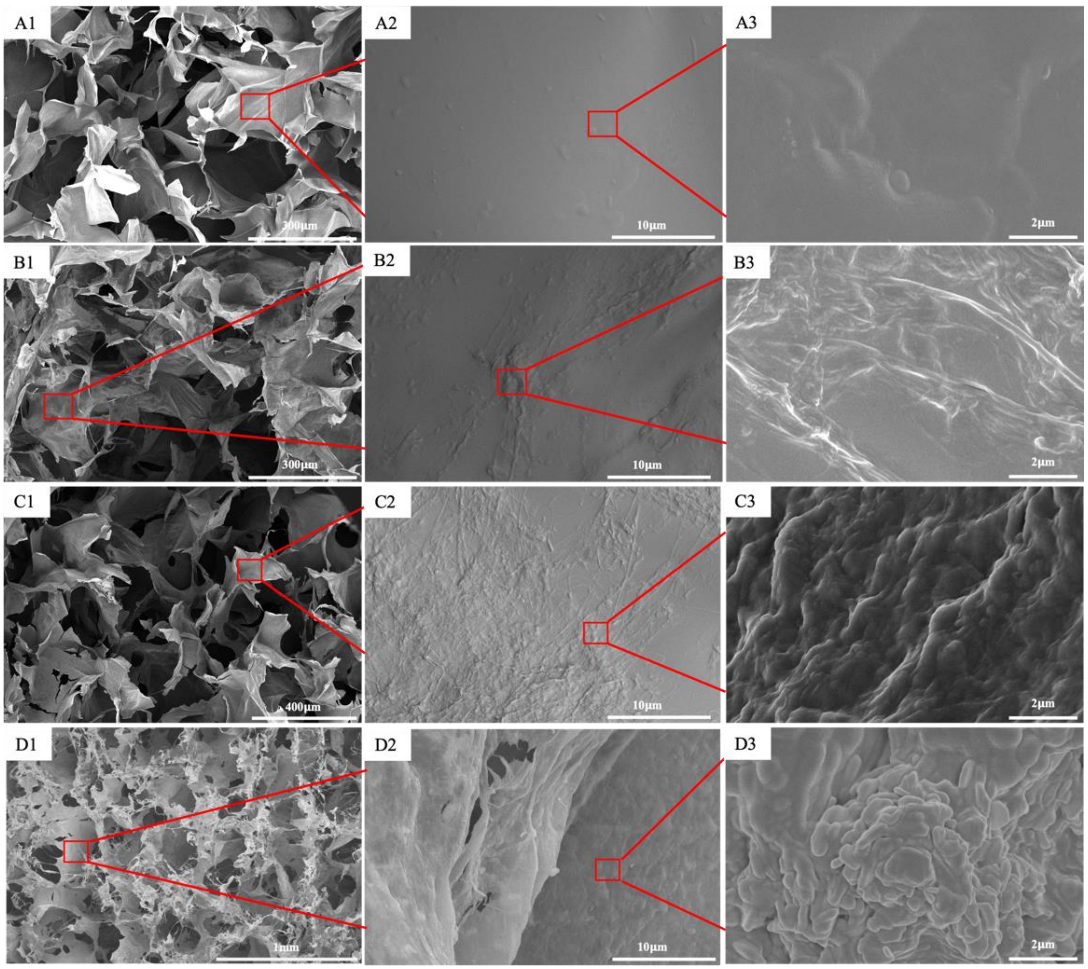

Figure 5. Scanning electron microscope (SEM)images of cross-section of NCFs-based aerogels with different ratios between NCFs and alginate: 0:5(A1-3), 1:1 (B1-3), 1:4 (C1-3), and 4:1 (D1-3).

3.4 Rheology assay

The mechanical properties of NCFs-based aerogels can be studied by rheology tests (Figure 6). The storage modulus (G') and loss modulus (G'') were tested at the constant strain (0.1%). In the whole angular frequency spectrum (0.1-100rad/s), the G' was higher than G'' which indicated that NCFs-based aerogels with different ratios of NCFs and alginate maintained a gel-like behaviour in the full angular frequency. As the fibers content increased, the storage modulus (G') and loss modulus (G'') increased progressively, demonstrating the presence of nanocellulose fibers enhanced

the mechanical properties of aerogels. The modulus of NCFs-alginate (1:1) aerogel and NCFs-alginate (4:1) aerogel are very similar which may because the two groups have high NCFs content, and NCFs play a dominant role in the aerogel system, while the latter is slightly higher than the former. Therefore, among the four groups, the NCFs-alginate (4:1) aerogel has the higher modulus which illustrates the aerogel has greater elastic behavior and mechanical performance in a wet condition (50). Besides, the result indicated that the mechanical performance of alginate-based aerogel has been improved by the incorporation of NCFs which may be owing to the reinforcement effect of NCFs. The similar result was reported in previous research (51–53).

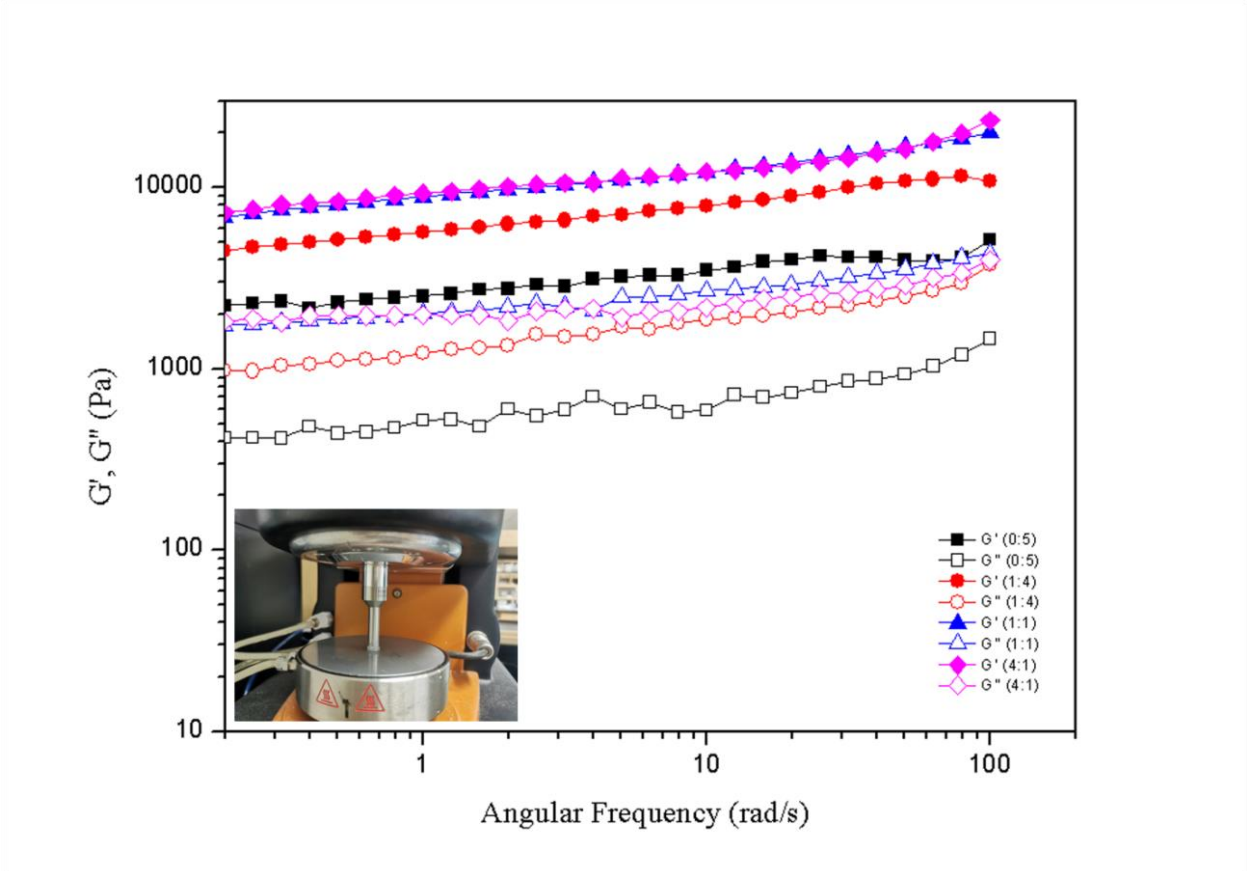

Figure 6. Rheology test for wet NCFs-based aerogels with different ratios of NCFs and alginate.

3.5 Compression test

To assess the mechanical properties of NCFs-based aerogels, compression tests were conducted, and the compressive stress-strain curves are shown in Figure 7. The process of the compression test is demonstrated in Figure 7A. In the compression test, the strains from 10% to 50% were used to calculate the curves. Figure 7B-E indicated the stress-strain plots of aerogels with different NCFs and alginate, namely 0:5, 1:4, 1:1, and 4:1. Meanwhile, three regions can be observed in the loading stress-strain curves of four groups: the Hookean region attributing to elastic bending deformation, a broad plateau relating to the collapse of the cell wall, and a densification region where the stress increases remarkably (26,54). A permanent residual deformation can be observed in the unloading curves after compression (55). Among the four groups, the aerogel (0:5), aerogel (1:4), and aerogel (1:1) have permanent residual deformation and loses its recoverability and elasticity from 10% strain (Figure 7B-D) (56,57). As Figure 3.7 E showed, the NCFs-alginate (4:1) aerogel has excellent compressibility and can completely recover back to its original shape at 30% strain. Other research also reported similar results (48). As Figure 3.7F indicates, in dry condition, the Young's modulus of NCFs-alginate (4:1) aerogel is much lower than aerogel (0:5) ($p<0.001$) and aerogel (1:4) ($p<0.001$), and has no significant difference with the aerogel (1:1), indicating the Yonge's modulus of NCFs-alginate aerogel decreases with increasing fibers content. Meanwhile, the tendency also proves that the aerogel (4:1) is softer than other groups because of the lower Young's modulus. The Young's modulus of aerogel (4:1) is similar with modulus of soft tissue, like livers, which can reduce the risk of stress shielding (58–60).

To further evaluate the recoverability and cyclic resilience properties of NCFs-alginate (4:1) aerogel, the compressive cycling test was carried out under 30% strain (Figure 7G). A hysteresis loop can be observed in the compressive stress-strain curves, which is similar to nanofiber-based aerogels(56,61). The loop of NCFs-alginate (4:1) aerogel

has shrunk after the first cycle, but it has remained largely constant after the fifth cycle (Figure 7G). The energy loss coefficient and maximum stress are assessed and demonstrated in Figure 7H. The value of maximum stress of the aerogel has not changed significantly since the first cycle and has remained at around 1.53kPa. However, the value of energy loss coefficient of NCFs-alginate (4:1) aerogel is the highest one in the first cycle, then it starts to decrease, and roughly maintains at 33%. The final energy loss coefficient is similar with other studies (54–57).

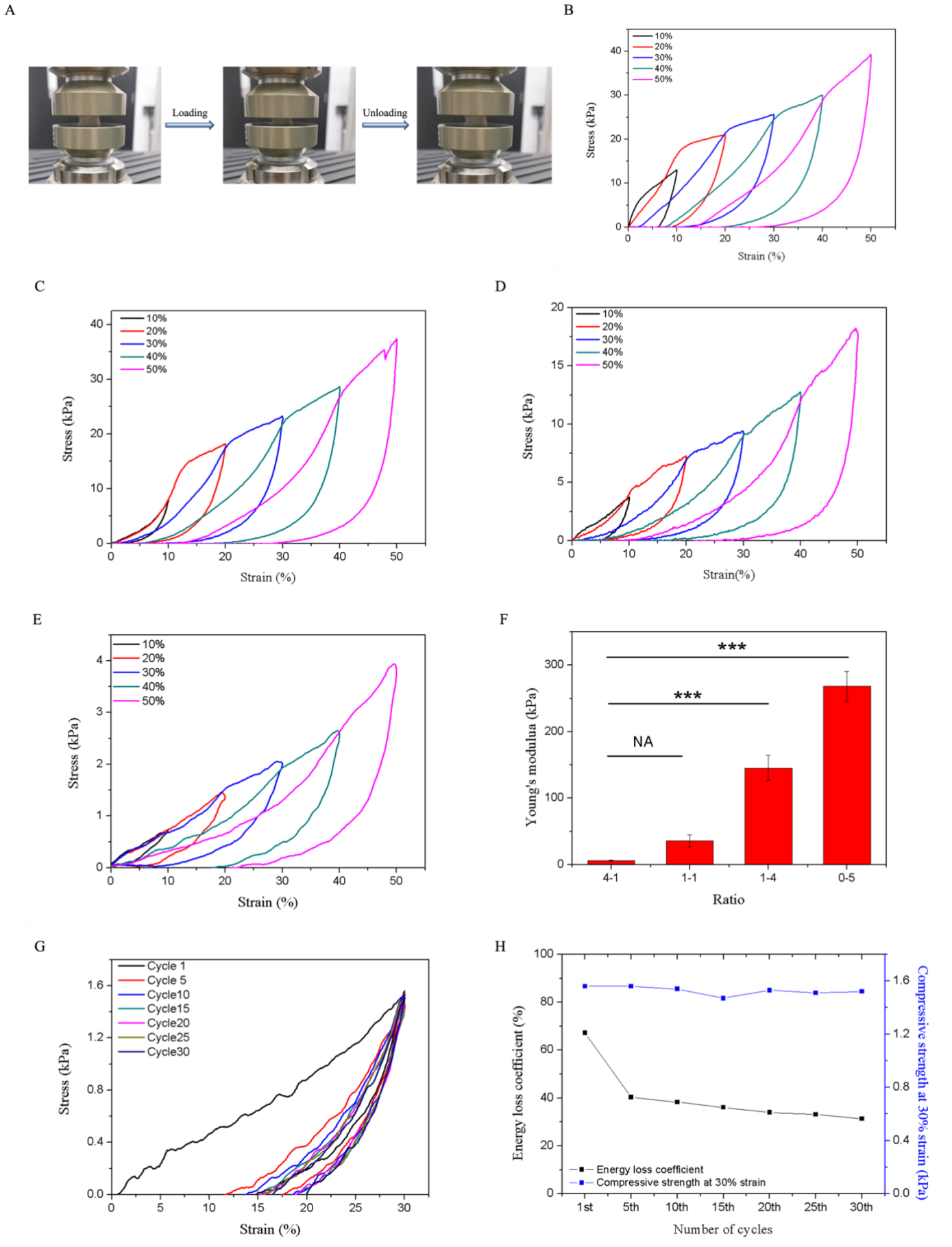
A
Loading
Unloading
B
10%
20%
30%
40%
50%
Stress (kPa)
Strain (%)
C
Stress (kPa)
Strain (%)
D
Stress (kPa)
Strain(%)
E
Stress (kPa)
Strain (%)
F
***
***
NA
Young's modulua (kPa)
4-1
1-1
1-4
0-5
Ratio
G
Cycle 1
Cycle 5
Cycle10
Cycle15
Cycle20
Cycle25
Cycle30
Stress (kPa)
Strain (%)
H
Energy loss coefficient (%)
Compressive strength at 30% strain (kPa)
Energy loss coefficient
Compressive strength at 30% strain
1st
5th
10th
15th
20th
25th
30th
Number of cycles

*Figure 7. Compression test of NCFs-alginate aerogels. (A) The loading-unloading process of NCFs-alginate (4:1) aerogel under 30% strain. The stress-strain curves during loading-unloading process under different compressive strains (10%, 20%, 30%, 40%, and 50%) for different rates between NCFs and alginate(n=3), (B) 0:5, (C) 1:4, (D) 1:1, and (E) 4:1. (F) Young's modulus of the four rates samples (n=3; ***, p<0.001). (G) 30 cycles compressive stress-strain curves of the aerogel (4:1) under 30% strain. (H) The energy loss coefficient and compressive stress at 30% strain for aerogel (4:1) during 30 compressive loading-unloading cycles in (G).*

3.6 Injectable and water-induced shape memory behaviours

The injectable ability and water-induced shape memory ability of aerogels have been indicated in Figure 8. As the images showed, the freeze-dried NCFs-alginate aerogels were squeezed to a certain shape and then put into tips with three designed diameters. The aerogels can be injected from the tips by a pipette and quickly back to its original shape within 4s when immersing in water. The shape recovery time of NCFs-alginate aerogel was consistent (39). The aerogels still returned to its original state when squeezing out again, which can be repeated. The aerogels exhibited a good water stability and structure stability due to freeze-dried NCFs and alginate-Zn^{2+} networks.

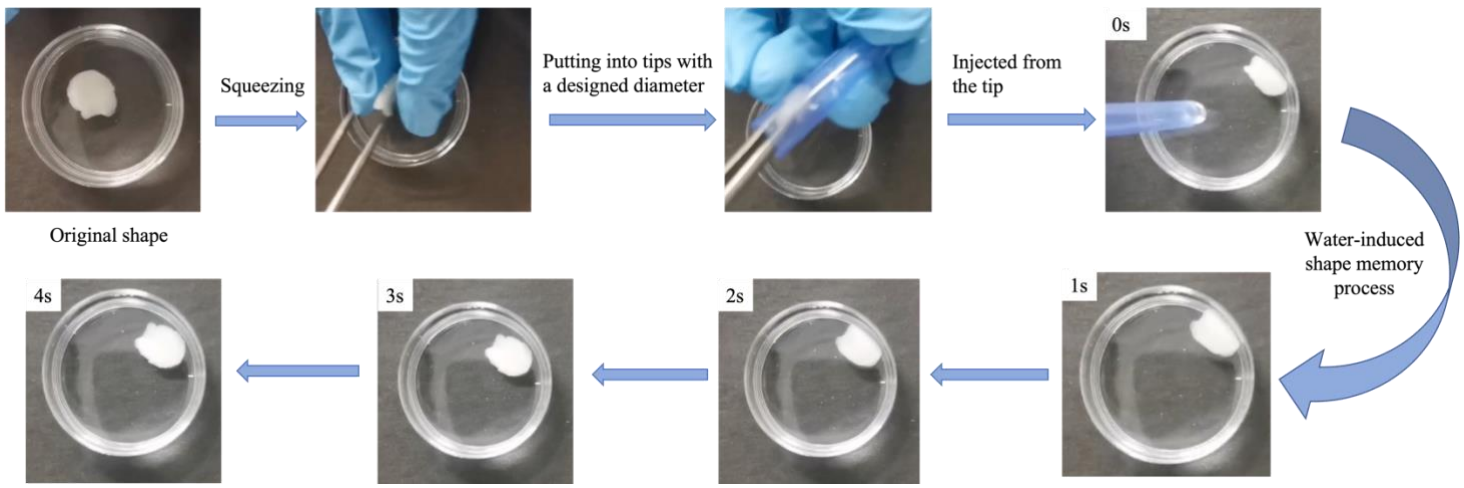

Figure 8. Images of NCFs-alginate aerogels with injectable and water-induced shape memory ability

3.7 Water absorption test

Because of its high porous, the NCFs-based aerogel has good water absorption ability. Figure 3.9A showed that in the first one minute, the water absorption of the aerogel (4:1) quickly increased to 36.28±2.23g/g. This means the water absorption of the aerogel reached 36 times its weight in the first one hour. After 1minute, the weight of aerogel (4:1) kept stable with slight fluctuation. The weight reached its peak at 1h, about 37.8±1.51g/g. The water absorption rates of the other three groups were higher than this aerogel (4:1). Among them, the aerogel (0:5) has a higher water absorption rate than other groups and the rate increased to 86.56 ± 22g/g within 30min. The water absorption of aerogel (0:5) was significantly higher than that of aerogel (0:4) ($p<0.01$) and was similar to that of aerogel (1:1) and aerogel (1:4) in 180min (Figure 3.9B). However, the weights of aerogel (0:5), aerogel (1:1), and aerogel (1:4) were decreased after their peak. This is because, in the three groups, the high proportion of alginate and the predominance of ionic bonds formed with zinc ions. Possibly, the ionic gel formed by alginate and zinc ions gradually dissolved, resulting in a decrease in the weight of the aerogels. On the contrary, the aerogel (4:1) maintain stably in water because of the high content of nanocellulose fibers. The water absorption ability of NCFs-alginate aerogel is much higher than methoxy polyethylene glycol/polycaprolactone nanofiber aerogels (24.11g/g) (62).

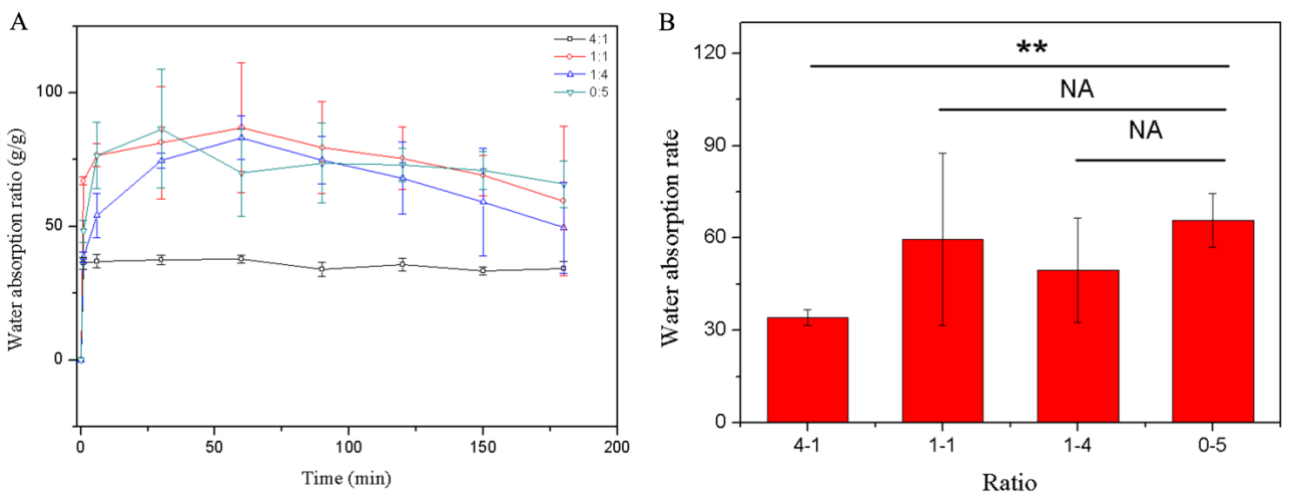

*Figure 9. Water absorption ability of NCFs-based aerogels with different rates between NCFs and alginate (n=3). (A) Water absorption of NCFs-based aerogels with time. (B) Statistical analysis of the water absorption of NCFs-based aerogels in 180min (**, p<0.01; NA, not significant. n=3).*

3.8 In vitro hemolysis assay

In vitro hemolytic assay was performed by using Sprague Dawley rat blood. As figure 10A illustration, the NCFs aerogel group, NCFs-alginate aerogel group, and negative control group (0.9% NaCl) did not observe any hemolysis, while the apparent hemolysis was observed in the positive control group (distilled water). Additionally, the hemolysis rate of positive control group was set as 100% and negative control group was 0. The hemolytic rates of NCFs-alginate aerogels are illustrated in Figure 10B. The hemolysis rates in NCFs aerogel (0.49±0.35) and NCFs-alginate aerogel (2.12±0.62) groups were both less than 5%. This indicated that the NCFs-alginate aerogels have excellent hemocompatibility and might be used as wound dressings to treat wounds.

A

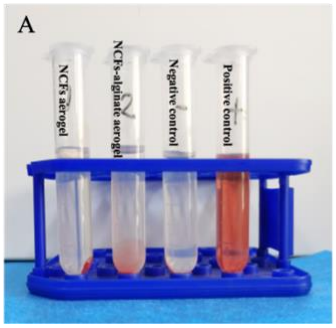

B

Group	Hemolysis (%)
NCFs aerogel	0.49±0.35
NCFs-alginate aerogel	2.12±0.62

Figure 10. (A) Hemolysis assay of NCFs-based aerogel. (B) Hemolysis ratio in the NCFs aerogel and NCFs-alginate aerogel groups (n=3).

3.9 Whole-blood clotting assay

The whole blood clotting evaluation was used to assess the in vitro coagulation ability of NCFs-alginate aerogels. The lower absorbance of hemoglobin solution, the faster blood clotting rate of NCFs-based aerogels and higher capacity to activate platelets (11,63). In here, gelatin hemostatic sponge and NCFs aerogel were set as the control group. As Figure 11 illustration, after adding whole blood (Figure 11A) and deionized water (Figure 11B), the solution of NCFs-alginate aerogel was clearer than other three groups which means the NCFs-alginate aerogel has excellent coagulation ability. Although NCFs aerogel can absorb the whole blood, the clotting effect of this group is lower than that of NCFs-alginate aerogel group. For gelatin hemostatic sponge, the hemoglobin release of solution is more than the NCFs-alginate aerogel and NCFs aerogel. This means the sponge cannot absorb the whole blood well and the blood is only accumulated on the sponge's surface. Figure 11C also supported the result. The hemoglobin absorbance value of NCFs aerogel was 84.33% lower than that of gelatin hemostatic sponge ($p<0.001$). However, the NCFs-alginate aerogel group has much lower hemoglobin solution absorbance of the two control groups, about 96.4% less than the gelatin hemostatic sponge and 76.85% less than the NCFs aerogel ($p<0.001$). It demonstrated that the addition of alginate and zinc chloride can promote blood coagulation ability of NCFs-based aerogels.

Scanning electron microscopy (SEM) was used to reveal the hemostatic mechanism of NCFs-alginate aerogels. Figure 11D illustrated the morphology and the degree of platelet activation on the NCFs-based aerogels and gelatin hemostatic sponges(2,11,64,65). In Figure 11Da, a large number of red blood cells and platelets are adsorbed on NCFs aerogel, however, very few platelets are activated. In Figure 11Db, the prominent deformation platelets were observed on the surface of NCFs-alginate aerogel, which indicated a large amount of platelets were activated and adhered on the aerogel because of the existence of carboxyl groups(2). Additionally, compared with NCFs aerogel and NCFs-alginate aerogel, the SEM images (Figure 11Dc) of gelatin hemostatic sponges illustrated that a small amount of red blood cells, very little fibrin, and activated platelets with adhered on its surface. Therefore, the NCFs-alginate aerogel with high porosity and water absorption ability can quickly absorb water from blood, attract blood cells and activate platelets to promote the formation of coagulation that stop bleeding and enhance in vitro clotting capacity(11).

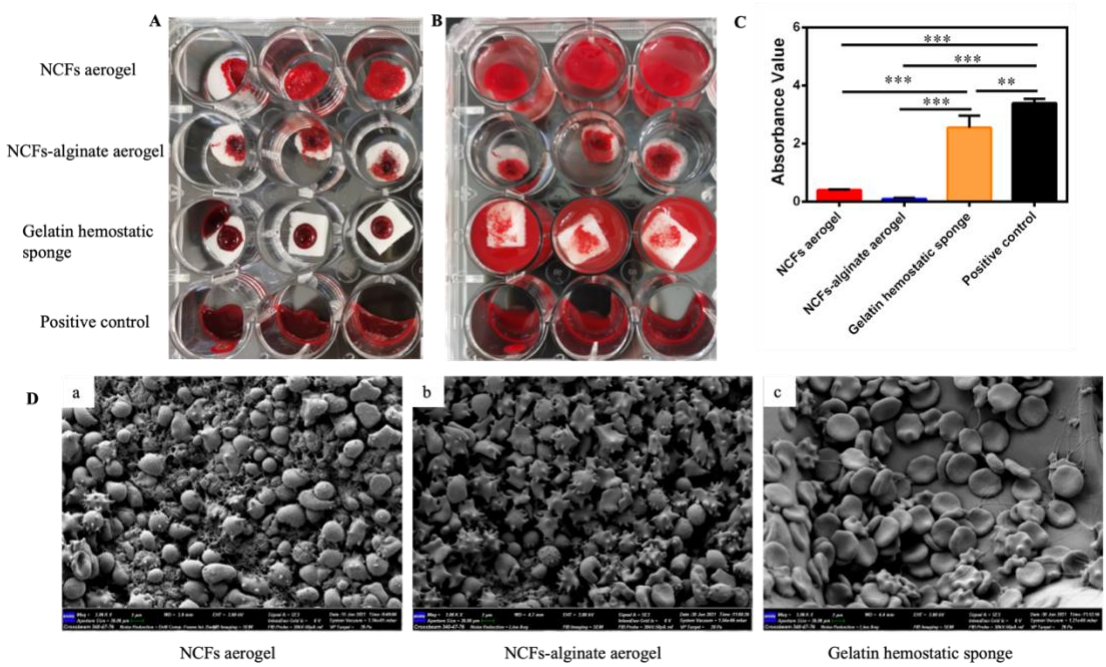

Figure 11. In vitro whole-blood clotting evaluation of NCFs-alginate aerogels. (A) Anticoagulant whole blood was added and reacted with NCFs aerogels, NCFs-alginate

aerogels, gelatin hemostatic sponge and anticoagulant whole blood (positive control) for 5min; (B) Adding distilled water to swell the unagglutinated red blood cells; (C) Hemoglobin absorbance values of the four groups (n=3); (D) SEM images of blood adhesion on NCFs aerogel(a), NCFs-alginate aerogel (b), and gelatin hemostatic sponge (c).

3.10 Antibacterial assay

Figure 12A illustrated antibacterial ability of NCFs-based aerogel within 24h. *E. coli* culture solution without material was set as the positive control. As the figure illustration, pure NCFs aerogel with low antibacterial properties just at 4 and 12h. However, after adding zinc chloride and alginate, the NCFs-alginate aerogel has more significant bacteria inhabitation than positive group and NCFs aerogel from 4-24h ($p<0.001$). Calculated by formula (Figure 12B), the inhibition bacterial rate of NCFs-alginate aerogel reached 80% at 4h and from 12h to 24h reached 86%. However, the inhibition bacterial rate of the NCFs aerogel group just 22% from 4h to 12h and decrease to 2% at 24h. Therefore, the result indicated that the NCFs-alginate aerogel can significantly inhibit the growth of bacteria due to the antibacterial ability of zinc ions(66). In other words, the NCFs-alginate aerogel can be used in emergency situations, especially hospitals and battlefields, to decrease wound infection rate, promote wound healing and improve survival rate of patients.

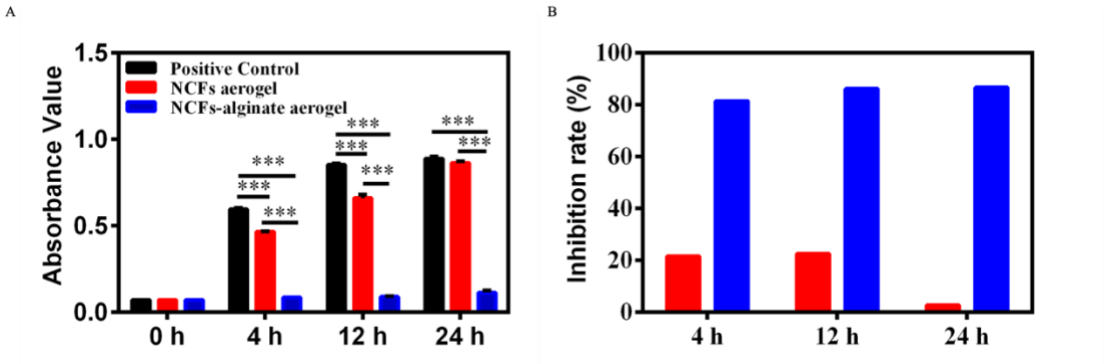

Figure 12. Antibacterial ability of NCFs-based aerogels. A. Statistical analysis chart of bacterial absorbance value(n=3), B. Absorbance mean conversion bacteriostatic rate statistical chart.

3.11 Cytotoxicity assay

The cytocompatibility of NCFs-based aerogels was tested by CKK-8 method at 24h and 72h (Figure 13). The cell viability of control group (without extract liquid) was set as 100%. Figure 13A and B respectively indicated the cell viability of 3T3 and Huvec cells at 24h and 72h. As presented, two groups, NCFs aerogel and NCFs-alginate aerogel, have more than 98% cell viabilities of 3T3 and Huvec cells after 24h and 72h of incubation. Figure 13C results also showed that the cells of control group, NCFs aerogel and NCFs-alginate aerogel group on 3T3 cells and Huvec cells had normal morphology and good growth status after cultured at 72h. The results prove that the NCFs-based aerogels have good cell safety.

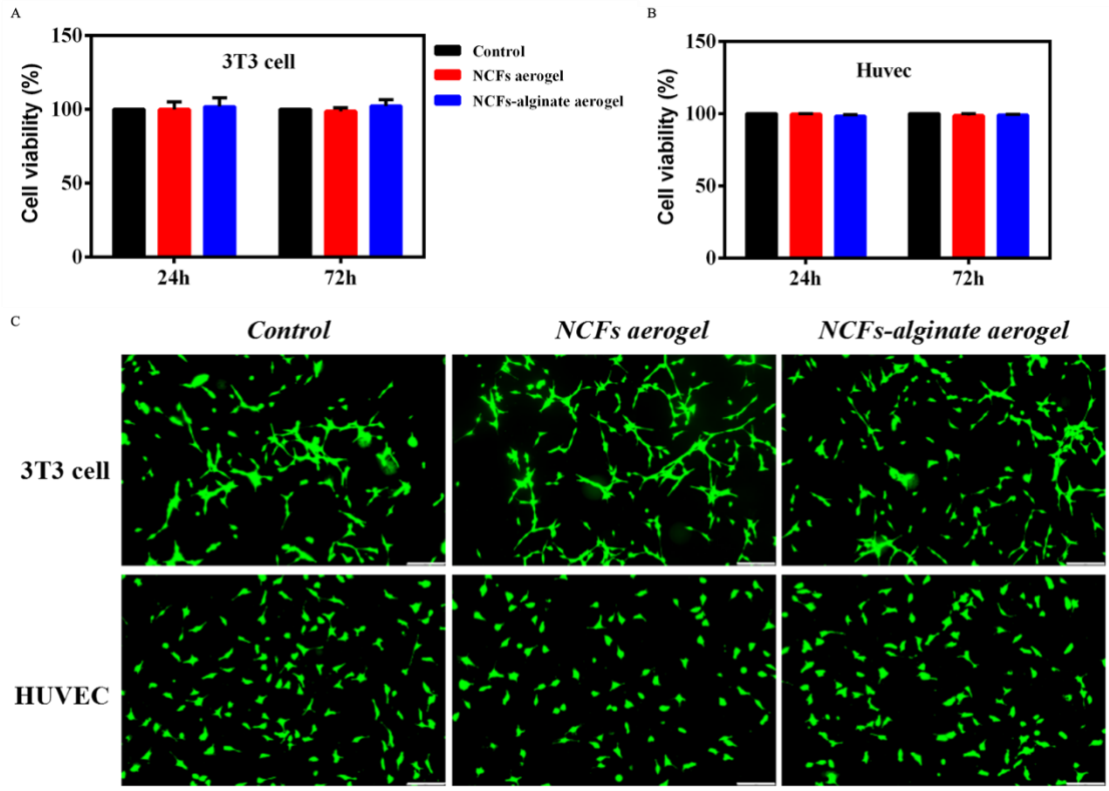

Figure 13. Cytotoxicity of materials on mouse embryonic fibroblasts (3T3) and Human Umbilical Vein Endothelial Cells (Huvec) in 24h and 72h. (A) Cell viability of control group, NCFs aerogel and NCFs-alginate aerogel on 3T3 cells (n=3). (B) Cell viability of control group, NCFs aerogel and NCFs-alginate aerogel on Huvec cells (n=3). Cell fluorescence images of NCFs-alginate aerogels on 3T3 cells and Huvec cells at 72h (C).

3.12 In vivo hemostatic assay

Currently, topical hemostatic materials have been widely used in battlefield and hospitals(67). In this project, rat liver injury and heart injury models were used to evaluate the in vivo hemostatic capacity of NCFs-based aerogels. As illustrated in Figure 14A, when samples of NCFs-alginate aerogel group (Figure 14Ac) and gelatin hemostatic sponges (Figure 14Ad) contacted with the wounds, the bleeding was blocked rapidly; oppositely, a large amount of blood was observed on the filter papers of control (Figure 14Aa) and NCFs aerogel (Figure 14Ab) groups. According to the statistics (Figure 14B), the bleeding loss in the NCFs-alginate aerogel group, only 0.187±0.034g, was much lower than that in control group and NCFs aerogel group (0.506±0.049g, $p<0.01$ and 0.420±0.076g, $p<0.05$, respectively), and with no significant difference from the gelatin sponge group (0.159±0.086g, $p>0.05$). Meanwhile, in Figure 14C, the bleeding time in the NCFs-alginate aerogel group was 20.67±0.882s, which is much shorter than that in control group and NCFs aerogel group (134±26.69s, $p<0.01$ and 91.67±23.702s, $p<0.05$, respectively). The bleeding time of gelatin hemostatic sponges was 18±4.163s, similar with the NCFs-alginate aerogel group ($p>0.05$). Thus, the hemostatic test of the rat liver injury model (Figure 14A, B and C) demonstrated that samples of NCFs-alginate aerogel group can significantly reduce the blood loss and bleeding time. The SEM images of Figure 14D as can be seen, after completing the liver hemostasis experiment, many red blood cells and fibrin were seen on the materials in each group, and the fibrin in the gelatin hemostatic sponge and the NCFs-alginate aerogel was more dense than the NCFs aerogel group. It shows that

the NCFs-alginate aerogel can promote hemostasis by better activating fibrinogen like gelatin hemostatic sponge. Figure 14E indicates the result of rat heart injury model tests. The hemostasis time of NCFs-alginate group and gelatin hemostatic sponges was significantly shorter than that of NCFs aerogel group and control groups. The result shows that the gelatin hemostatic sponge and NCFs-alginate aerogel can block wound bleeding completely. No re-bleeding traces after coagulation of the heart wound, the heart still filling and smooth. Therefore, the in vivo hemostatic tests indicate that the NCFs-alginate have excellent hemostatic capacity with lower blood loss and shorter hemostasis time.

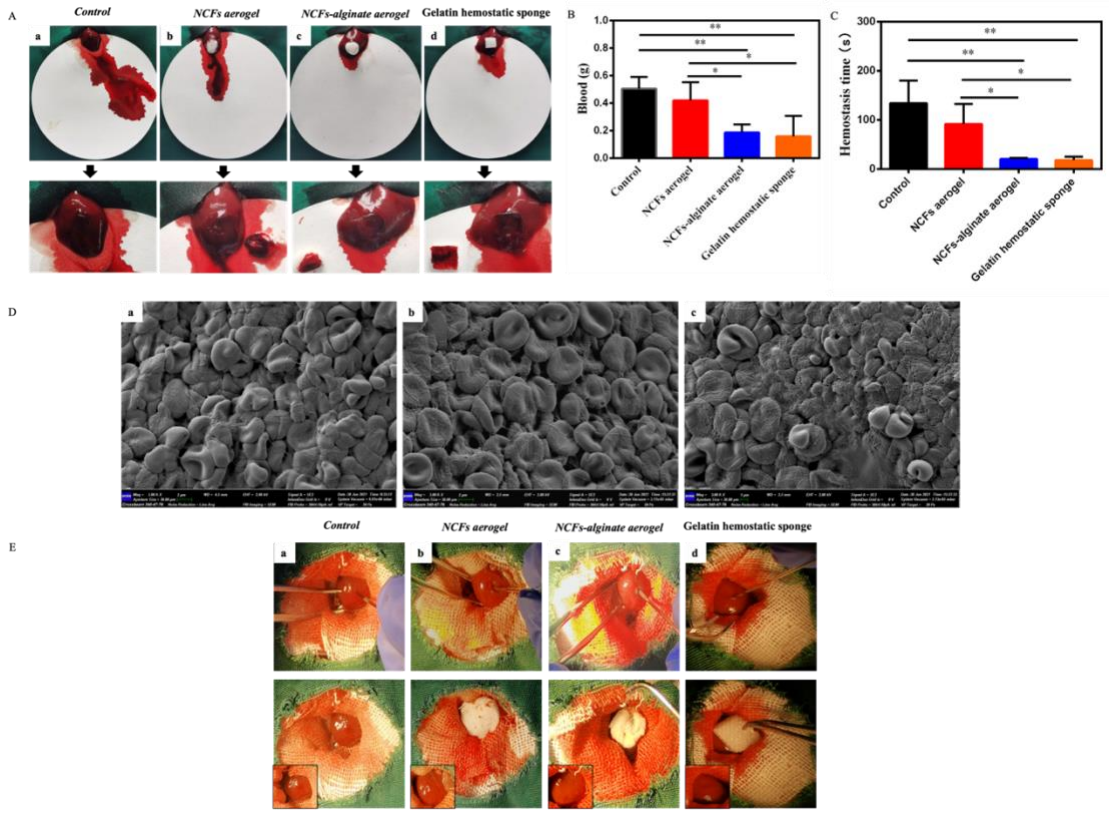

Figure 14. In vivo hemostatic test of aerogels in rat liver and heart injury model. Photographs of the rat liver injury model (A) and the rat heart injury model (E): (a) control group, (b) NCFs aerogel, (c)NCFs-alginate aerogel, and (d) gelatin hemostatic sponge groups. (B) Blood loss in the rat liver injury model (n=3). (C) Hemostatic time in rat liver injury model. (D) SEM

images of each group of materials after use in liver hemostasis experiment: (a)NCFs aerogel, (b)NCFs-alginate aerogel, and (c)gelatin hemostatic sponge.

4. Conclusion

A lightweight, antibacterial, injectable aerogel with high water absorption and excellent hemostatic ability was developed in this study. In this system, NCFs provided a substrate to improve the water stability and flexibility. In the meantime, addition of alginate and zinc chloride used to lock the network of NCFs-based network to increase the mechanical strength and endowed the aerogel with antibacterial ability, respectively. The lowest density of as-prepared aerogel was 10.66 mg/cm^3 with 2mg/ml NCFs. Compared with other ratios of NCFs and alginate, although the water absorption rate of the aerogel (4:1) was lower than other groups, only 37.8±1.51g/g, this aerogel has excellent water stability without any dissolution in water even after three hours. The introduction of NCFs can bestow the extreme compressive property and flexibility on NCFs-alginate aerogel. Besides, for hemostatic capacity, NCFs-based aerogel with the addition of alginate and zinc chloride has a good blood coagulation capacity, non-cytotoxicity, better antibacterial ability (89%), lower blood loss (0.124±0.1g) in the rat liver model and shorter hemostasis time (31s) in the rat heart model than NCFs aerogel and commercial gelatin hemostatic sponge. The NCFs-alginate aerogel will potentially be used as rapid hemostatic materials in emergency and surgery situations.

References

1. Zhao X, Guo B, Wu H, Liang Y, Ma PX. Injectable antibacterial conductive nanocomposite cryogels with rapid shape recovery for noncompressible hemorrhage and wound healing. Nat Commun. 2018;9(1):1–17.

2. Cheng F, Liu C, Wei X, Yan T, Li H, He J, et al. Preparation and Characterization of 2,2,6,6-Tetramethylpiperidine-1-oxyl (TEMPO)-Oxidized Cellulose Nanocrystal/Alginate Biodegradable Composite Dressing for Hemostasis Applications. ACS Sustain Chem Eng. 2017;5(5):3819–28.

3. Hu Z, Zhang DY, Lu ST, Li PW, Li SD. Chitosan-based composite materials for prospective hemostatic applications. Mar Drugs. 2018;16(8):1–25.

4. Cheng X, Shao Z, Li C, Yu L, Raja MA, Liu C. Isolation , Characterization and Evaluation of Collagen from Jellyfish Rhopilema esculentum Kishinouye for Use in Hemostatic Applications. PLoS One. 2017;12(1):1–21.

5. Hajosch R, Suckfuell M, Oesser S, Ahlers M, Flechsenhar K. A novel gelatin sponge for accelerated hemostasis. J Biomed Mater Res Part B Appl Biomater. 2010;94(2):372–9.

6. Thomas A, Harding KG, Moore K. Alginates from wound dressings activate human macrophages to secrete tumour necrosis factor-α. Biomaterials. 2000;21(17):1797–802.

7. Lan G, Lu B, Wang T, Wang L, Chen J, Yu K, et al. Chitosan / gelatin composite sponge is an absorbable surgical hemostatic agent. Colloids surfaces B Biointerfaces. 2015;136:1026–34.

8. Liu X, Lin T, Gao Y, Xu Z, Huang C, Yao G, et al. Antimicrobial electrospun nanofibers of cellulose acetate and polyester urethane composite for wound

dressing. J Biomed Mater Res - Part B Appl Biomater. 2012;100 B(6):1556–65.

9. Kai Jiang, Yun-Ze Long, Zhao-Jun Chen, Shu-Liang Liu, b Yuan-Yuan Huang XJ and Z-QH. Airflow-directed in situ electrospinning of a medical glue of cyanoacrylate for rapid hemostasis in liver resection. Nanoscale. 2014;6(14):7792–8.

10. Yang X, Liu W, Li N, Wang M, Liang B, Ullah I, et al. Design and development of polysaccharide hemostatic materials and their hemostatic mechanism. Biomater Sci. 2017;5(12):2357–68.

11. Fan X, Li Y, Li X, Wu Y, Tang K, Liu J, et al. Injectable antibacterial cellulose nanofiber/chitosan aerogel with rapid shape recovery for noncompressible hemorrhage. Int J Biol Macromol [Internet]. 2019;(xxxx). Available from: https://doi.org/10.1016/j.ijbiomac.2019.10.273

12. Baik SH, Kim JH, Cho HH, Park SN, Kim YS, Suh H. Development and analysis of a collagen-based hemostatic adhesive. J Surg Res. 2010;164(2):221–8.

13. Arnaud F, Tomori T, Carr W, McKeague A, Teranishi K, Prusaczyk K, et al. Exothermic reaction in zeolite hemostatic dressings: QuikClot ACS and ACS+®. Ann Biomed Eng. 2008;36(10):1708–13.

14. Duong HM, Lim ZK, Nguyen TX, Gu B, Penefather MP, Phan-Thien N. Compressed hybrid cotton aerogels for stopping liquid leakage. Colloids Surfaces A Physicochem Eng Asp. 2018 Jan 20;537:502–7.

15. Ibrahim NA, Abo-Shosha MH, Gaffar MA, Elshafei AM, Abdel-Fatah OM. Antibacterial properties of ester - Cross-linked cellulose-containing fabrics post-treated with metal salts. Polym - Plast Technol Eng. 2006;45(6):719–27.

16. Shin JU, Gwon J, Lee SY, Yoo HS. Silver-Incorporated Nanocellulose Fibers for Antibacterial Hydrogels. ACS Omega. 2018;3(11):16150–7.

17. Hu J, Liu Z, Yu Q, Ma T. Preparation of reactive oxygen species-responsive antibacterial hydrogels for efficient anti-infection therapy. Mater Lett [Internet]. 2020;263:127254. Available from: https://doi.org/10.1016/j.matlet.2019.127254

18. Llor C, Bjerrum L. Antimicrobial resistance: Risk associated with antibiotic overuse and initiatives to reduce the problem. Ther Adv Drug Saf. 2014;5(6):229–41.

19. Friedman ND, Temkin E, Carmeli Y. The negative impact of antibiotic resistance. Clin Microbiol Infect [Internet]. 2016;22(5):416–22. Available from: http://dx.doi.org/10.1016/j.cmi.2015.12.002

20. Roca I, Akova M, Baquero F, Carlet J, Cavaleri M, Coenen S, et al. The global threat of antimicrobial resistance: Science for intervention. New Microbes New Infect [Internet]. 2015;6(January 2015):22–9. Available from: http://dx.doi.org/10.1016/j.nmni.2015.02.007

21. Ding BP, Wu F, Chen SC, Wang YZ, Zeng JB. Synthesis and characterization of a polyurethane ionene/zinc chloride complex with antibacterial properties. RSC Adv. 2015;5(16):12423–33.

22. Jin G, Cao H, Qiao Y, Meng F, Zhu H, Liu X. Osteogenic activity and antibacterial effect of zinc ion implanted titanium. Colloids Surfaces B

Biointerfaces [Internet]. 2014;117:158–65. Available from: http://dx.doi.org/10.1016/j.colsurfb.2014.02.025

23. Cummins D. Zinc citrate/Triclosan: a new anti-plaque system for the control of plaque and the prevention of gingivitis: short-term clinical and mode of action studies. J Clin Periodontol. 1991;18(6):455–61.

24. Nouri S, Sharif MR, Tabatabaei F, Farokhi S. Investigating the Effect of Zinc Chloride to Control External Bleeding in Rats. Nurs Midwifery Stud. 2014;3(3).

25. Basu A, Hong J, Ferraz N. Hemocompatibility of Ca2+-Crosslinked Nanocellulose Hydrogels: Toward Efficient Management of Hemostasis. Macromol Biosci [Internet]. 2017 Nov 1 [cited 2020 Mar 25];17(11):1700236. Available from: http://doi.wiley.com/10.1002/mabi.201700236

26. Françon H, Wang Z, Marais A, Mystek K, Piper A, Granberg H, et al. Ambient-Dried, 3D-Printable and Electrically Conducting Cellulose Nanofiber Aerogels by Inclusion of Functional Polymers. Adv Funct Mater. 2020;

27. Wang D, Peng H, Yu B, Zhou K, Pan H, Zhang L, et al. Biomimetic structural cellulose nanofiber aerogels with exceptional mechanical, flame-retardant and thermal-insulating properties. Chem Eng J [Internet]. 2020;389(February):124449. Available from: https://doi.org/10.1016/j.cej.2020.124449

28. De France KJ, Hoare T, Cranston ED. Review of Hydrogels and Aerogels Containing Nanocellulose. Chem Mater. 2017;29(11):4609–31.

29. Hutchinson RW, George K, Johns D, Craven L, Zhang G, Shnoda P. Hemostatic efficacy and tissue reaction of oxidized regenerated cellulose hemostats. Cellulose. 2013;20(1):537–45.

30. Davis FE, Kenyon K, Kirk J. A Rapid Titrimetric Method for Determining the Water Content of Human Blood. Adv Sci. 1953;118(3062):276–7.

31. Françon H, Wang Z, Marais A, Mystek K, Piper A, Granberg H, et al. Ambient-Dried, 3D-Printable and Electrically Conducting Cellulose Nanofiber Aerogels by Inclusion of Functional Polymers. Adv Funct Mater. 2020;30(12).

32. Soni B, Hassan EB, Mahmoud B. Chemical isolation and characterization of different cellulose nanofibers from cotton stalks. Carbohydr Polym. 2015 Aug 24;134:581–9.

33. Fiedot-Toboła M, Ciesielska M, Maliszewska I, Rac-Rumijowska O, Suchorska-Woźniak P, Teterycz H, et al. Deposition of zinc oxide on different polymer textiles and their antibacterial properties. Materials (Basel). 2018 Apr 30;11(5).

34. Praglowska J, Piątkowski M, Janus Ł, Korniienko V, Husak E, Holubnycha V, et al. Chitosan-Based Bioactive Hemostatic Agents with Antibacterial Properties—Synthesis and Characterization. Molecules. 2019;24:17.

35. Wang Y, Yin M, Zheng X, Li W, Ren X. Chitosan/mesoporous silica hybrid aerogel with bactericidal properties as hemostatic material. Eur Polym J. 2021 Jan 5;142.

36. Cao S, Yang Y, Zhang S, Liu K, Chen J. Multifunctional dopamine modification of green antibacterial hemostatic sponge. Mater Sci Eng C

[Internet]. 2021;127(April):112227. Available from: https://doi.org/10.1016/j.msec.2021.112227

37. Yang X, Cranston ED. Chemically cross-linked cellulose nanocrystal aerogels with shape recovery and superabsorbent properties. Chem Mater. 2014;26(20):6016–25.

38. Wågberg L, Decher G, Norgren M, Lindström T, Ankerfors M, Axnäs K. The build-up of polyelectrolyte multilayers of microfibrillated cellulose and cationic polyelectrolytes. Langmuir. 2008;24(3):784–95.

39. Jiang F, Hsieh Y Lo. Super water absorbing and shape memory nanocellulose aerogels from TEMPO-oxidized cellulose nanofibrils via cyclic freezing-thawing. J Mater Chem A. 2014;2(2):350–9.

40. Dhahri M, Rodriguez-Ruiz V, Aid-Launais R, Ollivier V, Pavon-Djavid G, Journé C, et al. In vitro and in vivo hemocompatibility evaluation of a new dermatan sulfate-modified PET patch for vascular repair surgery. J Biomed Mater Res - Part B Appl Biomater. 2017 Oct 1;105(7):2001–9.

41. Wang Y, Liu Y, Liu M, Qian W, Zhou D, Liu T, et al. Short fluorocarbon chains containing hydrophobic nanofibrous membranes with improved hemocompatibility, anticoagulation and anti-fouling performance. Colloids Surfaces B Biointerfaces. 2019 Aug 1;180:49–57.

42. Reithofer MR, Lakshmanan A, Ping ATK, Chin JM, Hauser CAE. In situ synthesis of size-controlled, stable silver nanoparticles within ultrashort peptide hydrogels and their anti-bacterial properties. Biomaterials. 2014;35(26):7535–42.

43. Lu D, Wang H, Li T, Li Y, Dou F, Sun S, et al. Mussel-Inspired Thermoresponsive Polypeptide-Pluronic Copolymers for Versatile Surgical Adhesives and Hemostasis. ACS Appl Mater Interfaces. 2017;9(20):16756–66.

44. Hong Y, Zhou F, Hua Y, Zhang X, Ni C, Pan D, et al. A strongly adhesive hemostatic hydrogel for the repair of arterial and heart bleeds. Nat Commun [Internet]. 2019;10(1):1–11. Available from: http://dx.doi.org/10.1038/s41467-019-10004-7

45. Ramli S, Ja'afar SM, Sisak MAA, Zainuddin N, Rahman IA. Formulation and physical characterization of microemulsions based carboxymethyl cellulose as vitamin c carrier. Malaysian J Anal Sci. 2015;19(1):275–83.

46. Onyianta AJ, Dorris M, Williams RL. Aqueous morpholine pre-treatment in cellulose nanofibril (CNF) production: comparison with carboxymethylation and TEMPO oxidisation pre-treatment methods. Cellulose. 2018 Feb 1;25(2):1047–64.

47. Maver T, Hribernik S, Mohan T, Smrke DM, Maver U, Stana-Kleinschek K. Functional wound dressing materials with highly tunable drug release properties. RSC Adv. 2015 Sep 9;5(95):77873–84.

48. Zhang A, Zou Y, Xi Y, Wang P, Zhang Y, Wu L, et al. Fabrication and characterization of bamboo shoot cellulose/sodium alginate composite aerogels for sustained release of curcumin. Int J Biol Macromol [Internet]. 2021;192(October):904–12. Available from: https://doi.org/10.1016/j.ijbiomac.2021.10.027

49. Hossen MR, Dadoo N, Holomakoff DG, Co A, Gramlich WM, Mason MD. Wet stable and mechanically robust cellulose nanofibrils (CNF) based hydrogel. Polymer (Guildf). 2018 Aug 29;151:231–41.

50. Tajvidi M, Falk RH, Hermanson JC. Effect of natural fibers on thermal and mechanical properties of natural fiber polypropylene composites studied by dynamic mechanical analysis. J Appl Polym Sci. 2006;101(6):4341–9.

51. Ochbaum G, Davidovich-Pinhas M, Bitton R. Tuning the mechanical properties of alginate-peptide hydrogels. Soft Matter. 2018;14(21):4364–73.

52. Baniasadi M, Minary-Jolandan M. Alginate-collagen fibril composite hydrogel. Materials (Basel). 2015;8(2):799–814.

53. Pang L, Sun P, Dong X, Tang T, Chen Y, Liu Q, et al. Shear viscoelasticity of electrospinning PCL nanofibers reinforced alginate hydrogels. Mater Res Express. 2021;8(5).

54. Zhu C, Han TYJ, Duoss EB, Golobic AM, Kuntz JD, Spadaccini CM, et al. Highly compressible 3D periodic graphene aerogel microlattices. Nat Commun. 2015;6:1–8.

55. Wang L, Zhang X, He Y, Wang Y, Zhong W, Mequanint K, et al. Ultralight Conductive and Elastic Aerogel for Skeletal Muscle Atrophy Regeneration. Adv Funct Mater. 2019;29(1):1–17.

56. Wang H, Zhang X, Wang N, Li Y, Feng X, Huang Y, et al. Ceramic Nanofiber Sponges. Sci Adv. 2017;(June):1–10.

57. Si Y, Wang X, Dou L, Yu J, Ding B. Ultralight and fire-resistant ceramic nanofibrous aerogels with temperature-invariant superelasticity. Sci Adv. 2018;4(4).

58. Bai Y, Deng Y, Zheng Y, Li Y, Zhang R, Lv Y, et al. Characterization, corrosion behavior, cellular response and in vivo bone tissue compatibility of titanium-niobium alloy with low Young's modulus. Mater Sci Eng C [Internet]. 2016;59:565–76. Available from: http://dx.doi.org/10.1016/j.msec.2015.10.062

59. Zou Y, Liu PX, Cheng Q, Lai P, Li C. A New Deformation Model of Biological Tissue for Surgery Simulation. IEEE Trans Cybern. 2017;47(11):3494–503.

60. Kim HN, Kang DH, Kim MS, Jiao A, Kim DH, Suh KY. Patterning methods for polymers in cell and tissue engineering. Ann Biomed Eng. 2012;40(6):1339–55.

61. Yang J, Xia Y, Xu P, Chen B. Super-elastic and highly hydrophobic/superoleophilic sodium alginate/cellulose aerogel for oil/water separation. Cellulose [Internet]. 2018;25(6):3533–44. Available from: https://doi.org/10.1007/s10570-018-1801-8

62. Jia J, Wang C. A facile restructuring of 3D high water absorption aerogels from methoxy polyethylene glycol-polycaprolactone (mPEG-PCL) nanofibers. Mater Sci Eng C [Internet]. 2019;94(August 2017):965–75. Available from: https://doi.org/10.1016/j.msec.2018.10.044

63. Wang Y, Zhao Y, Qiao L, Zou F, Xie Y, Zheng Y, et al. Cellulose fibers-reinforced self-expanding porous composite with multiple hemostatic efficacy and shape adaptability for uncontrollable massive hemorrhage treatment.

Bioact Mater [Internet]. 2021;6(7):2089–104. Available from: https://doi.org/10.1016/j.bioactmat.2020.12.014

64. Quan K, Li G, Luan D, Yuan Q, Tao L, Wang X. Black hemostatic sponge based on facile prepared cross-linked graphene. Colloids Surfaces B Biointerfaces [Internet]. 2015;132:27–33. Available from: http://dx.doi.org/10.1016/j.colsurfb.2015.04.067

65. Cheng X, Shao Z, Li C, Yu L, Raja MA, Liu C. Isolation, characterization and evaluation of collagen from jellyfish Rhopilema esculentum kishinouye for use in hemostatic applications. PLoS One. 2017;12(1).

66. Xie T, Ding J, Han X, Jia H, Yang Y, Liang S, et al. Wound dressing change facilitated by spraying zinc ions. Mater Horizons [Internet]. 2020;7(2):605–14. Available from: http://dx.doi.org/10.1039/C9MH01255A

67. Yu P, Zhong W. Hemostatic materials in wound care. Vol. 9, Burns and Trauma. Oxford University Press; 2021.